Ph.D. Dissertation in Agricultural Biotechnology

The molecular mechanism of lamin assembly and development of functional foods for anti-aging

라민 조립의 분자 메커니즘과 노화 방지를 위한 기능성 식품의 개발

February 2020

The Graduate School
Seoul National University
Department of Agricultural Biotechnology

Jinsook Ahn

The molecular mechanism of lamin assembly and development of functional foods for anti-aging

Advisor: Nam-Chul Ha

Submitting a Ph.D. Dissertation in Agricultural Biotechnology

February, 2020

The Graduate School
Seoul National University
Department of Agricultural Biotechnology

Jinsook Ahn

Confirming the Ph.D. Dissertation written by Jinsook Ahn
February, 2020

Chair	_____(Seal)
Vice Chair	_____(Seal)
Examiner	_____(Seal)
Examiner	_____(Seal)
Examiner	_____(Seal)

Abstract

The molecular mechanism of lamin assembly and development of functional foods for anti-aging

Jinsook Ahn
Department of Agricultural Biotechnology
The Graduate School
Seoul National University

Intermediate filament (IFs) proteins form flexible fibrous structures that provide vital mechanical support in cells of higher eukaryotes. Nuclear structure and function are governed by lamins, which are intermediate filaments mostly consisting of α-helices. Therefore, it is necessary to determine the mechanism of lamin assembly to understand the dynamic functions of the nuclear membrane. Different lamin assembly models have been proposed based on low resolution or fragmented structures. However, their assembly mechanisms at the molecular level are poorly understood. Here, I present a crystal structure of a long human lamin fragment at a 3.2 Å

resolution, which allows for the visualization of the full-length features. The structure shows the anti-parallel arrangement of two coiled-coil dimers, which is important for the assembly process. The anti-parallel interaction corresponded to the ‘A11 interaction’ of vimentin. Furthermore, another new interaction (eA22) involved in longitudinal elongation of lamin filament was discovered by using chemical cross-linking and mass analysis. Based on these two interactions (A11 and eA22 interaction), a molecular mechanism of lamin assembly was proposed that is in agreement with a recent model representing the native state and could explain pathological mutations.

Furthermore, it was observed that the altered binding strength of eA22 interaction when the mutations were introduced to the residues at a, d position of coil 1a to discover the role of coil 1a on the longitudinal extension of filament. The result indicated that the binding affinity of eA22 interactions is altered depending on the stability of coil 1a dimer. Consistent results were obtained in the nuclear shapes and the distribution of the lamin A/C when the mutant lamin genes were overexpressed in the cell lines. This study provides an insight to understand the role of coil 1a as a molecular switch in the eA22 interaction, which contributes to the molecular basis for the development of a new treatment against laminopathies.

A silent mutation of the lamin A/C gene, leading to the production of a C-terminally truncated protein (called progerin), causes Hutchinson-Gilford progeria syndrome (HGPS). A deformed nuclear shape is a hallmark of HGPS cells, which shares with normal aged cells. A recent study found that progerin makes a direct interaction with a middle fragment of lamin A/C, which leads to nuclear deformation. A synthetic compound (called JH4), blocking the interaction between the progerin and meddle fragment of lamin A/C, ameliorated the aging phenotypes both in cells and mouse models. The natural compounds were discovered that interrupt progerin-mediated interaction. Of these, the flavonoid morin was investigated further characterization. Morin showed an effect on the interruption of the progerin-mediated interaction. Treatment of morin to progerin-expressing cells and HGPS cells alleviated the nuclear deformation, which is comparable to the previous synthetic compound JH4. Since morin is a naturally occurring substance with the antioxidant activity, it has the potential to develop as a functional food to improve lifespan and health in both HGPS patients and normal aged persons.

Keyword: intermediate filament, nuclear lamin A/C, nuclear membrane, crystal structure, assembly mechanism, laminopathies, HGPS, morin

Student Number: 2017-39169

Table of Contents

List of Figures

List of Tables

Chapter 1. Introduction

1.1. Intermediate filament

1.1.1. The domain organization of intermediate filament

The intermediate filament (IF) proteins form flexible fibrous structures that provide vital mechanical support in the higher eukaryote cells. Intermediate filaments refer to the intermediate fibers (~10 nm), whose diameter is between actin filaments (~6 nm) and microtubules (~25 nm) (Goldman, 1971; Ishikawa et al., 1968). All IF proteins follow a common structural principle comprising of a central α-helical rod, unstructured N-terminal head, and non-helical C- terminal tail domains. The rod domain is comprised of three segments interrupted by two linkers; coil 1a, L1, coil 1b, L12, and coil 2 (Chou and Fasman, 1978). Those of structural features and length of central rod domain are conserved in the IF proteins. Since the central rod domains have a high propensity to form coiled-coil dimer, a dimer of the IF proteins has been considered as a minimal unit to assemble into higher-order structures. The assembly mechanism of the canonical IF proteins (IF proteins except for lamins) has been reported that mature 10 nm-thick filaments.

1.1.2. Classification of intermediate filament proteins

Comparing the amino acid sequences of various IF proteins, it has been classified into “type I” - “type V” (Conway and Parry, 1988). Interestingly, this sequence-derived classification has been interpreted to reflect its biological functions and tissue origin. According to the classification, types I and II consist of two groups of keratins. The acidic keratins were termed type I and the neutral-basic keratins type II (Jacob et al., 2018; Schweizer et al., 2006), which are expressed in epithelial cells. Type III intermediate filament proteins consist of vimentin and desmin, which is specifically expressed in glial cells (Franke et al., 1979; Herrmann and Aebi, 2016; Lazarides and Hubbard, 1976). The type IV intermediate filament proteins contain synemin, nestin, and three neurofilaments (NF) proteins including light NF (NF-L), medium NF (NF-M), and heavy NF (NF-H) (Hoffman and Lasek, 1975; Lendahl et al., 1990).

1.2. Nuclear lamins

1.2.1. Expression of nuclear lamins

Based on the genomic structure and sequence homology, the nuclear lamins were identified as type V of five subtypes of the IF superfamily. According to the expression patterns, two major types of lamins are recognized; A-type and B-type. B-type lamins are expressed in all metazoan cells. On the other hand, A-type lamins are only expressed in the differentiated cells of the higher complex organisms (Burke and Stewart, 2013).

In mammalian cells, three genes encode predominantly four major isoforms, two A-type lamins; A and C and two B-type lamins; B1 and B2, and three minor lamin isoforms; A△10, C2, and B3. The *LMNA* gene encodes the A-type lamins including the major isoforms A and C, whereas *LMNB1* and *LMNB2* genes encode B-type lamins containing B1 and B2, respectively.

Lamin A and B have been considered as that they are co-assembled to form the filament (Gruenbaum and Foisner, 2015; Kapinos et al., 2010). However, several lines of experimental results indicate that lamin A and B polymerize to form separate filament networks that concentrate underneath the INM in the somatic cell (Goldberg et al.,

2008). At the cellular level, both types of proteins contribute to maintaining the mechanical properties of the nucleus. Elastic mechanical properties of the nucleus are determined by B-type lamins, which regulate the deformation of the nuclear envelope (Dahl et al., 2004). A-type lamins contribute to nuclear stiffness by giving the deformation-resistant viscosity to the nucleus (Broers et al., 2004; Lammerding et al., 2006).

1.2.2. The domain organization of lamins

Like other IF proteins, lamins share similar protein domains; an unstructured N-terminal head domain, a coiled-coil central rod domain, and a C-terminal tail domain. The three a-helical domains (coils 1a, 1b, and 2) in the central rod domain are separated by two linkers (linkers L1 and L2). Unlike the other IF proteins, lamins contain an additional 42 residues in their coil 1B segments. The tail domain of lamins contains a nuclear localization signal (NLS), a globular immunoglobulin fold (Ig-like domain), and a conserved CaaX motif (C, cysteine residue; a, aliphatic residue; and X, any residue) (Gruenbaum and Foisner, 2015; Holtz et al., 1989).

1.2.3. Post-translational modification of lamins

Lamin proteins initially expressed as pre-lamins and undergo post-translationally modification in several ways to become mature lamins. Almost all lamins contain a CaaX motif at the carboxyl terminus, which is modified to post-translational farnesylation. The cysteine residue of the CaaX motif is farnesylated by farnesyltransferase. Subsequently, the last three amino acids (aaX) is removed by an endoprotease including Ras-converting enzyme (Rce1) or Zinc metalloprotease (Zmpste24). The third modification is a process of carboxymethylation, the cysteine residue is catalyzed by isoprenylcysteine carboxyl methyltransferase (ICMT). Unlike B-type lamins including the farnesylated cysteine in their mature form, lamin A undergoes an additional cleavage of the last 15 amino acids, containing the farnesylated cysteine by ZMPSTE24. Lamin C does not undergo the post-translational farnesylation since it has a shorter C-terminal which does not contain the CaaX motif.

Early studies revealed that the lamins are phosphorylated during mitosis, resulting in the reversible disassembly of the nuclear lamina (Ottaviano and Gerace 1985). Lamins contain numerous phosphorylation sites of the serine and threonine residues, with more than 30 known sites. The N-terminal head domain of all lamins contains

highly conserved sites, which are phosphorylated by the mitotic cyclin-dependent kinase CDK1 (Machowska et al., 2015). The phosphorylation of lamin by CDK1 and protein kinase C (PKC) derives the disassembly of lamins during the nuclear envelop breakdown at the beginning of mitosis (Dessev et al., 1990; Mall et al., 2012; Peter et al., 1990). During the telophase/early G1 transition, protein phosphatase 1a is involved in the dephosphorylation of the mitotic sites for re-assembly of lamins (Thompson et al., 1997). In addition, phosphorylation of serine and threonine residues adjacent to the NLS sequence by PKC is known to regulate the import of lamins into the nucleus (Hennekes et al., 1993; Leukel and Jost, 1995).

1.2.4. Assembly of lamins

The central rod domain consisting of α-helices is essential for the assembly of the nuclear lamina. Each α-helical segment has a high propensity to form coiled-coil dimers in parallel with each other. The coiled-coil interactions follow the seven-residues (heptad; a, b, c, d, e, f, and g) periodicity. Positions a and d preferentially contain hydrophobic residues and the charged polar residues are occupied repeats e and g. The α-helical segment following the heptad repeat pattern likely to form a

left-handed coiled-coil structure (Herrmann and Aebi, 2016).

Electron microscope analysis has shown that parallel associated lamin dimers with two globular domains corresponding to the C-terminal tail domain which has 52–55-nm-long rod-like shape (Heitlinger et al., 1991). The lamin dimers associate longitudinally to form the head-to-tail manner (Heitlinger et al., 1991; Stuurman et al., 1996). Tetrameric protofilaments lead to the formation of 10-nm-thick filaments (Ben-Harush et al., 2009; Stuurman et al., 1996).

Recently, cryo-electron tomography (cryo-ET) study revealed that lamins form 3.5-nm-thick filaments (Turgay et al., 2017) that are remarkably different from other canonical 10-nm thick IF proteins and the proposed assembly model of lamins (Guzenko et al., 2017; Herrmann and Aebi, 2016; Herrmann et al., 1999; Herrmann and Strelkov, 2011; Wickert et al., 2005)

1.3. Functions of lamins

1.3.1. Protein interactions

Lamins interact with numerous functionally diverse proteins in the inner nuclear membrane (INM) and nucleoplasm (Wilson and Foisner, 2010). Lamin-binding proteins together with lamins have been described supporting nuclear architecture and mechanics as well as several nuclear functions (Dechat et al., 2008; Gruenbaum et al., 2005). Most of the lamin-interacting proteins identified to be caused by A-type lamins. Numerous direct or indirect interactions have been recognized by using various proteomics-based studies (Kubben et al., 2010).

The lamina-associated polypeptide 1 (LAP1) proteins have been first identified among the lamin binding proteins (LBPs) (Foisner and Gerace, 1993; Martin et al., 1995). LAP1 protein regulates ATPase torsin A activity, and this interaction might be important in neuronal cells (Waterham et al., 2003). Since the torsin A mutant has strengthened binding affinity to LAP1 protein, and it causes a disease of the central nervous system (Goodchild and Dauer, 2005).

The nuclei are mechanically connected to the cytoskeleton by SUN and KASH domain proteins which localized in the INM and ONM, respectively. Trimeric SUN proteins interact with three KASH proteins

forming LINC complexes in the perinuclear space (Crisp et al., 2006; Sosa et al., 2012). The LINC complexes have been emphasized in diverse functions important for migrating cells, nuclear positioning, nucleus morphology, and mechanics (Bouzid et al., 2019; Starr and Han, 2003; Tapley and Starr, 2013).

The LEM proteins together with lamins contribute to maintaining the nuclear architecture and anchor heterochromatin to the lamina (Laguri et al., 2001; Wilson and Foisner, 2010). LEM proteins share the LEM domain which interacts with the Barrier to Auto integration Factor, BAF (Furukawa, 1999; Shumaker et al., 2001). Several LEM proteins interfere with signaling components in the INM by inducing away from their active transcription complexes (Gruenbaum and Foisner, 2015).

1.3.2. Chromatin organization

Heterochromatin is highly organized and normally located at the nuclear peripheral regions of the lamina in mammalian cells (Dechat et al., 2008). Gene-poor chromosome regions, such as telomeres, centromeres, and the inactive X chromosome, have preference to locate in the region of the nuclear lamina (Croft et al., 1999). Early biochemical evidence

supporting that C-terminal non-a helical domain of lamin A and N- and C-terminal tail domain of histones are involved in the interaction between lamins and chromatin (Hoger et al., 1991; Schmidt and Krohne, 1995; Yuan et al., 1991).

Furthermore, lamins can bind directly DNA associated with the scaffold/matrix attachment regions, which has been recognized to involve in DNA replication, chromosome organization, chromatin condensation and regulation of transcription (Baricheva et al., 1996; Dechat et al., 2008). It was demonstrated that lamins directly regulate chromosome in studies from Lmna-/- mice, which show the dissociation of heterochromatin from the nuclear peripheral regions (Nikolova et al., 2004; Sullivan et al., 1999).

In the cells from HGPS patients, altered specific histone marks were identified; reduced levels of the constitutive heterochromatin (H3K9me3 and H3K27me3) and increased levels of H4K20me3 which identify facultative heterochromatin (Columbaro et al., 2005; Martin and Zhang, 2005; Shumaker et al., 2006). Taken together, these findings reveal that mutations of lamin lead to global changes in the epigenetic organization of chromatin.

1.3.3. DNA damage and repair

Recent studies have suggested the role of lamins for DNA repair. An unprocessed lamin A protein, named progerin or farnesylated prelamin A leads to defect DNA repair. In the Zmpste24(-/-) cells, recruitment of the repair factor p53-binding protein (53BP1) to DNA damage region is impaired and sensitive to DNA damaging agents is increased since DNA damage is increased (Liu et al., 2005). Taken together, these findings emphasize the importance of normal lamin A functions in DNA repair.

1.3.4. Cellular signaling

A number of studies demonstrated that lamins directly associate with signaling components for cellular differentiation and homeostasis (Andres and Gonzalez, 2009; Naetar and Foisner, 2009). These interactions affect the repression of transcription by recruiting transcription factors and activation of transcription by taking away from their promoters (Heessen and Fornerod, 2007). Binding of lamins A/C and LAP2α stabilize the tumor suppressor protein retinoblastoma (Rb) which is a master regulator of cell proliferation (Markiewicz et al., 2002; Nitta et al., 2006; Ozaki et al., 1994). Lamin A complex provides a scaffold for the phosphatase 2A to efficiently dephosphorylate Rb, which

is required for the cell cycle arrest (Van Berlo et al., 2005). Conversely, when ERK1/2 is combined with lamin A, the complex releases Rb and which followed its cyclin-dependent kinase-mediated phosphorylation, resulting in the cell proliferation (Naetar and Foisner, 2009; Rodriguez et al., 2010).

A-type lamins regulate AP-1 activity by recruiting c-Fos to the nuclear lamina in an ERK1/2-dependent manner, thereby inhibiting AP-1-dependent transcription (Gonzalez et al., 2008; Ivorra et al., 2006). Conversely, c-Fos is rapidly released from the nuclear envelope by the ERK1/2-dependent phosphorylation which activates via mitogenic stimulation, resulting in the AP-1 activation. (Andres and Gonzalez, 2009; Gonzalez et al., 2008). Thus A-type lamins affect the AP-1 activation, transcriptional activity, and enhanced proliferation by regulating c-Fos.

1.3.5. Transcription

Several lines of evidence support the direct interaction of A-type lamins to associated proteins mediate the transcriptional regulation (Dittmer and Misteli, 2011). These interactions might affect the transcriptional regulation by recruiting the transcriptional regulators in the nuclear

peripheral regions, altering the posttranslational modifications of them, and influencing the assembly of transcriptional complexes. Lamin A/C directly or indirectly associates with several transcriptional regulators including Rb, cFos, Srebp1, and Mok2 (Malhas et al., 2009). These functions are highlighted since the laminopathy-associated mutations appear to disrupt these processes.

1.4. Laminopathies

By the discovery of a variety of diseases associated with mutations in *LMNA*, the functional roles of nuclear lamins have been emphasized (Capell and Collins, 2006). Lamin associated diseases, which are referred to as 'laminopathies', have been discovered since 1999, resulting in the discovery of over 450 disease-related mutations to date (http://www.umd.be/LMNA/, (Bonne et al., 1999)). Most laminopathies include Emery Dreifuss muscular dystrophy (EDMD), dilated cardiomyopathy (DCM), Dunnigan-type familial partial lipodystrophy (FPLD), and Hutchinson-Gilford progeria syndrome (HPGS) which is a premature aging disorder (Schreiber and Kennedy, 2013; Worman and Bonne, 2007). These mutations might interfere to the nuclear stability, cause the defects of lamin assembly, or affect their biochemical properties which is important to interaction with lamin itself or lamin-associated proteins (Bank et al., 2012; Bollati et al., 2012; Burke and Stewart, 2002a; Krimm et al., 2002).

1.4.1. Emery Dreifuss muscular dystrophy (EDMD)

Emery-Dreifuss muscular dystrophy (EDMD) is one of muscular dystrophy. It was first designated and named by Alan Emery and Fritz

Dreifuss. Mutations in LMNA cause autosomal dominant EDMD, autosomal recessive EDMD, and sporadic cases of EDMD (Bonne et al., 1999; Manilal et al., 1998; Raffaele Di Barletta et al., 2000; Yates and Wehnert, 1999). Most missense mutations have been mapped in LMNA exons encoding the central rod domain of both lamin A and C (Bonne et al., 2000; Lin and Worman, 1993). The rod domain of lamins is considered essential for the formation of filament assembly. Therefore, misfolding of lamin proteins or failure to correctly filament assembly causes partial or complete loss of functions (Brown et al., 2001).

1.4.2. Dilated Cardiomyopathy (DCM) and Limb Girdle Muscular Dystrophy type 1B (LGMD1B)

DCM associated with LMNA mutations accounts for up to at least one-third of DCM families reported up to now, indicating ventricular dilation, impaired systole and conduction defects (Sylvius et al., 2005). Numerous types of *LMNA* mutations also attributed to limb girdle muscular dystrophy type 1B (LGMD1B) affects the skeletal and cardiac muscles (Muchir et al., 2000; Todorova et al., 2003). The major features of LGMD1B are the absence of early tendon contractures and progressive muscle weakness (Helbling-Leclerc et al., 2002). These phenotypes have

been preserved in a single-family. For example, the classic phenotypes of DCM1A, LGMD1B, and EDMD were exhibited in each of the three family members. These studies give an insight into the potential for genetic background and/or epigenetic and environmental factors to influence laminopathy phenotypes (Burke and Stewart, 2002a).

1.4.3. Dunnigan-type familial partial lipodystrophy (FPLD)

Laminopathies associated with Dunnigan-type familial partial lipodystrophy (FPLD) is inherited in an autosomal dominant manner (Worman and Bonne, 2007). The major features of FPLD are loss of white adipose tissue from limbs, gluteal, and truncal regions, insulin resistance, and diabetes mellitus. There are three substitutions on Arg482 residue (R482W, R482Q, and R482L) of lamin A/C which are responsible for FPLD (Cao and Hegele, 2000; Shackleton et al., 2000; Tu et al., 2016; Vigouroux and Capeau, 2005). LMNA mutations associated with FPLD are positioned on the surface of the Ig-like domain mutations, which cause Dunnigan-type familial partial lipodystrophy without change the structure, but inducing the modification of the binding site for biological target of lamin A/C (Krimm et al., 2002).

1.4.4. Hutchinson-Gilford progeria syndrome (HPGS)

Hutchinson-Gilford progeria syndrome (HGPS) is a premature aging syndrome caused by aberrant processing of post-translational modification of lamin A (Ghosh and Zhou, 2014; Scaffidi and Misteli, 2006). HGPS patients usually die in their teens and suffer from sarcopenia, lipodystrophy, diabetes, cataracts, and atherosclerosis. Most common mutations causing HGPS is a silent mutation (G608G) which generates abnormal splicing donor site within exon 11 of the *LMNA* gene (Eriksson et al., 2003). The result of the mis-splicing product 50 amino acid deleted abnormal lamin, referred to progerin (De Sandre-Giovannoli et al., 2003). The farnesylated C-terminal cysteine of progerin remains intact since the deleted 50 amino acids contain the cleavage sites catalyzed by Zmpste24 (Liu and Zhou, 2008; Maraldi et al., 2005; Qin et al., 2011). However, the retained farnesylation of progerin could not fully explain all features with HGPS.

1.5. Purpose of research

Nuclear lamins maintaining the nuclear envelope have been implicated in a wide range of nuclear functions, including DNA repair, chromatin regulation, cellular signaling, DNA replication, and transcription. Mutations in lamins interfere with the normal function of lamins in the nuclear stability which causes the defects of lamin assembly or affects their biochemical properties which are important to interaction with lamin itself or lamin-associated proteins. Despite the numerous studies on lamin, it still has been a lack of understanding of the assembly mechanism of lamin at the molecular level. A recent study presented that progerin caused by a silent mutation of the lamin A/C gene could be synthesized during the normal aging process, leading to the nuclear deformation. This finding indicates an emphasis on the importance of lamin function.

In this study, I tried to identify the structure of lamin to present the mechanism of how lamin became assembly, and to interpret the cause of laminopathies at a molecular level, which only stayed in the understanding of the phenomenon. Furthermore, I tried to discover drug or functional food candidates that inhibit the combination of progerin

and lamin produced during the normal aging process and interfered with normal lamin functions.

Chapter 2.

Structural basis for lamin assembly at the molecular level

Published in *Nature communications*

Ahn, J., Jo, I., Kang, S.M., Hong, S., Kim, S., Jeong, S., Kim, Y.H., Park, B.J., and Ha, N.C. (2019). Structural basis for lamin assembly at the molecular level. *Nat Commun 10*, 3757.

2.1. Introduction

Intermediate filament (IF) proteins form flexible fibrous structures that provide vital mechanical support in higher eukaryotic cells (Fuchs and Cleveland, 1998; Herrmann et al., 2007). All IF proteins have three domains: an unstructured N-terminal head, a central α-helical rod, and non-helical C-terminal tail domains (Guzenko et al., 2017; Herrmann et al., 2007; Herrmann and Strelkov, 2011). The central rod domain is further divided into three coiled-coil segments (coil 1a, 1b, and 2) and two flanking linkers (L1 and L12). The central rod domains have a high propensity to form coiled-coil dimers, which are further assembled into a 10-nm-thick filament in cells in several hierarchical steps in most IF proteins (Quinlan et al., 1986).

The nuclear envelope structures are the hallmark of all eukaryotic cells, and the intact structures are important for the proper functioning of the nucleus and the cells. Nuclear lamins are IF proteins that play an essential role in maintaining the nuclear envelope structure (Aaronson and Blobel, 1975; Burke and Stewart, 2013). They have been implicated in diverse cellular processes, including mitosis, chromatin organization, DNA replication, and transcription (Dechat et al., 2010; Lee et al., 2016; Mattout et al., 2006). Many lamin mutations have been found to be

closely related to various human diseases, including muscular dystrophy and Hutchinson Gilford progeria syndrome (Dittmer and Misteli, 2011; Liu and Zhou, 2008; Maraldi et al., 2005).

Compared to the canonical IF proteins, such as vimentin and keratin, the central rod domain of lamins has a longer coil 1b, and the non-helical C-terminal tail region contains an additional immunoglobulin (Ig)-like domain (Herrmann et al., 2007; Kapinos et al., 2010). The fundamental soluble unit of lamin is a dimer, which is different from the tetrameric vimentin (Kapinos et al., 2010; Strelkov et al., 2004). The lamin assembly is formed by longitudinal and lateral association based on the coiled-coil dimers (Chernyatina et al., 2015; Turgay et al., 2017). Initially, many researchers studied lamin using the refolded proteins, proposing an assembly model with 2-4 nm overlap between the dimers by emphasizing the head-to-tail interaction between the dimeric units of lamin (Kapinos et al., 2010). Several fragments structures, together with vimentin fragment structures, have been determined, and full-length models of vimentin in the tetrameric arrangement have been proposed by combining the fragment structures and binding mapping with the electron paramagnetic resonance spectroscopy (Aziz et al., 2012; Chernyatina et al., 2015). Recently, a

cryo-electron tomography (cryo-ET) study revealed that lamins form 3.5-nm-thick filaments (Turgay et al., 2017) that are remarkably different from other canonical 10-nm thick IF proteins and the proposed assembly model of lamin (Guzenko et al., 2017; Herrmann et al., 1999; Turgay et al., 2017; Wickert et al., 2005). The Ig-like domains of lamins were decorated at both sides of the filament with an interval of ~20 nm and various cross-sections (Turgay et al., 2017).

The lamin filaments make up the three-dimensional meshwork underlying the inner nuclear envelope (Aebi et al., 1986; Dechat et al., 2010; Goldman et al., 2002; Holaska et al., 2002). The intrinsic structural flexibility and self-aggregative properties of lamin have allowed the determination of only low-resolution electron microscopy (EM) structures and crystal structures of short fragments (Dhe-Paganon et al., 2002; Krimm et al., 2002; Strelkov et al., 2004). To date, their assembly mechanisms at the molecular level are poorly understood (Kapinos et al., 2011; Strelkov et al., 2001; Strelkov et al., 2004; Turgay et al., 2017). In this study, I determined the crystal structure of an N-terminal half fragment of the human lamin A/C, which was stably expressed and amenable to studies for the seamless full-length structures of lamin. This study provides a structural basis for how the lamin filament is assembled

with two interactions, giving insights into the assembly mechanisms of other IFs.

2.2. Materials and Methods

2.2.1. Plasmid construction

For overexpression of lamin proteins, amplified DNA fragments coding for residues 1-300 (wild-type and A146C mutant), 1-125, 175-300, 250-400 and 406-567 of lamin A/C were inserted into the pProEx-HTa vector (Thermo Fisher Scientific, MA, USA). The used oligonucleotide primer sequences were shown in Table 2.1. The resulting plasmids encoded the His-tag and the tobacco etch virus (TEV) protease cleavage site at the N-terminus of the lamin proteins. To prevent overlapping of the peptides from the lamin 300 and 250-400 fragments digested by chymotrypsin for mass spectrometry analysis, a 286-400 fragment was constructed. The arginine 388 residue was replaced with cysteine, which enabled crosslinking of a lysine residue in the lamin 300 fragment through the primary amine and sulfhydryl reactive spacer of sulfosuccinimidyl 4-(*N*-maleimidophenyl)butyrate (Sulfo-SMPB; Sigma Aldrich, USA). For immunofluorescence staining, amplified DNA fragments encoding wild type and the Y45C and L59R mutants of full-length lamin A/C were inserted into the pcDNA3.1(+) vector (Thermo Fisher Scientific, MA, USA).

Table 2.1. Oligonucleotide primer sequences of human lamin fragments

lamin fragments	forward primers (5'→3')	reverse primers (5'→3')
lamin 1-125	ggcgaattcatggagaccccgtcccag	ggcaagcttttaaccctccttcttggttatg
lamin 1-300	ggcgaattcatggagaccccgtcccag	ggcaagcttttagtcgatgcggatgcg
lamin 175-300	ggcgaattcatggccctaggtgaggcc	ggcaagcttttagtcgatgcggatgcg
lamin 250-400	ggcccatggcccagcatgaggac	ggcctcgagctagccacggctgcgctg
lamin 286-400	ggcgaattctgggggctgcccacgagg	ggcctcgagctagccacggctgcgctg
lamin 406-567	ggcgaattctcatcccagacacagggtg	gccaagcttttagtggtggtgatggagcag
lamin Y45C	cgcttggcggtctgcatcgaccgtgtg	cacacggtcgatgcagaccgccaagcg
lamin L59R	gagaacgcagggcggcgccttcgcatcaccgag	gatgcgaaggcgccgccctgcgttctccgtttc
lamin A146C	ctgaactccaaggagtgcgcactgagcactgc	gcagtgctcagtgcgcactccttggagttcag
lamin R388C	aggaggagaggctatgcctgtccccc	gggggacaggcatagcctctcctcct

2.2.2. Purification of the recombinant proteins

To obtain the selenomethionyl-labeled protein for crystallization, the *E. coli* strain B834 (DE3; Novagen, USA) harboring the plasmid encoding the lamin A/C fragment (residues 1-300) was cultured in M9 medium supplemented with L-(+)-selenomethionine. The protein expression was induced by 0.5 mM IPTG at 30°C. The cells were harvested by centrifugation and resuspended in lysis buffer containing 20 mM Tris-HCl (pH 8.0) and 150 mM NaCl. The cells were disrupted using sonication and the cell debris was removed using centrifugation. The supernatant was loaded onto Ni–NTA affinity agarose resin (Qiagen, The Netherlands), pre-incubated with lysis buffer. The target protein was eluted with lysis buffer supplemented with 250 mM imidazole. The eluate was treated with TEV protease to cleave the His-tag and then was loaded onto a HiTrap Q column (GE Healthcare, USA). A linear gradient of increasing NaCl concentration was applied to the HiTrap Q column. The fractions which contained the protein were applied onto a size-exclusion chromatography column (HiLoad Superdex 200 26/600 column; GE Healthcare), pre-equilibrated with lysis buffer. The purified protein containing lysis buffer was concentrated to 7 mg/mL and frozen at −70°C.

For biochemical assays, each plasmid encoding the lamin A/C fragments was transformed into *E. coli* BL21 (DE3; Novagen, USA) and cultured in LB or TB medium. The same procedure was used to purify the proteins. For the His-tagged proteins, the TEV protease treatment was not applied.

2.2.3. Crystallization and structure determination

The selenomethionine-labelled lamin protein (7 mg/mL) whose His-tag was cleaved off was crystallized in a precipitation solution containing 0.1 M Tris-HCl (pH 8.5), 0.9 M lithium chloride, and 7% (w/v) PEG 8000 using the hanging-drop vapor diffusion method at 14°C. Crystals with a size of ~ 300 μm were used for structure determination. The crystals were dipped in a cryoprotectant solution containing 3.75% (v/v) diethylene glycol, 3.75% (v/v) ethylene glycol, 3.75% (v/v) (+/-)-2-methyl-2,4-pentanediol, 3.75% (v/v) 1,2-propanediol, 3.75% (v/v) dimethyl sulfoxide, and 3.75 mM 3-(1-pyridino)-1-propane sulfonate and flash-frozen in a nitrogen stream at −173°C. A single-wavelength anomalous diffraction (SAD) dataset was collected at Pohang Accelerator Laboratory Beamline 5C using Pilatus 3 6M Detector (Henrich et al., 2009) and processed with the HKL2000 package

(Otwinowski and Minor, 1997; Rice et al., 2000). The crystals belong to space group $P2_12_12$ with unit-cell dimensions of a = 231.3 Å, b = 85.0 Å, and c = 92.4 Å. Heavy atom searching was performed using SHELXC/D of the CCP4i package (McCoy et al., 2007; Sheldrick, 2010). The lamin 300 fragment contained three Met residues in the sequence. However, two Se-Met were identified per protomer in the SAD date by SHELXD. Eight Se-Met sites were identified because the asymmetric unit contained 4 protomers. Phase calculation and density modification were performed using Phaser of the PHENIX (Afonine et al., 2010; Headd et al., 2012). The programs COOT and PHENIX were used for model building and refinement (Afonine et al., 2012; Emsley and Cowtan, 2004; Headd et al., 2012). The final structure was refined at a 3.2 Å resolution (R_{factor} and R_{free} of 20.7% and 26.1%, respectively; Table 2.2)(Brunger, 1992).

Table 2.2. X-ray diffraction and refinement statistics

Data collection	**Lamin 300 fragment (residues 1-300)**
Beamline	Pohang Accelerator Laboratory Beamline 5C
Wavelength (Å)	0.9795
Space group	$P2_12_12$
Cell dimensions	
a, *b*, *c* (Å)	231.3, 85.0, 92.3
α, *β*, *γ* (°)	90, 90, 90
Resolution (Å)	50-3.2 (3.26-3.21)
No. of reflections	40335
R_{merge}	0.11 (0.37)
R_{pim}	0.04 (0.21)
$I/\sigma I$	11.5 (3.11)
Completeness (%)	93.5 (80.8)
Redundancy	5.7 (3.4)
Refinement	
Resolution (Å)	46.2-3.20 (3.26-3.21)
No. reflections	40280
R_{work}/R_{free}	0.207/0.260
Total no. of atoms	7161
No. ligands	0
No. water molecules	0

Wilson B-factor (Å^2)	39.3
Average B-factor (Å^2)	46.0
R.M.S deviations	
Bond lengths (Å)	0.002
Bond angles (°)	0.453
Ramachandran plot	
Favoured (%)	99.09
Allowed (%)	0.93
Outliers (%)	0.0
PDB ID	6JLB

* Values in parentheses are for the highest resolution shell.

** $R_{merge} = \Sigma_{hkl}\Sigma_i|I_i(hkl) - [I(hkl)]|/\Sigma_{hkl}\Sigma_i I_i(hkl)$, where $I_i(hkl)$ is the intensity of the *i*th observation of reflection *hkl* and [I(*hkl*)] is the average intensity of *i* observations.
*** $R_{p.i.m.} = \Sigma_{hkl}\ (1/(n-1))^{1/2}\ \Sigma_i|I_i(hkl) - [I(hkl)]|/\Sigma_{hkl}\Sigma_i I_i(hkl)$. R_{pim} is the precision-indicating (multiplicity-weighted) R_{merge}.
****R_{free} calculated for a random set of 7.8% of reflections not used in the refinement.

2.2.4. SEC-MALS

Molecular mass was determined with analytical size exclusion chromatography coupled with multi-angle light scattering (SEC-MALS). The protein samples (wild type and A146C mutant of the lamin 300 fragment; 2.5mg/ml) were applied to a Superdex 200 Increase 5/150 GL column (GE healthcare), pre-equilibrated with a buffer containing 20 mM Tris-HCl (pH 8.0), 150 mM NaCl, 2 mM tris (2-carboxyethyl) phosphine (TCEP) or a non-reducing buffer containing Tris-HCl (pH 8.0) and 150 mM NaCl. The mass-averaged molecular weights were calculated using Debye analysis with ASTRA 6 software (WYATT, USA).

2.2.5. Pull-down assays

For Figure. 2.11, a pull-down assay was conducted by using immobilized lamin 300 A146C mutant protein. The lamin 300 A146C mutant protein was coupled to CNBr-activated Sepharose resin (GE Healthcare) and/or blocked with excessive 0.1 M Tris-HCl (pH 8.0) buffer containing 150 mM NaCl. Four purified lamin fragments (residues 1-125, 175-300, 250-400, and 406-567; 66 μM) were incubated with the lamin-coupled resin or Tris-blocked resin (for control), which were pre-equilibrated with a

20 mM Tris-HCl (pH 8.0) buffer containing 150 mM NaCl. After washing with the buffer, the resin was analysed using SDS-PAGE.

For Figure. 2.11c, His-tagged lamin proteins were immobilized on the Ni-NTA resin as bait. BSA or His-tag cleaved lamin proteins as prey were incubated on the His-lamin immobilized resin pre-equilibrated in a 20 mM Tris-HCl (pH 8.0) buffer containing 150 mM NaCl (or 50 mM NaCl) at room temperature for 30 min. After washing with the buffer supplemented with 20 mM imidazole, the resin was analysed using SDS-PAGE.

2.2.6. Cross-linking reaction and MS/MS analysis

Purified lamin 286-400 R388C protein was incubated with 2 mM DTT and changed to a 20 mM HEPES (pH 7.5) buffer containing 50 mM NaCl, and 1 mM EDTA using a HiPrep 26/10 desalting column (GE Healthcare). Sulfo-SMPB (100 mM stock solution) was added in 0, 2.5, 25, 125, and 250 μM to a mixture containing 20 μM lamin 300 and coil 2 (286-400) R388C proteins for 1 h, and the reactions were stopped by a solution containing 40 mM Tris-HCl pH 7.5 and 40 mM L-cysteine. The reaction mixture was subjected to SDS-PAGE, and the protein bands of coil 2 R388C (14 kDa), lamin 300 (38 kDa), and their cross-

linked structure (52 kDa) were further analysed by the MS/MS spectrometry.

The corresponding protein bands were excised from the SDS-polyacrylamide gel and were digested in-gel by chymotrypsin (Promega, USA) with a low specificity towards the C-termini of tyrosine, phenylalanine, tryptophan, and leucine according to the manufacturer's manual. The digested peptides were extracted from the gel slices, as previously described[48], and analysed on a nLC-Velos Pro mass instrument equipped with a PicoFrit^{TM} column, 100 mm, packed with 5 μm Biobasic® C18 and an EASY-Column^{TM}, 2 cm, packed with 5 μm C18 (Thermo Fisher Scientific). The LC condition operated at 0.3 μL min^{-1} was a 45-min linear gradient from 5% to 40% ACN in a 0.1% formic acid buffer solution, followed by a 10 min column wash with 80% ACN and a 20 min re-equilibration to the initial buffer condition. The full mass (MS1) scan was performed in a range of *m/z* 300 – 2000 in a positive ion mode. Data-dependent MS2 scans of the 7 most intense ions were performed from the full scan with scan options of 1.5 *m/z* isolation width, 25% normalized collision energy, and 30 s dynamic exclusion duration. The acquisitioned MS2 data were primarily analysed by a SEQUEST search with a maximum miscleavage of 2, precursor mass

tolerance 1.5 Da, fragment mass tolerance 1.0 Da, dynamic modification of lysine either blocked with a cysteine-conjugate cross-linker (Cys~K, +*m/z* 362.4) or cross-linked with a Cys388-Leu389 dipeptide (CL~K, +*m/z* 475.5) of the coil 2 R388C fragment, and static modification of the Cys388 residue blocked with a Tris-conjugate cross-linker (Tris~C, *m/z* 362.4) in the coil 2 fragment band (14 kDa). After filtering out the peptide-to-spectrum matches (PSM) with a peptide probability above 90%, the tandem mass spectra of the cross-linked peptides were manually assigned to the fragment ions generated from the collision-induced dissociation of the precursor ion. The manually assigned tandem mass spectra of Tris-crosslinker conjugate Cys388-Leu389 dipeptide and target Lys171 cross-linked with the Cys388-Leu389 dipeptide are shown with extracted ion chromatograms in Figures 2.1 and 2.2.

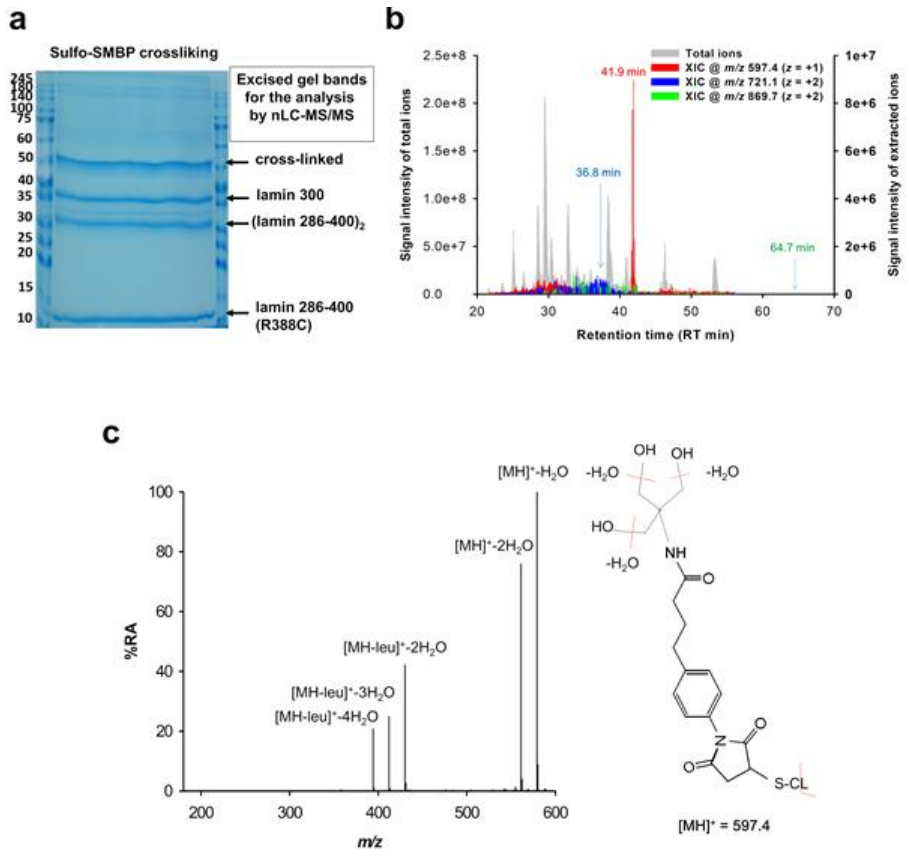

Figure 2.1. Extracted ion chromatogram (XIC) and a tandem mass spectrum of Tris-blocked cross-linker bound to Cys388-Leu389 dipeptide in the coil 2 (286-400) R388C mutant protein

(a) Excised gel bands for the analysis by nLC-MS/MS. Protein bands of the lamin 300 fragment and the cross-linked sample are labelled. To block the unreacted chemical cross-linker, excess cysteine was added. The major bands of 'cross-linked' (52 kDa), lamin 300 (38 kDa), (lamin

286-400 R388C)$_2$ (30 kDa), and lamin 286-400 R388C (14 kDa) were excised and subjected to the subsequent MS/MS analysis.

(b) Total ion (left y-axis) and extracted ion (right y-axis) chromatogram signals of Tris-blocked cross-linker bound to the asterisked cysteine sites of C*L (*m/z* = 597.4, z = +1), EGEEERLC*L (*m/z* = 721.1, z = +2), and C*LSPSPTSQRSRG (*m/z* = 869.7, *z* = +2) from in-gel chymotrypsin digestion of a coil 2 (286-400) R388C mutant protein, as described in the Materials and methods in the main text and Table 2.3.

(c) Tandem mass spectrum and proposed structure of a CL dipeptide bound to a Tris-blocked cross-linker. * MS/MS analysis was performed by Yong-Hak Kim's lab.

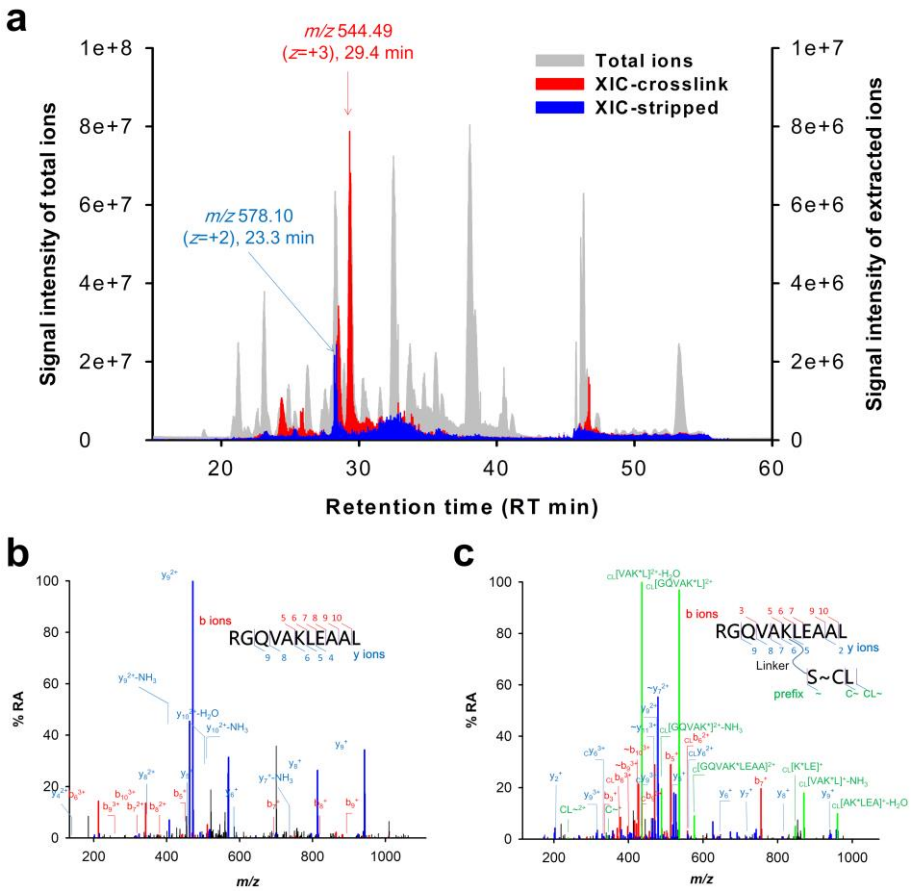

Figure 2.2. The most probable target peptide in the lamin 300 fragment, ^{166}RGOVAK*LEAAL^{176}, with or without modification of the asterisked Lsy171 position by a chemical cross-linker bound to a CL-dipeptide in the coil 2 (286-400) R388C mutant protein

(a) Total ion (left y-axis) and extracted ion (right y-axis) chromatogram signals of the unmodified Lys171-containing peptide ion (stripped *m/z* = 578.1, *z* = +2) at the RT of 23.2 min and the CL-crosslinked Lys171-containing peptide ion (*m/z* 544.49, *z* = +3) at the RT of 29.4 min.

(b) An electrospray ionization-tandem mass spectrum of an unmodified Lys171-containing peptide.

(c) An electrospray ionization-tandem mass spectrum of a Lys171-containing peptide crosslinked with a CL dipeptide in the coil 2 286-400 R388C mutant protein. * MS/MS analysis was performed by Yong-Hak Kim’s lab.

2.2.7. Isothermal Titration Calorimetry

Isothermal titration calorimetry (ITC) experiments were carried out using an Auto-iTC200 Microcalorimeter (GE healthcare) at Korea Basic Science Institute (Ochang, Korea). His-tagged wild type or L59R mutant of lamin 300 fragment (20 μM; 0.7 mg/ml) was prepared in the sample cell (370 μL) and his-tagged 250-400 fragment (160 μM; 3 mg/ml) was loaded into the injectable syringe. All samples were prepared in PBS. Titration measurements of 19 injections (2 μL) with 150 sec spacing were performed at 25°C while the syringe was stirred at 750 rpm. The data were analyzed using the MicroCal Origin^{TM} software.

2.2.8. Immunofluorescence staining

A human fibrosarcoma cell line (HT1080) and human neuroblastoma cell line (SH-SY-5Y) obtained from ATCC were maintained in liquid medium (DMEM) containing 10% (v/v) FBS, 1% (v/v) antibiotics at 37°C. HT1080 or SH-SY-5Y cells were seeded on a cover glass and transfected with the plasmid coding wild type, Y45C or L59R mutant of full-length lamin A/C using jetPEI (Polyplus Transfection). After fixing with 1% (w/v) paraformaldehyde (PFA) for 1 h at 4°C, cells were permeabilized with 0.1% (v/v) Triton X-100 including 2.5 U/ml

benzonase (Calbiochem; 71206-3) or mock for 5 min and incubated with a blocking buffer containing PBS and anti-human antibodies (1:400) for 1 h. After washing with PBS twice, the cells were incubated with anti-lamin A/C (sc-376248; Santa Cruz Biotechnology) and anti-emerin (sc-15378; Santa Cruz Biotechnology) primary antibodies (1:200) in the blocking buffer overnight, followed by secondary antibodies (anti-mouse Ab-FITC and anti-rabbit Ab-rhodamine; 1:400) in the blocking buffer for 7 h and mounted. The nucleus was stained with DAPI. The immunofluorescence signal was detected using fluorescence microscopy (Logos).

2.3. Results

2.3.1. Structural determination of the lamin fragment

I determined the crystal structure of an N-terminal half fragment of human lamin A/C (residues 1-300; referred to as 'lamin 300 fragment' in this study) at a resolution of 3.2 Å. This spans the N-terminal head, coil 1a, L1, coil 1b, L12, and the first half of coil 2 (Figure. 2.3a and Table 2.1). The asymmetric unit consists of four protomers (chains A-D), which are bundled by an anti-parallel pair of parallel helical dimers (chain A:B and C:D). The four helical bundle structure showed the α-helical conformations in an ~38-nm-long structure (Figure. 2.3b).

The analyses of the two helical dimers using the program TWISTER (Figure. 2.5a) (Strelkov and Burkhard, 2002) showed two different superhelical structures with regular α-helical regions. A typical left-handed coiled-coil conformation was found in most of the coil 1a and the N-terminal four-fifths of coil 1b (Figure. 2.5a), in which hydrophobic residues were regularly found at the heptad positions a and d (Figures. 2.4a and 2.5b; highlighted in yellow). Remarkably, significant bending was found in the regions near L1, probably caused by the crystal packing interactions (Figure. 2.4b *left*). The junction

between coil 1a and L1 (residues 65-69) showed a short α-helical segment without an inter-helical hydrophobic interaction (Figure. 2.4). Linker L1 and an adjacent coil 1b segment (residues 70-84) showed the hendecad pattern (Gruber and Lupas, 2003; Lupas and Bassler, 2017), which induces the formation of an untwisted helical section (Figures. 2.4 and 2.5). The hendecad pattern is composed of 11 amino-acid repeats, where the residues at the a, d, and h positions are involved in the inter-helical hydrophobic interactions (Figures. 2.4a and 2.5b; highlighted in magenta).

In the helical dimers, coil 1b consists of the 18 N-terminal heptad repeats (residues 79-204) forming a left-handed coiled-coil structure (~22 nm; one and a half super-helical turn) and the two C-terminal hendecad repeats (residues 204-222) forming an untwisted helical section (Figures. 2.4 and 2.5). The hendecad repeat region in coil 1b is continuous to the N-terminal half of L12 (residues 223-230; Figures. 2.4a and 2.5b), unlike previous predictions proposing a flexible hinge conformation (Chernyatina et al., 2015; Strelkov et al., 2004). The untwisted helical section is bent asymmetrically near the junction between L12 and coil 2 (Figures. 2.4 and 2.5b), leading to mismatched inter-helical hydrophobic interactions (Figure. 2.6a). Interestingly, the

C-terminal end of the lamin 300 fragment interacts with the symmetry-related molecules through hydrophobic interactions, as observed in the coil 2 structure of vimentin (Nicolet et al., 2010) (Figure. 2.6).

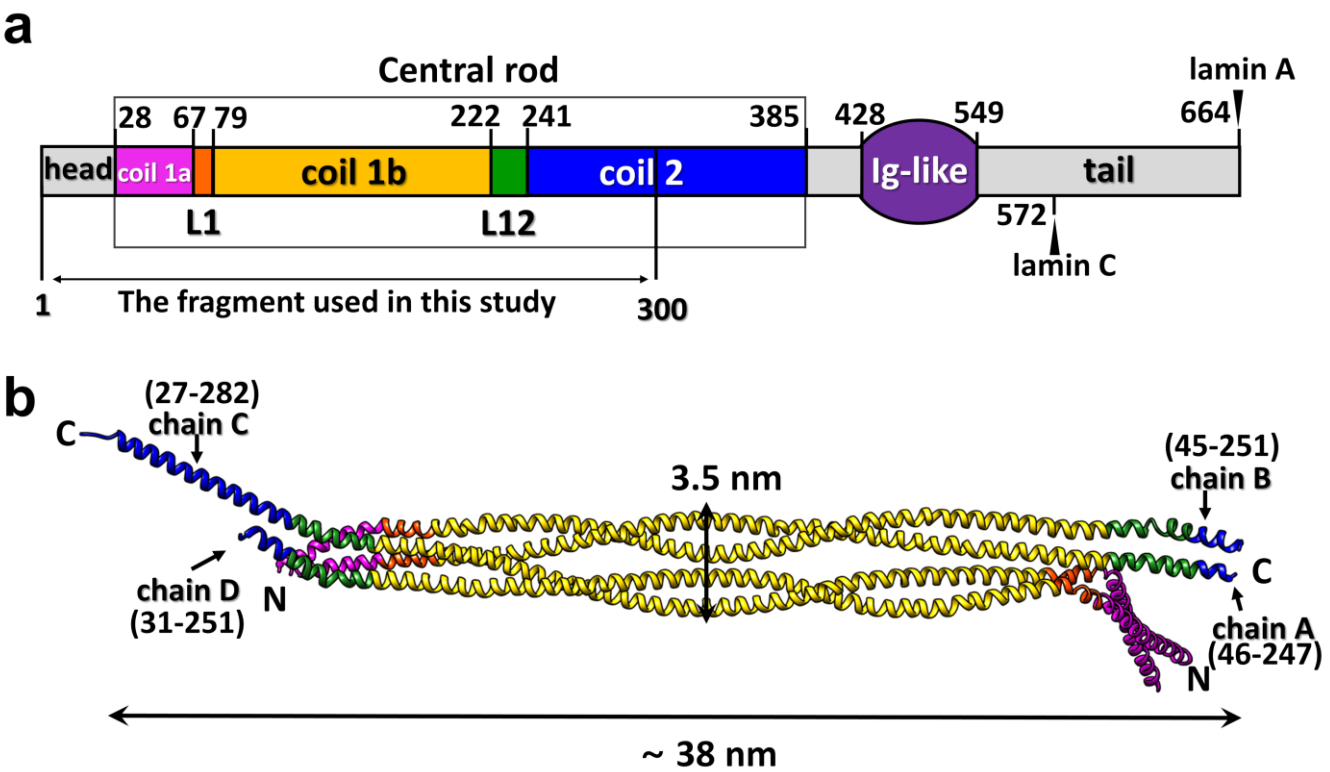
a
Central rod
lamin A
28
67
79
222
241
385
428
549
664
head
coil 1a
coil 1b
coil 2
Ig-like
tail
L1
L12
572
lamin C
1
The fragment used in this study
300
b
(27-282)
chain C
C
3.5 nm
(45-251)
chain B
C
chain D
(31-251)
N
chain A
(46-247)
N
~ 38 nm

Figure 2.3. Structure of the asymmetric unit of the human lamin A/C fragment

(a) Structural organization of human lamin A/C, consisting of the head, central rod, Ig-like, and C-terminal tail domains. The central rod domain is divided into subdomains (coil 1a, L1, coil 1b, L12, and coil 2). The start and end residues of coils 1a, 1b, and 2 are labeled with different C-termini in lamin A and lamin C. See also Table 2.2.

(b) The asymmetric unit in the crystal of an N-terminal fragment (residues 1 - 300) of lamin A/C consists of four chains: A, B, C, and D. The ordered region in the crystal structure is indicated. Each subdomain is coloured according to the colour code in (**a**).

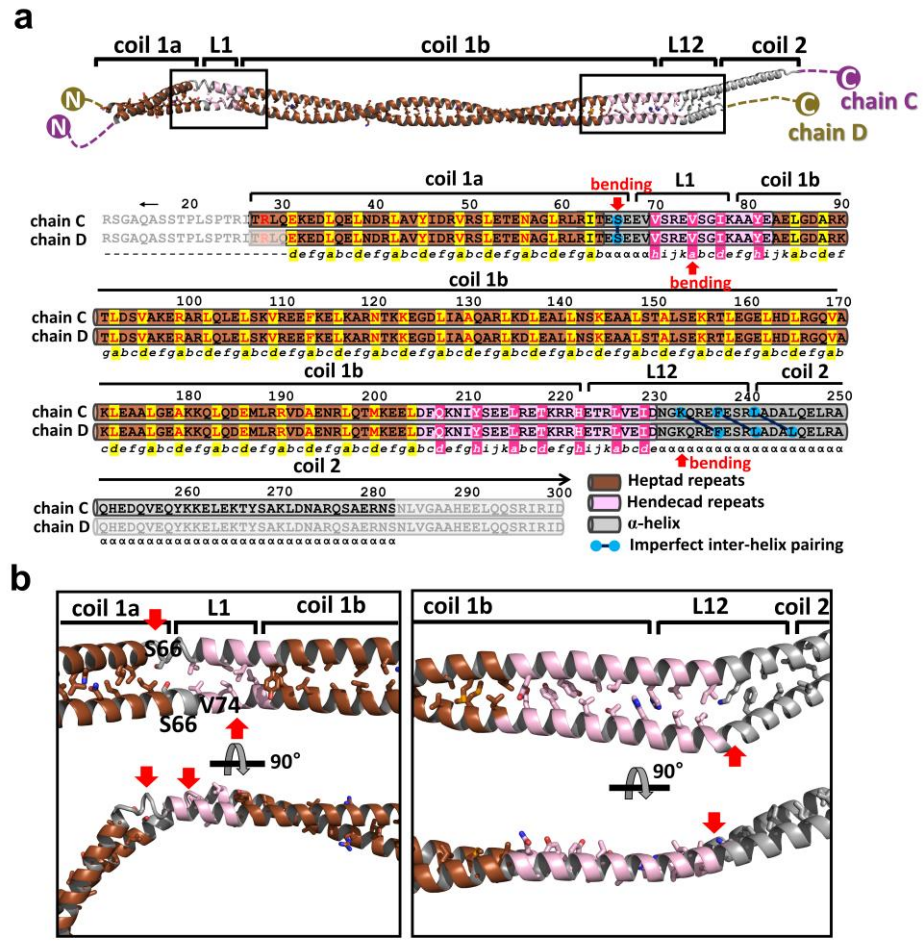

Figure 2.4. Structural-based superhelicity and sequence periodicity of the lamin C:D dimer

(a) Structure-based analysis of the sequence periodicity of the heptad (shaded in brown or yellow) or hendecad (shaded in pink or magenta) repeats. The phases of the heptad (abcdefg) and hendecad (abcdefghijk)

repeats are described below the sequences. The hydrophobic residues (a, d, and h) involved in the inter-helical interaction are highlighted by shadowing. If no inter-helical interaction occurs, α is used instead. Bends in the α-helices are indicated by red arrows. The mismatched interaction between two α-helices is highlighted with linked blue circles. The disordered regions are masked with semi-transparent boxes. The analyses of the A:B dimer are provided in Figure 2.5b.

(b) Inter-helical hydrophobic interactions of the linkers L1 and L12 proximal regions in the C:D dimer. Heptad repeat periodicity exhibiting the left-handed coiled-coil structure is coloured brown, whereas the hendecad repeat periodicity in the untwisted α-helical dimer is coloured pink. Grey α-helices indicate an unmatched hydrophobic interaction between two α-helices in the dimer. Hydrophobic residues associated with inter-helical interactions in the L1 and L12 proximal regions are shown in stick representations in the orthogonal views. The bending in the α-helices is indicated by red arrows.

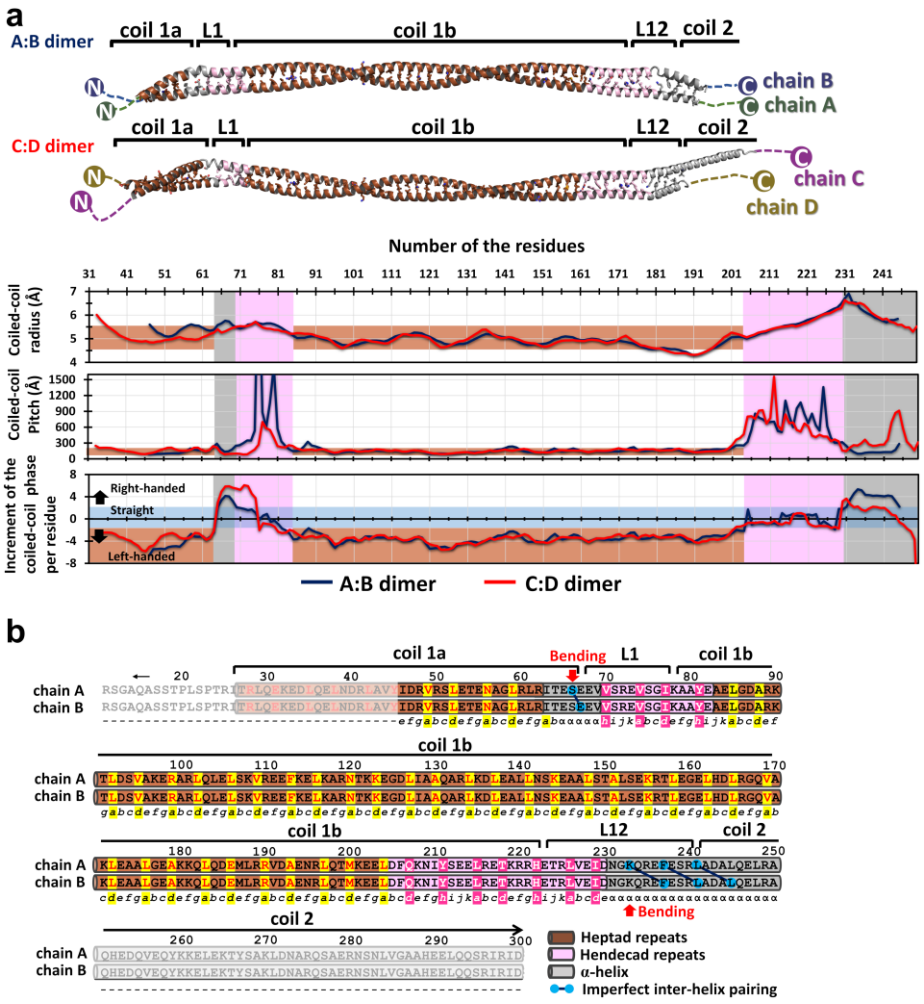

Figure 2.5. Structural and geometrical analyses of the A:B and C:D helical dimers

(a) Structure and geometry of coiled-coil were analysed using the program TWISTER (Strelkov and Burkhard, 2002). The heptad repeat periodicity is in brown, with the coiled-coil (CC) pitch ranging from 100-200 Å. The hendecad repeat periodicity is shown in pink with more than

300 Å of the CC pitch. Regions lacking regular inter-helical interaction are shown in grey. Graphs representing the CC radius, CC pitch, and the increment of the coiled phase per residue are displayed.

(b) Structure-based superhelicity and sequence periodicity of the A:B dimer in the lamin A/C fragment (residues 1-300). The colour schemes are shown as in Figure. 2.3a. Structure-based analysis of the sequence periodicity of the heptad (shaded in brown or yellow) or hendecad (shaded in pink or magenta) repeats. The phases of the heptad (abcdefg) and hendecad (abcdefghijk) repeats are described below the sequences. The hydrophobic residues (a, d, and h) are highlighted by shadowing. α indicates an α-helix that does not follow the heptad nor the hendecad rules. The bends in the α-helices are indicated by red arrows. The mismatched interaction between two α-helices is highlighted with linked blue circles. The disordered regions are masked with semi-transparent boxes.

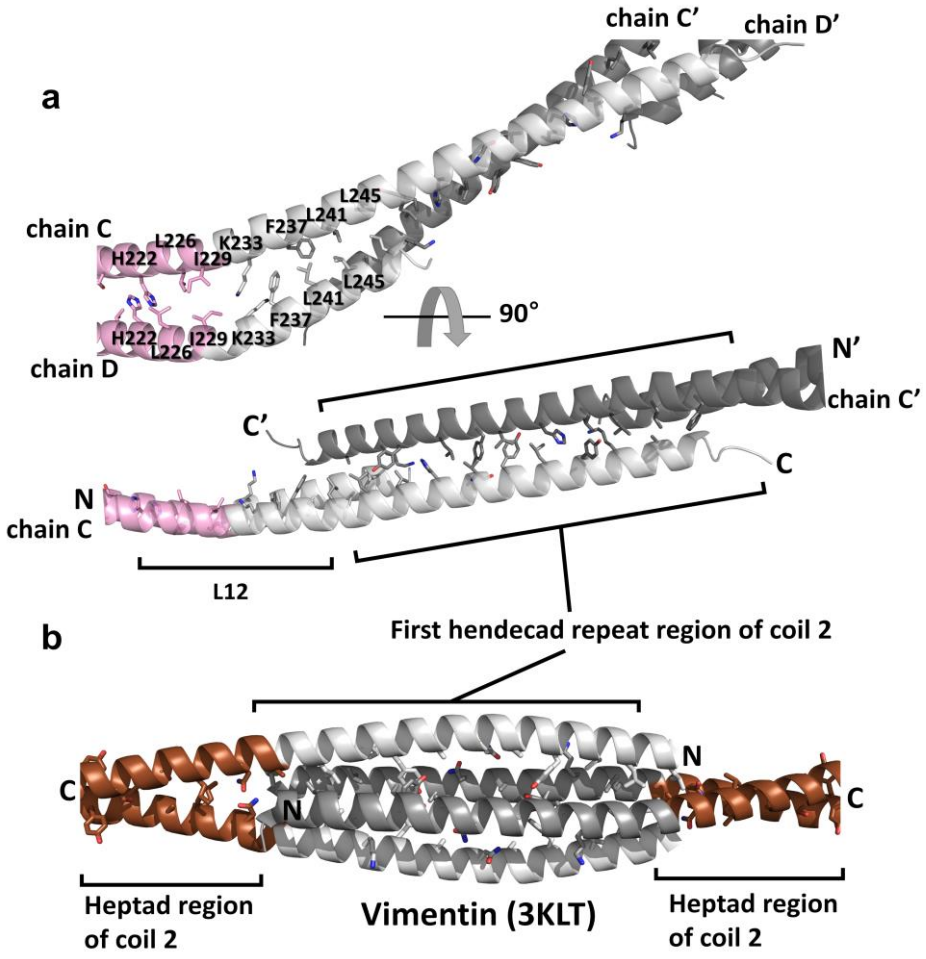

Figure 2.6. Anti-parallel α-helical interactions of lamin and vimentin found in their crystal structures

(a) The orthogonal view of the coil 2 region in the C:D dimer of the lamin 300 structure in the crystal. Chains C and D (pink or grey) and their symmetry-related chains C' and D' (dark grey) are displayed in ribbon representations with inter-helical hydrophobic residues (stick

representations). The first hendecad repeat region (residues 241-277) of coil 2 is involved in the packing interactions.

(b) The coil 2 region of the vimentin fragment (PDB code: 3KLT(Nicolet et al., 2010)) in the crystal. Similar to that of lamin A/C, the first hendecad repeat region (residues 265-301, corresponding to residues 241-277 in lamin A/C) of coil 2 is involved in the packing interactions.

2.3.2. Antiparallel interaction between two coiled coils

The tetrameric arrangement in the asymmetric unit is noteworthy. Coil 1b and its flanking linker segments (residues 67-221) form the anti-parallel contacts between coiled-coil dimers, and the remaining parts (coil 1a and coil 2) are bifurcated from both sides of the contacting region (Figure. 2.7a). The anti-parallel contact region is subdivided into a central compartment and two side compartments, and each compartment is composed of a pair of half super-helical turns of two α-helical dimers (Figure. 2.7a). The two side compartments with the internal pseudo-2-fold symmetry exhibit cross-sectional variation. At the central compartment, the four α-helices form two dimers arranged in juxtaposition (Figures. 2.7a; c, 2.7b; c). The cross-section in the middle region is ~ 3.5 nm in width, which is similar to the thickness of the lamin filament model determined by cryo-ET (Turgay et al., 2017) (Figure. 2.3b).

Structural comparison of the anti-parallel contact region of lamin to the vimentin coil 1b structure depicting the A11 interaction revealed a striking structural similarity between the side compartments of lamin and the vimentin coil 1b (Figure. 2.7a). I further noticed that the insertion sequence of coil 1b of lamin on the sequence alignment to vimentin

represents the central compartment of the anti-parallel contact region (Figure. 2.8). Each side compartment has two hydrophobic patches for the anti-parallel inter-dimer interaction (Figures. 2.7b; a, b, d, and e). The inter-dimer interactions were not mediated by residues at the a, d, and h positions in the hendecad repeat regions, and neither was in vimentin (Figures. 2.8 and 2.9). In contrast, only slight contacts were found in the central compartment (Figure. 2.7b; c). At the junctions between the central and side compartments, each dimer is twisted by 90°, resulting in a parallel arrangement without direct contacts (Figure. 2.7a). From these observations, I concluded that the anti-parallel interaction between the two coiled-coil dimers in the asymmetric unit of lamin corresponds to the ‘A11 interaction’ of vimentin (Aziz et al., 2009; Aziz et al., 2012; Chernyatina et al., 2012; Steinert et al., 1993) (Figures. 2.7a and 2.9). Thus, the anti-parallel contact between the two dimers of lamin was referred to an ‘A11 interaction’ in this study.

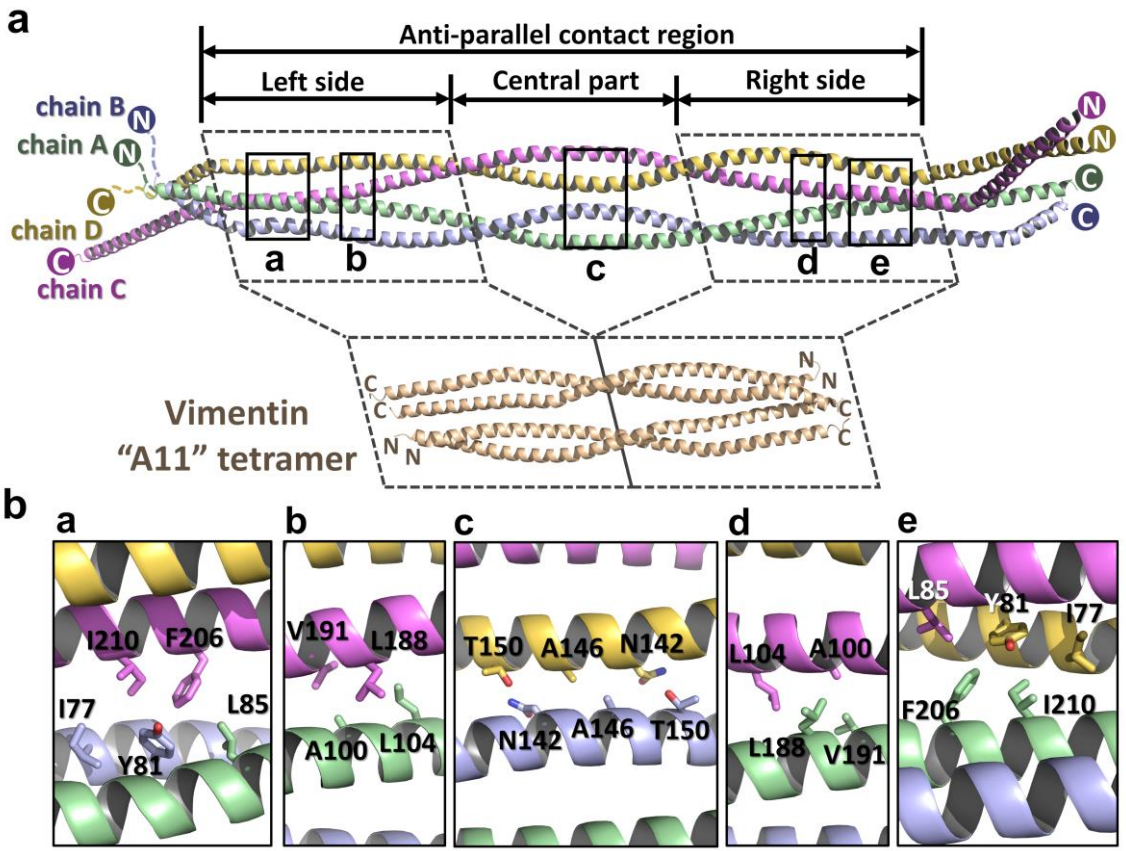
a
Anti-parallel contact region
Left side
Central part
Right side
chain B
chain A
chain D
chain C
a
b
c
d
e
Vimentin
"A11" tetramer
b
a
I210
F206
I77
L85
Y81
b
V191
L188
A100
L104
c
T150
A146
N142
N142
A146
T150
d
L104
A100
L188
V191
e
L85
Y81
I77
F206
I210

Figure 2.7. A11 interaction of the lamin 300 fragment

(a) Structural comparison of the tetrameric structures of the lamin 300 fragment (this study, residues 75-213) and vimentin coil 1b (PDB code: 3UF118, residues 144-251). Top panel, the anti-parallel contact region and its three compartments (left side, central part, and right side) of the lamin 300 fragment are indicated by double-headed arrows. Four chains (chain A-D) are in green, blue, violet, and yellow, respectively. Left and right-side parts of the lamin 300 fragment and vimentin are marked as dotted boxes. The N and C terminus of each chain are indicated by N and C, respectively. The contact interfaces between chain A:B and C:D are marked as black boxes labeled with a, b, c, d, and e, which are enlarged in b.

(b) Residues involved in hydrophobic or molecular contacts are shown in the stick representations. See also Figure. 2.9 for interfaces of the vimentin.

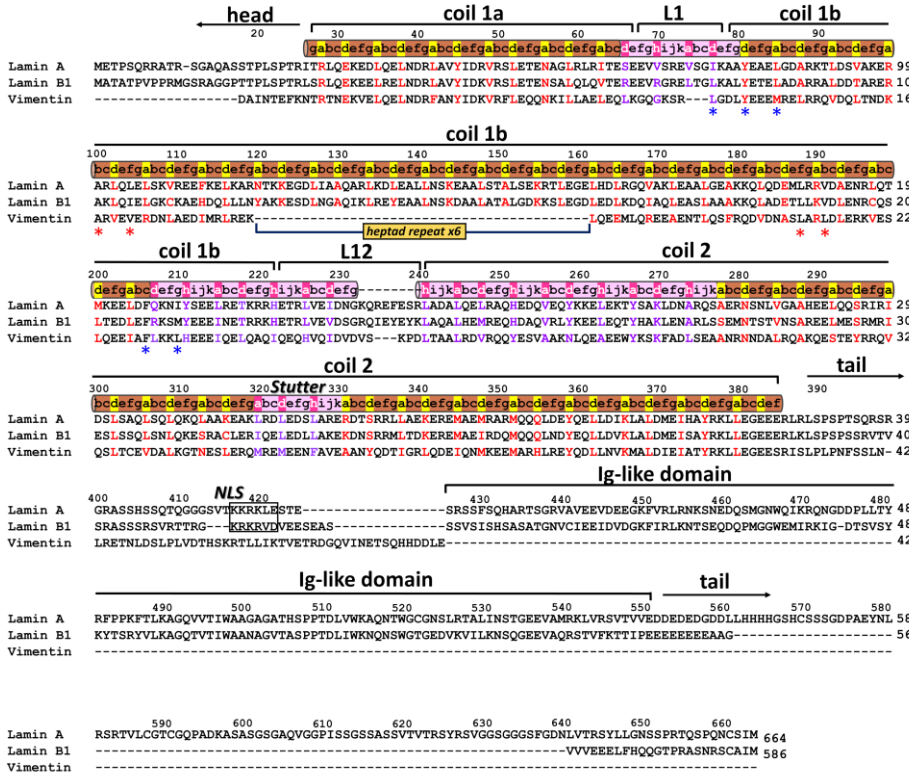

Figure 2.8. Sequence comparison of lamin A, lamin B1, and vimentin

The domains and subdomains are indicated. The phases in the heptad (brown) or hendecad (pink) repeat, which was previously predicted 3, 4, are displayed above the sequences. Gaps in vimentin coil 1b were generated based on the structural comparison. Note that the nuclear localization signal (NLS) and Ig-like domains are found only in lamins. The conserved residues associated with the tetramer interaction between lamin and vimentin are marked with asterisks.

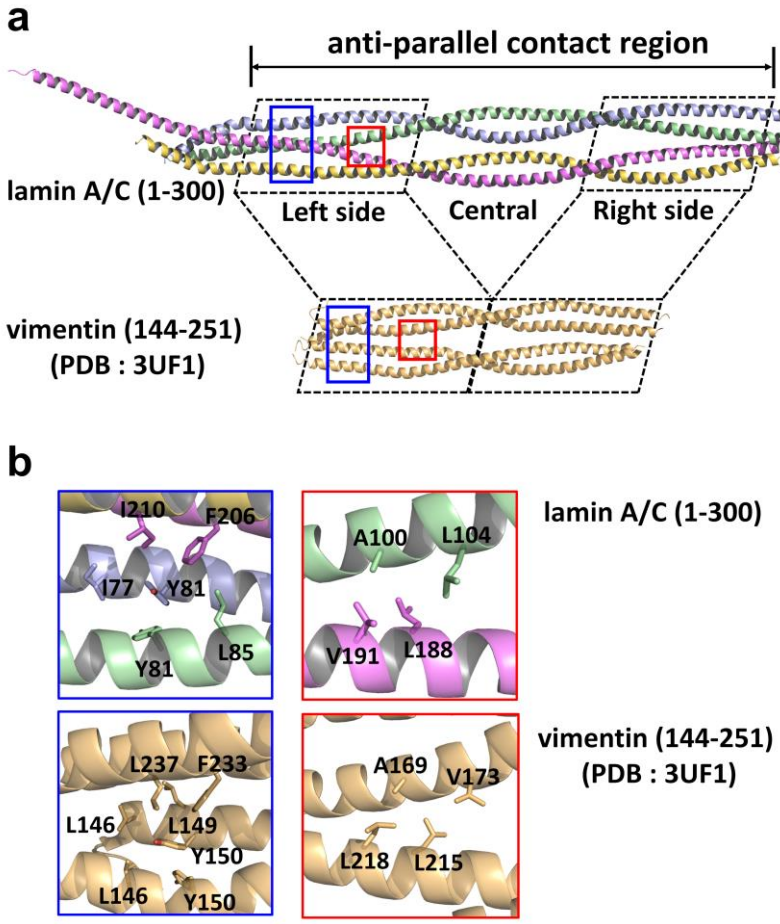

Figure 2.9. Structural comparison of the anti-parallel contact regions of the lamin 300 fragment (this study, residues 75-213) and vimentin coil 1b (PDB code: 3UF1(Aziz et al., 2012), residues 144-251)

(a) Left and right-side parts of the vimentin structure (*bottom*) are directly joined to the corresponding regions in the lamin 300 fragment (*top*).

(b) Interface regions forming the tetramer (boxed regions in A) are enlarged (*top* for lamin, *bottom* for vimentin).

2.3.3. The lamin A11 interaction for the lamin assembly process

It is known that lamin proteins exist in the dimeric form in solution before forming the filament (Goldman et al., 2002; Strelkov et al., 2004). To probe the A11 interaction of lamin during the filament formation, I noted Ala146 at the center of the anti-parallel coiled-coil dimers, which would be close enough to make a disulfide bond if it is changed to cysteine (Figure. 2.7b; c). It was first observed that the A146C variant protein of the lamin 300 fragment formed a disulfide bond in SDS-PAGE, suggesting that the tetrameric arrangement is formed in solution (Figures. 2.10c and d).

Next, the molecular masses of the wild type and A146C variant of the lamin 300 fragment were compared by using size exclusion chromatography-multiangle light scattering (SEC-MALS). The A146C variant protein partially formed a larger complex indicating a tetramer, while the wild-type fragment mostly remained as a dimer. Moreover, the larger tetrameric complex was shifted into the dimeric size in the presence of a reducing agent (Figure. 2.10d). These results indicate that Ala146 makes a close contact between two dimers during the assembly process, as predicted from the crystal structure, and further suggests that

the tetrameric lamin formed by the A11 interaction represents a snapshot of the assembly processing.

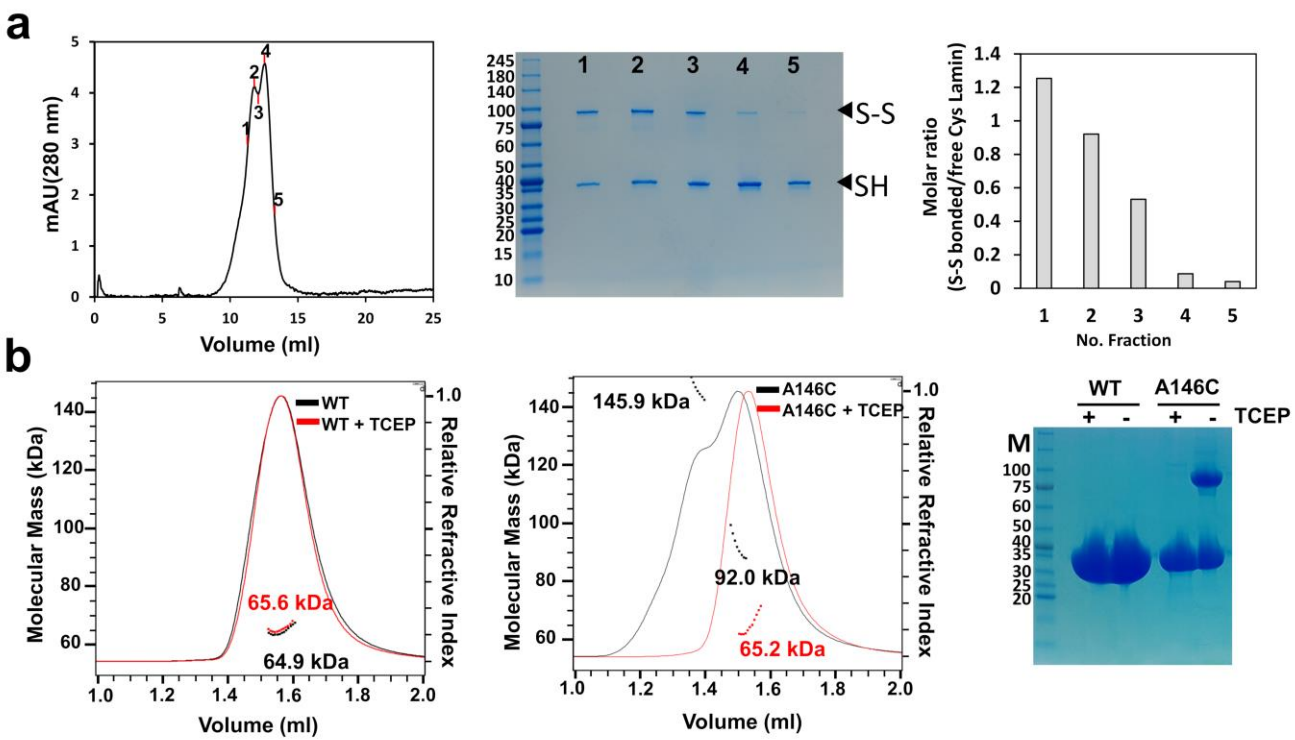

Figure 2.10. The oligomeric state of A146C mutant

(a) SEC profile of the lamin 300 fragment A146C mutant and a molar ratio of disulfide-bonded proteins in each peak

on Superdex 200 10/300 column. Five labeled fractions (*left*) were analysed using non-reducing SDS-PAGE (*middle*), and the relative portion of disulfide-bonded protein (tetramer) to free Cys protein (dimer) was calculated based on the band intensity using ImageJ (*right*).

(b) SEC-MALS analysis of lamin 300 fragment (2.5 mg/ml, wild type; left and A146C mutant; *middle*) in the absence (black line) or presence of a reducing agent TCEP (red line). The relative refractive index (right y-axis) and molecular weight of each peak (left y-axis) are plotted against the elution volume. The protein samples were also analysed using SDS-PAGE in the presence or absence of the reducing agent TCEP (*right*). Molecular sizes (kDa) of the marker proteins (M) are labeled on the left. Note that MALS might not give accurate values when two peaks were not resolved. Considering the SDS-PAGE analysis of the fractions (in **c**), the two peaks (*middle*) correspond to the tetramer and dimer, respectively.

2.3.4. Enhanced binding of coil 2 by the A11 interaction

I attempted to find the binding partners of the lamin 300 fragment with four candidate fragments, as shown in Figure. 2.11a. A binding assay was performed by using the A146C variant of the lamin 300 fragment that makes more stable A11 interactions than the wild type lamin 300 fragment. Only the F3 fragment (residues 250-400) was bound to the A146C variant of the lamin 300 fragment (Figure. 2.11b). The F3 fragment is roughly matched to coil 2 (residues 240 – 385) without the N-terminal 10 residues. The binding of the coil 2 fragment was weakened when the disulfide bond was reduced in the A146C variant of the lamin 300 fragment, and the wild-type of the lamin 300 fragment also bound to the coil 2 fragment with a weaker affinity than the A146C variant of the lamin 300 fragment (Figure. 2.11c). These results showed that coil 2 is bound to the lamin 300 fragment, and the binding affinity is increased by the A11 interaction.

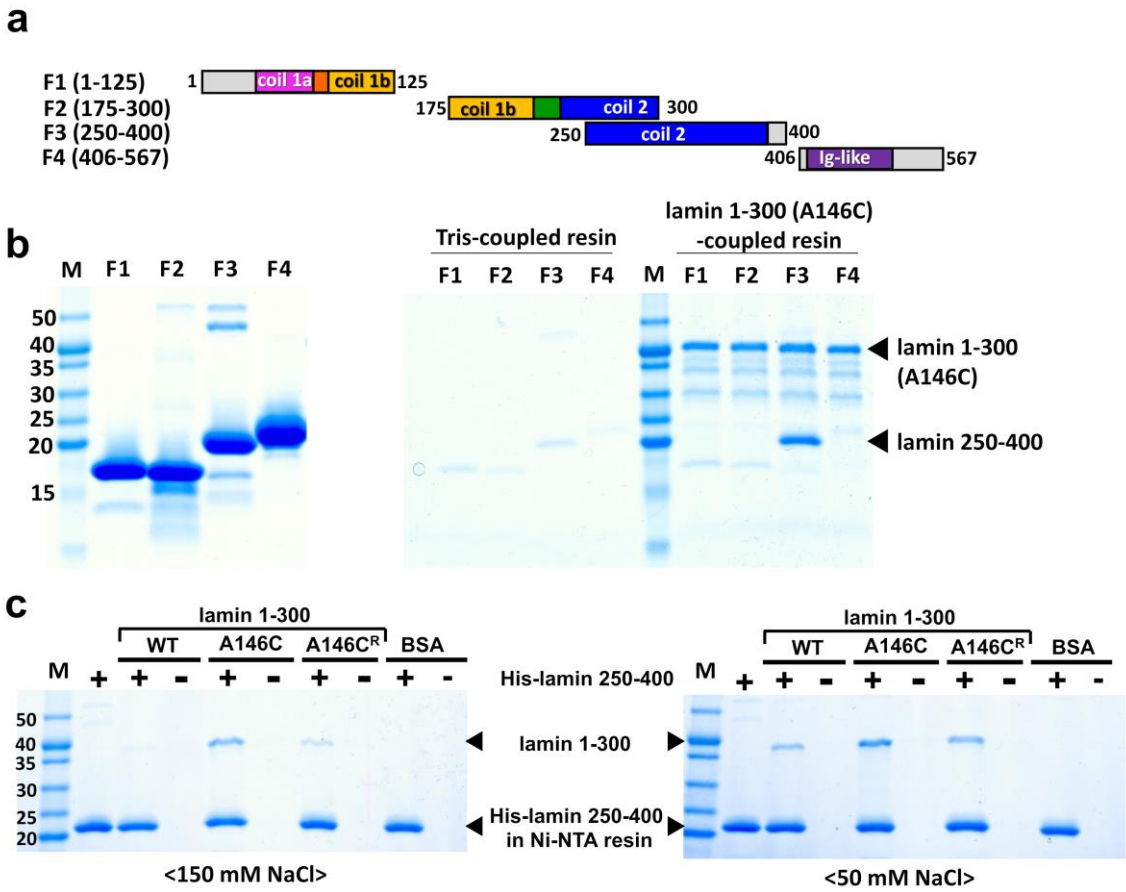
a
F1 (1-125)
F2 (175-300)
F3 (250-400)
F4 (406-567)
1
coil 1a
coil 1b
125
175
coil 1b
coil 2
300
250
coil 2
400
406
Ig-like
567
b
M F1 F2 F3 F4
50
40
35
30
25
20
15
Tris-coupled resin
lamin 1-300 (A146C)
-coupled resin
F1 F2 F3 F4
M F1 F2 F3 F4
lamin 1-300
(A146C)
lamin 250-400
c
lamin 1-300
WT
A146C
A146C^R
BSA
M
+ + - + - + - + -
50
40
35
30
25
20
<150 mM NaCl>
His-lamin 250-400
lamin 1-300
His-lamin 250-400
in Ni-NTA resin
lamin 1-300
WT
A146C
A146C^R
BSA
M
+ + - + - + - + -
<50 mM NaCl>

Figure 2.11. Direct binding between the lamin fragments depending on the A11 interaction

(a) Lamin fragments (F1-F4) were used for the binding assay. The sub-domains are coloured differently as shown in Figure. 2.3a. The start and end residues of the four fragments are indicated.

(b) Identification of the binding partners of the lamin 300 fragment. Four purified fragments are shown in the *left* SDS-PAGE gel. An *in vitro* pull-down assay was conducted using the immobilized lamin 300 A146C mutant on CNBr-activated resin. Four candidate fragments (66 μM) were incubated with lamin 300 A146C-coupled resin or Tris-coupled resin under the non-reducing condition (*right* SDS-PAGE gel).

(c) Comparison of binding affinity between the lamin 300 variants and F3 depending on A11 interaction. An *in vitro* pull-down assay was conducted using His-F3 (residues 250-400)-bound Ni-NTA resin. BSA and wild-type (WT; dimer), non-reduced A146C (A146C; tetramer), and reduced A146C ($A146C^{R}$; dimer) of the lamin 300 fragment were incubated on the empty (-) or His-F3-bound (+) Ni-NTA resins. The resins were pre-equilibrated and washed with the 20 mM Tris-HCl (pH 8.0) buffer containing 150 mM (*left***)** or 50 mM NaCl (*right*). For $A146C^{R}$, the buffer was supplemented with 2 mM TCEP (reducing agent). The bound proteins in the resins were analysed using SDS-

PAGE. Molecular weights (kDa) of the marker (M) are labeled on the *left*.

2.3.5. The eA22 interaction

To identify the binding sites between the lamin 300 fragment and the bound coil 2 fragment, a chemical cross-linking assay was conducted, followed by MS/MS analysis. Since both fragments contain many lysine residues without any cysteine residue, a cysteine residue was introduced at the Arg388 site in the C-terminal end region of a shorter coil 2 fragment (residues 286 – 400). The cysteine residue would be covalently linked to a lysine residue of the lamin 300 fragment via sulfo-SMPB [sulfosuccinimidyl 4-(N-maleimidophenyl) butyrate] cross-linker if the coil 2 fragment is bound to the lamin 300 fragment. The treatment of the cross-linker at low concentration (2.5 μM) built up specific conjugate bands (~52 and ~30 kDa) on SDS-PAGE (Figure. 2.12a). The MS/MS analysis of the conjugate band (~52 kDa) indicated that the Cys388 site of coil 2 is near Lys171 in the lamin 300 fragment in the highest proportion among all modified lysine residues at each position (Figure. 2.12b and Table 2.3). It is also possible that Lys180 and Lys181, which are close to the Lys171 site, are involved in this eA22 interaction if the length of cross-linker and surface geometry of the coiled-coil is considered. These results indicated that the entire coil 2 dimers make an extensive anti-parallel interaction with each other (Figure. 2.12c). This

interaction was referred as an eA22 (extensive anti-parallel binding between coil 2s) interaction in this study and is distinguished from the ‘A22 interaction’ of vimentin, where only the C-terminal half parts of coil 2 (called coil 2b) are involved (Hess et al., 2004). Additionally, the ~30 kDa conjugate band was revealed to be the coil 2 fragment dimer.

Since the eA22 interaction was enhanced by the A11 interaction, the eA22 interaction should be considered in terms of the tetramer made by the A11 interaction. The possible overlapping region was structurally evaluated for the coil 2 region in the presence of the A11 and eA22 interactions. In the tetrameric arrangement by the A11 interaction, I noted ~6-nm-long spaces between the bifurcated coil 1a and coil 2 on both sides (Figure. 2.13). The bifurcated coils appear to hold a long α-helix or coiled-coil dimer like a crocodile clip if they are stretched from the core anti-parallel contact part (Figure. 2.13b), which would be allowed by the conformational flexibility at the linker segments (L1 and L12; Figures. 2.4 and 2.5). Next, ~4-nm-long grooves was noted in the tetrameric arrangement at each side compartment in the anti-parallel contact part (Figure. 2.13a). The grooves would accommodate a longer structural motif together with the bifurcated coils, since they are continuous to the space between the bifurcated coil 1a and coil 2, making

a 10-nm-long binding motif (Figure. 2.13b). The groove and space would provide the major part of the long overlapping region with the 6 α-helical intersections.

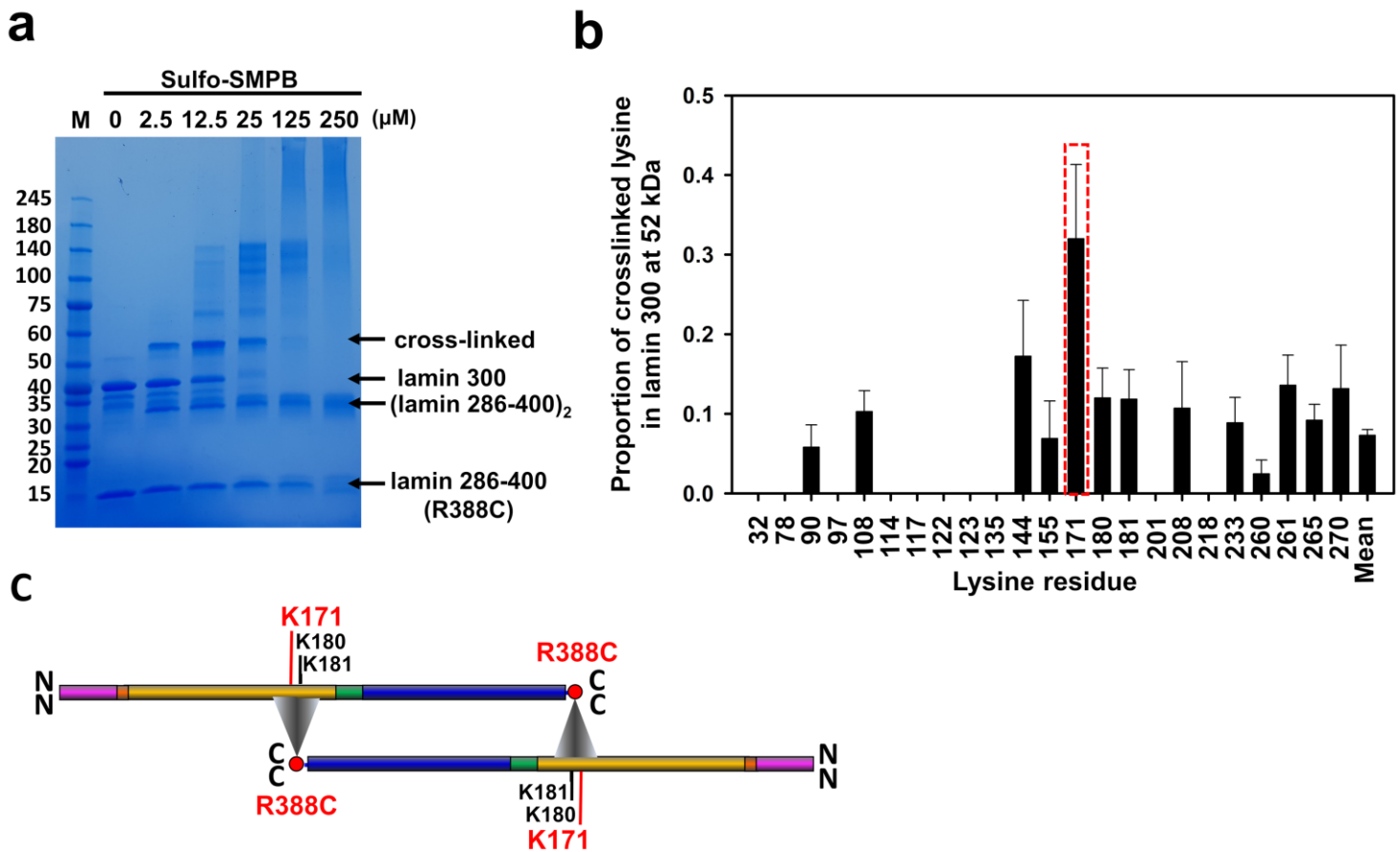
a
Sulfo-SMPB
M 0 2.5 12.5 25 125 250 (μM)
245
180
140
100
75
60
50
40
35
30
25
20
15
cross-linked
lamin 300
(lamin 286-400)2
lamin 286-400
(R388C)
b
Proportion of crosslinked lysine in lamin 300 at 52 kDa
0.5
0.4
0.3
0.2
0.1
0.0
32 78 90 97 108 114 117 122 123 135 144 155 171 180 181 201 208 218 233 260 261 265 270 Mean
Lysine residue
C
K171
K180
K181
R388C
N
N
C
C
C
C
R388C
N
N
K181
K180
K171

Figure 2.12. The eA22 interaction mapping by MS/MS analysis with cross-linked proteins

(a) The chemical cross-linking assay with the lamin 300 fragment and lamin 286-400 R388C mutant in SDS-PAGE. Protein bands of the lamin 300 fragment and the cross-linked sample are labeled. To block the unreacted chemical cross-linker, excess cysteine was added. The major bands of 'cross-linked' (52 kDa), lamin 300 (38 kDa), dimerized lamin 286-400 R388C [$(\text{lamin 286-400})_2$; 30 kDa], and lamin 286-400 R388C (14 kDa) were excised and subjected to the subsequent MS/MS analysis.

(b) Proportion ($\hat{p}$) of the Cys388-bound lysine residues at each position was determined by dividing the number of Cys388-bound lysine residues by the total number of observed lysine residues in the pooled data of cross-linked bands. Position of the most probable Lys171 to be cross-linked to Cys388 is shown in a red box in the plot. The error bars indicate each standard error of a proportion, which was calculated by $\sqrt{\frac{\hat{p}*(1-\hat{p})}{\text{number of observed peptides}}}$. See also Table 2.3.

* MS/MS analysis was performed by Yong-Hak Kim's lab.

(c) Schematic representation of the central rod domains of two coiled-coil dimers in the colour code of Figure. 2.3a, displaying the eA22 interaction based on the results of the MS/MS analysis. Triangles indicate that Arg388 (or Cys388) of coil 2 is around Lys171 (or its neighboring Lys180 or Lys181) of coil 1b in lamin 300 fragment.

Table 2.3. Summary of the 52 kDa bands (52 kDa #1 and 52 kDa #2).

residue number	# observed peptides	# CL-linked peptides	proportion of cross-liking ($\hat{p}$)	standard error of p
K32	38	0	0	0
K78	ND	ND	ND	ND
K90	69	4	0.06	0.028
K97	73	0	0	0
K108	136	14	0.11	0.026
K114	49	0	0	0
K117	61	0	0	0
K122	61	0	0	0
K123	61	0	0	0
K135	26	0	0	0
K144	29	5	0.17	0.070
K155	29	2	0.07	0.047
K171	25	8	0.32	0.093
K180	75	9	0.12	0.037
K181	76	9	0.12	0.037
K201	12	0	0	0
K208	28	3	0.11	0.058
K218	8	0	0	0
K233	79	7	0.09	0.032
K260	81	2	0.02	0.017
K261	81	11	0.14	0.038
K265	207	19	0.09	0.020
K270	38	5	0.13	0.055

* ND = not detected

** standard error of $p = \sqrt{\frac{\hat{p}*(1-\hat{p})}{\text{number of observed peptides}}}$

*** MS/MS analysis was performed by Yong-Hak Kim's lab.

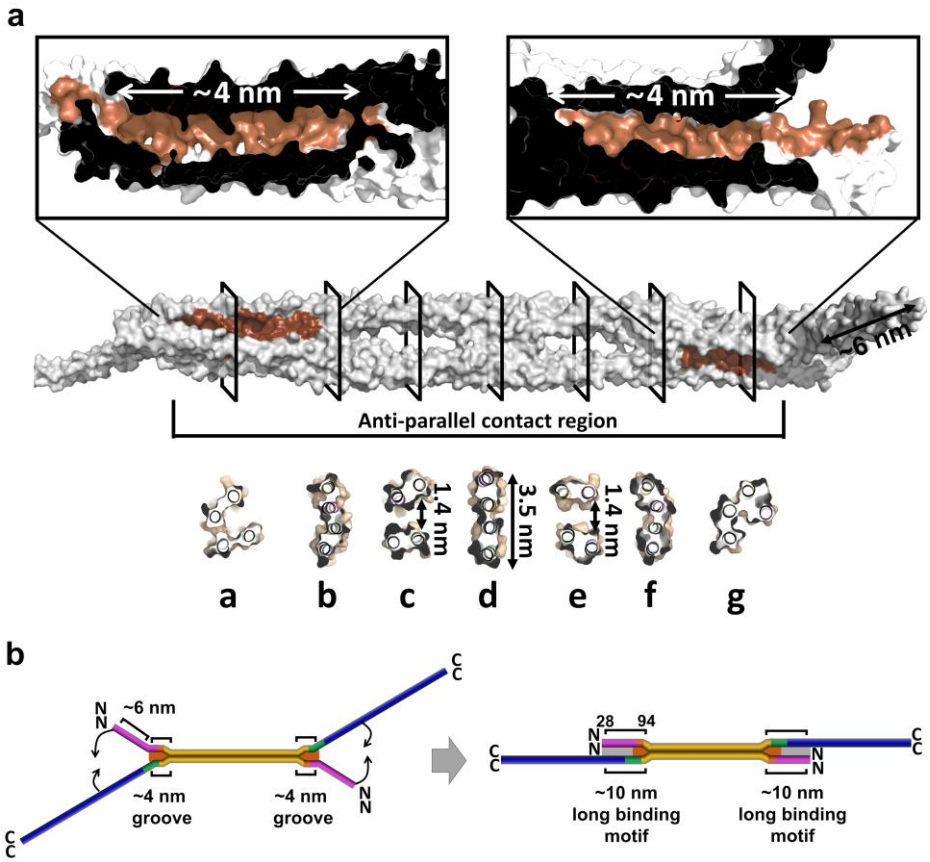

Figure 2.13. The grooves and the space in the lamin A11 tetramer

(a) The lamin tetramer is shown in the surface representation (grey), and the anti-parallel contact region is marked. Two ~4-nm-long grooves are in brown and enlarged in the top panel. The cross-sections, marked with Roman numerals, are shown in the *bottom* panel.

(b) The bent model of the full-length rod domain reflecting the crystal structure of the lamin A11 tetramer is shown in the left panel and the

straightened model is shown in the right panel. The sub-domains are coloured differently as shown in Figure. 2.3a. The ~4 nm grooves and ~6-nm-long spaces are in brown and light grey, respectively. Detailed information for the model construction is depicted in Figure 2.15.

2.3.6. Proposed lamin assembly model at the molecular level

To build the assembly model of the lamin filament, it was started from a 54 nm-long coiled-coil dimer model of the central rod domain by combining this structure with fragmented structures (Krimm et al., 2002; Nicolet et al., 2010; Strelkov et al., 2004) (Figure. 2.14a). The missing parts (residues 283-385) were presumed by the typical coiled-coil structure with a rise per residue of 1.5 Å. The A11 interactions were applied between coiled-coil dimers, leading to the formation of a 72-nm long tetramer with 19-nm-long overhangs of coil 2 on both sides (Figure 2.15a). Sequentially or simultaneously, coil 2 of the coiled-coil dimer was inserted to the tetramer by the eA22 interaction with ~14 nm-long overlapping, including a 10-nm-long binding motif. This assembly resulted in ~40 nm-long intervals between the C-terminal ends of two coiled-coil dimers in the same direction (Figures. 2.14b and 2.15b). Due to the two-fold symmetry in the four lamin subunits, an interval averaging ~20-nm is generated between the Ig-like domains attached to coil 2 (Figure. 2.14c). I believe that the A11 and eA22 interactions would occur simultaneously and synergistically for the further extensions of the lamin filament (Figures. 2.14b and c). This assembly model is well matched to the previous cryo-ET structure representing the native state,

including the features of different cross-section shapes and the interval between the adjacent Ig-like domains (Turgay et al., 2017).

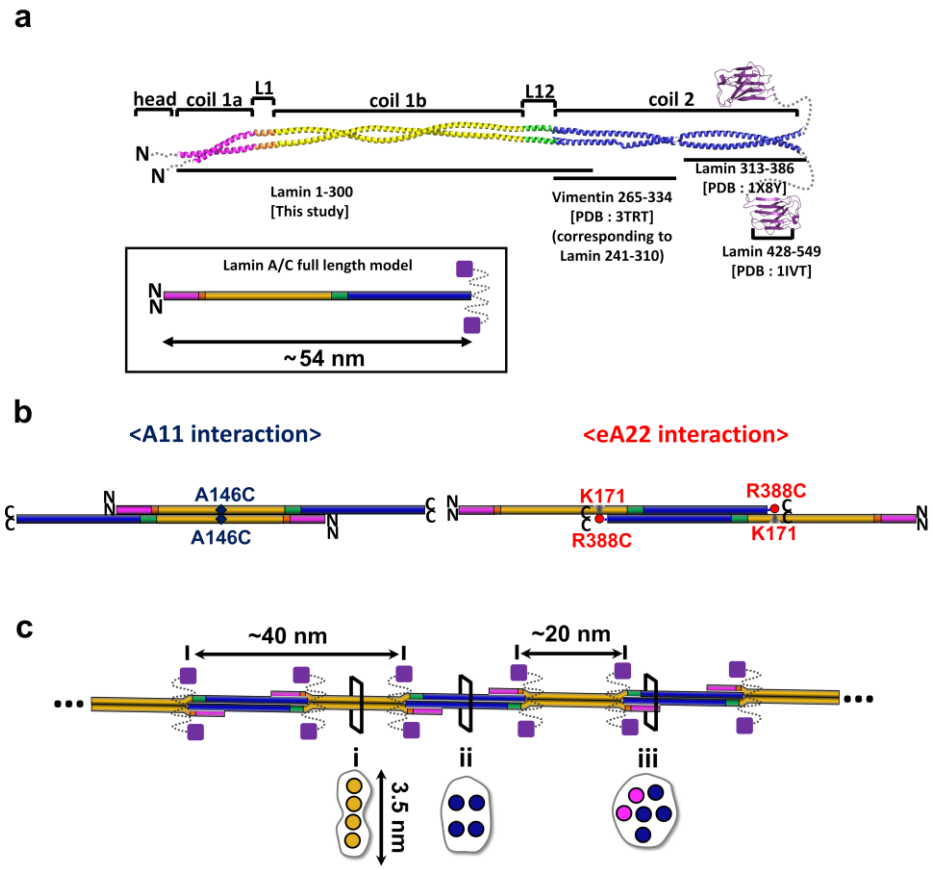

Figure 2.14. Proposed assembly mechanism of lamin by the A11 and eA22 interactions

(a) Coiled-coil dimer model of full-length lamin based on the lamin 300 fragment structure. The C-terminal region of coil 2 (residues 313-386; PDB code: 1X8Y (Strelkov et al., 2004)) and the Ig-like domain (residues 428-549; PDB code: 1IVT (Krimm et al., 2002)) of human

lamin A/C, were added to the structure described in this study. For the N-terminal region of coil 2, the corresponding vimentin fragment (PDB code 3TRT (Chernyatina and Strelkov, 2012); corresponding to residues 241-310 in lamin A/C) was used. The missing part (residues 283-385) in the central rod domain was built with the typical coiled-coil structure with a rise per residue of 1.5 Å. The unstructured regions (N-terminal head, NLS, and C-terminal tail) are indicated by dotted lines. Schematic drawings of the dimer model of the 54-nm long full-length lamin A/C is in the box.

(b) Two different tetrameric assemblies by the A11 or eA22 interactions. Each band in the same colour code as in Figure. 2.3a represents the coiled-coil dimer. Left, the A11 interaction-based tetrameric assembly. Right, the eA22 interaction-based tetrameric assembly. The nearby residues mapped by the disulfide or the chemical cross-linking assays are labelled.

(c) The model of the mature lamin filament, formed by the successive and alternative A11 and eA22 interactions between the dimers. When a pair of Ig-like domains (violet square) are placed on both sides of the tetramers, the distance between the neighboring Ig-like domains is ~20 nm. Schematic cross-sections (a, b, and c) of the lamin filament model

are shown in the bottom (circles represent the intersection of an α-helix, the binding motif is in brown). The cross-section a is equivalent to Figure. 2.13d, and b to Figure. 2.13e, while c is an arbitrary arrangement of 6 α-helices.

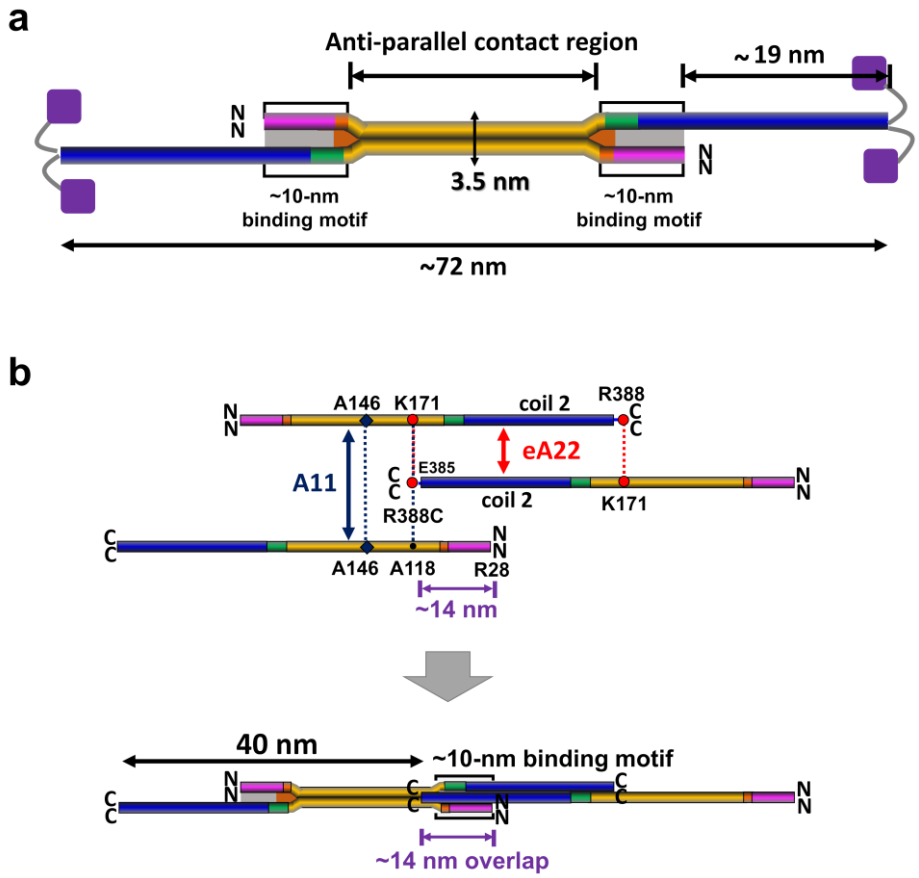

Figure 2.15. Construction of a full-length model for lamin A/C

(a) Schematic drawing of the full-length tetramer model based on the tetramer structure of the lamin 300 fragment. Black boxes indicate the 10-nm-long site in the anti-parallel contact region of the lamin tetramer. The lengths are indicated by double-headed arrows.

(b) The two interactions are combined in three coiled-coil dimers. The A11 interactions are indicated by blue lines and the eA22 interactions by the red lines (*top*). The combined interactions result in ~14-nm-long overlapping of three dimers consisting of 6 α-helices in the intersection, and a ~40-nm-long interval between the C-terminal ends of two coiled-coil dimers in the same direction (*bottom*). The ~10-nm binding motif in the A11 tetramer, described in Figure. 2.13, is indicated.

2.3.7. Laminopathies correlated with A11 and eA22 interactions

It is noted that many genetic mutations causing laminopathies were mapped on the interfaces of the A11 and eA22 interactions, suggesting their importance in the formation of a functional nucleus (Figure. 2.16). To gain insights into the laminopathies at the molecular level, two mutations Y45C and L59R were selected which are related to muscular dystrophy (Bonne et al., 2000; Scharner et al., 2011) and dilated cardiomyopathy (Dittmer and Misteli, 2011; McPherson et al., 2009; Nguyen et al., 2007) respectively. The binding affinity of the lamin 1-300 fragments to the C-terminal part of coil 2 was compared in low and high salt buffers containing 50 or 150 mM NaCl (Figure. 2.11c), where the eA22 interaction was strengthened in the low salt buffer more than that in a high-salt buffer (Figure. 2.11c). The Y45C mutation in the lamin 300 fragment abolished binding to the C-terminal part of coil 2 (Figures. 2.16b and 2.17). In contrast, it was observed that the L59R mutation increased the eA22 interaction in the high salt buffer (Figure. 2.17a *right*). Furthermore, isothermal titration calorimetry (ITC) results showed a ~40-fold higher binding affinity of L59R mutation than the wild type against the C-terminal part of coil 2 in the phosphate-buffered saline, based on K_D values (Figure. 2.18). Consistent results were obtained in

the nuclear shapes and the distribution of the lamin A/C when the mutant lamin genes were overexpressed in the cell lines (HT1080 and SHSY5Y). Lamin A-Y45C formed a blebbing in the nucleus, and they diffused to the cytosol when mechanical stress was applied to the nucleus by cleaving the chromosomal DNA with a nuclease (benzonase). When lamin A-L59R was overexpressed, stronger lamin aggregates were found at the peripheral region of the nuclear envelopes, probably by reinforced filament formation (Figures 2.17b, 2.19, and 2.20).

To explain the opposite effects of the Y45C mutation for muscular dystrophy and the L59R mutation for dilated cardiomyopathy, the locations of the two residues were noted. Both Tyr45 and Leu59 residues are in the d position in the heptad repeat (Figure. 2.4a). The crystal structure further revealed that Tyr45 makes an awkward interaction (with Ile46 at the e position) and Leu59 is ideally positioned in the coiled-coil (Figures. 2.17c and d). The Y45C mutation is likely to stabilize the coiled-coil interaction in coil 1a with the small and hydrophobic residue by relieving the awkward interaction. This appears to inhibit the interaction with the coil 2. However, the potential disulfide bond formation between the cysteine residues might not be important in the Y45C mutant (Figure 2.16b). In contrast, the L59R mutation would

destabilize the coiled-coil interaction through the non-homologous change, which would augment the interaction with the coil 2 region as shown in Figure. 2.17a. The reinforced filament formation would also deteriorate dynamic remodeling or correct mesh formation in cells for the robust nuclear envelope. Thus, these findings suggest that the stronger or weaker interactions may be responsible for pathological states since both cases could cause adverse effects in the formation of robust nuclear structures.

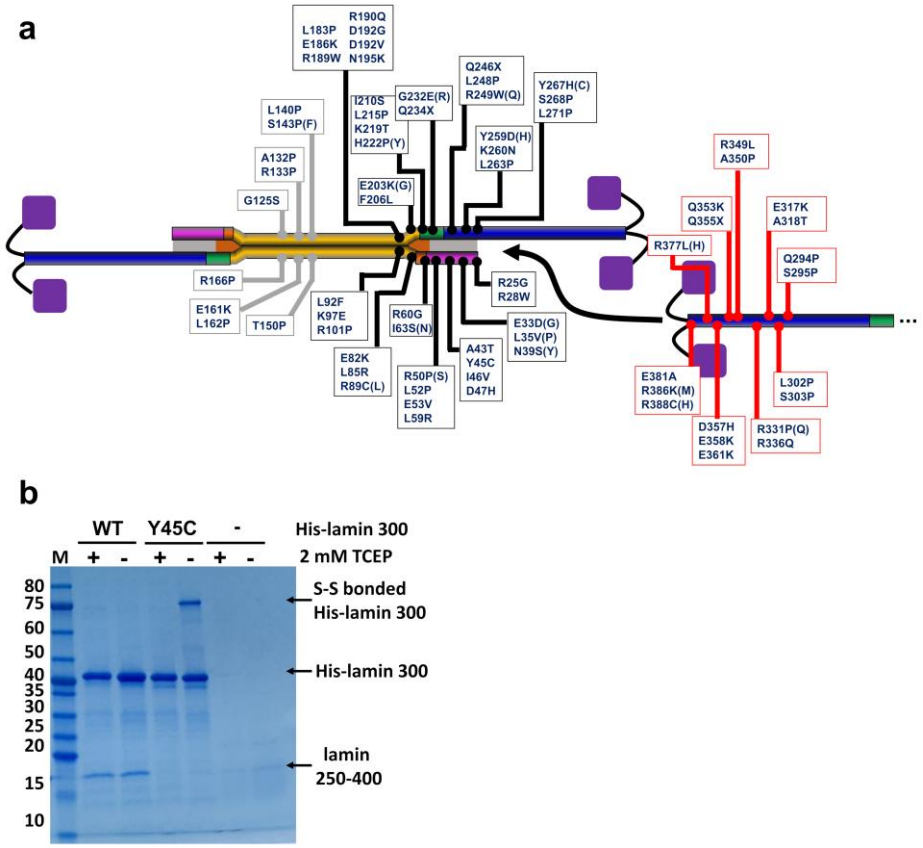

Figure 2.16. Association of the lamin assembly and laminopathies with preferential involvement of skeletal and cardiac muscle on the lamin rod domain

(a) Mapping of mutations associated with skeletal and cardiac muscular related laminopathies on the lamin rod domain, based on the assembly model (Dittmer and Misteli, 2011; Szeverenyi et al., 2008). For detailed information, see the mutations in the red of Figure. 2.13 in reference

(Dittmer and Misteli, 2011). Black dots are in the 10-nm-long site, red dots are in the C-terminal coil 2, and grey dots are in the central part of the anti-parallel contact region.

(b) *In vitro* binding assay using the wild type lamin 300 fragment or Y45C mutant protein-bound Ni-NTA resin. A lamin fragment (residues 250-400) was incubated on resin pre-equilibrated with a high-salt buffer containing 20 mM Tris-HCl (pH 8.0) and 150 mM NaCl. The buffer did not contain reducing agents for non-reducing SDS-PAGE, while 2 mM TCEP was added to the buffer to break the disulfide bonds of the sample. Molecular weights (kDa) of the marker (M) are labeled on the *left*.

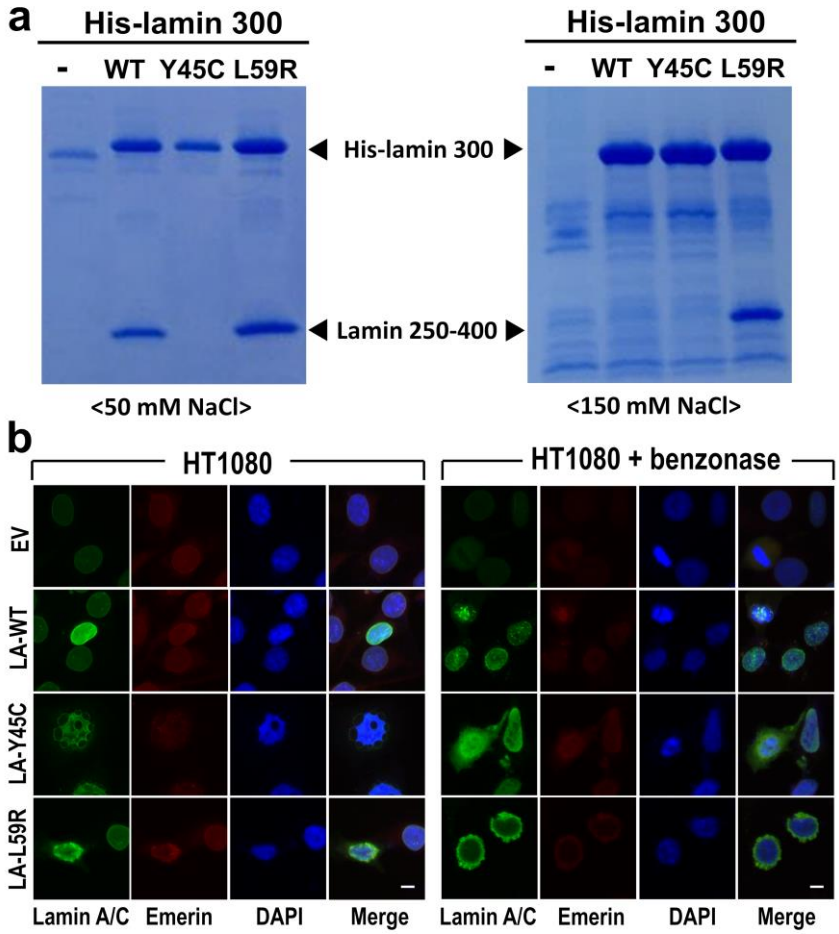
a
His-lamin 300
- WT Y45C L59R
His-lamin 300
Lamin 250-400
<50 mM NaCl>
His-lamin 300
- WT Y45C L59R
<150 mM NaCl>
b
HT1080
HT1080 + benzonase
EV
LA-WT
LA-Y45C
LA-L59R
Lamin A/C
Emerin
DAPI
Merge
Lamin A/C
Emerin
DAPI
Merge

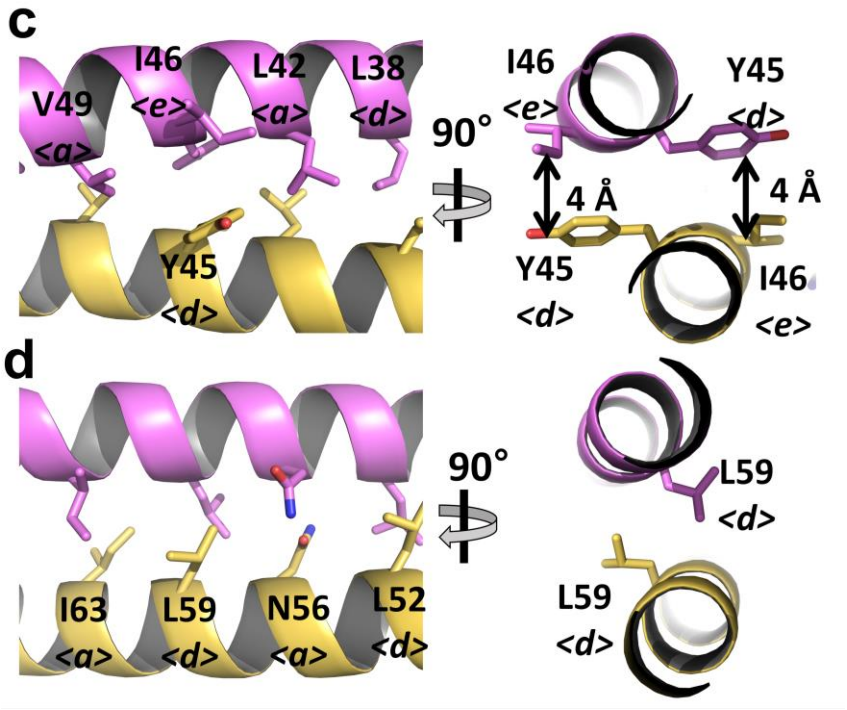

Figure 2.17. The laminopathy-related mutations

(a) Altered eA22 interaction by mutations Y45C or L59R, revealed by *in vitro* binding assay. Wild type, Y45C, or L59R mutant proteins of the His-tagged lamin 300 fragment were immobilized on Ni-NTA resin. Lamin 250-400 fragment were incubated on the empty (-) or His-lamin-bound (+) Ni-NTA resins. The resins were pre-equilibrated and washed with the 20 mM Tris-HCl (pH 8.0) buffer containing 50 mM (*left*) or 150 mM NaCl (*right*). After washing, the bound proteins were analysed using SDS-PAGE.

(b) Nuclear shapes and distribution of lamin A/C Y45C and L59R mutant proteins. Nuclear morphology was examined using fluorescence confocal microscopy after transfection of empty vector (*EV*), wild type, or Y45C or L59R mutant of lamin A/C (*LA-WT, LA-Y45C, LA-L59R*) into HT1080 cells with or without treatment of 2.5 U benzonase for 5 min. For visualization of the nuclear membrane, cells were stained with lamin A/C (green), emerin (red) and DAPI for DNA (blue). See also Figures 2.19 and 2.20. * The immunofluorescence assay was conducted by Bum-Jun Park's lab.

(c), (d) Structural environment around Tyr45 and Leu59. The orthogonal view of the coiled-coil structure around **(c)** Tyr45 and (**d**) Leu59 residues are represented. Each Tyr45 residue interacts with Ile46 residue in another protomer (double-headed arrows). Leu59 residues adopt ideal inter coiled-coil interaction. 'a', 'd', and 'e' positions of the residues in the heptad repeat are labelled with an italic letter.

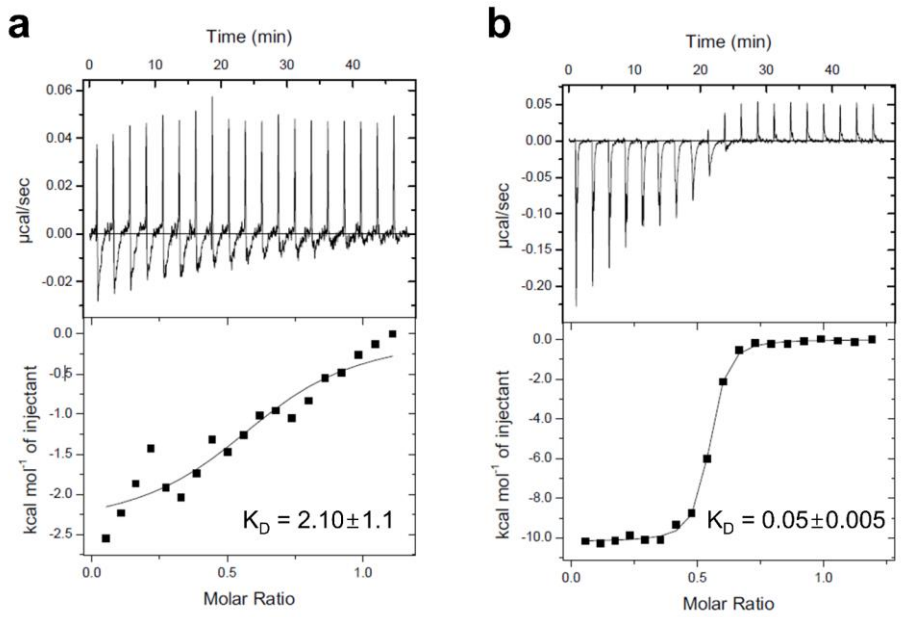

Figure 2.18. Isothermal titration calorimetry (ITC) analysis for the binding of lamin 300 fragments (WT; a and L59R; b) to the coil 2 fragment (residues 250-400)

The *top* panels represent the raw data plots as a series of peaks corresponding to the heat change (µcal/s) resulting from titration of lamin 300 fragment (20 µM; 370 µL) with 19 injections of the coil 2 fragment (160 µM; 2 µL per one injection). The *bottom* panels show the integrated heat pulses in the *top* panels.

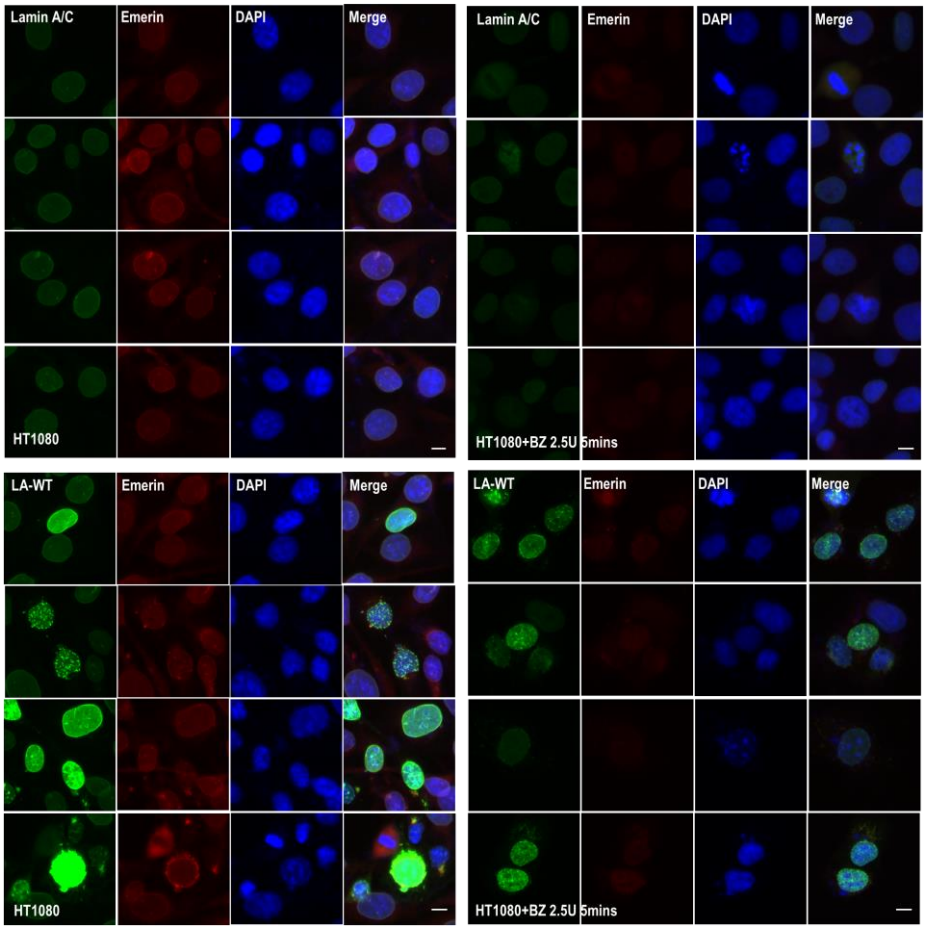
Lamin A/C
Emerin
DAPI
Merge
HT1080
HT1080+BZ 2.5U 5mins
LA-WT
Emerin
DAPI
Merge
HT1080
HT1080+BZ 2.5U 5mins

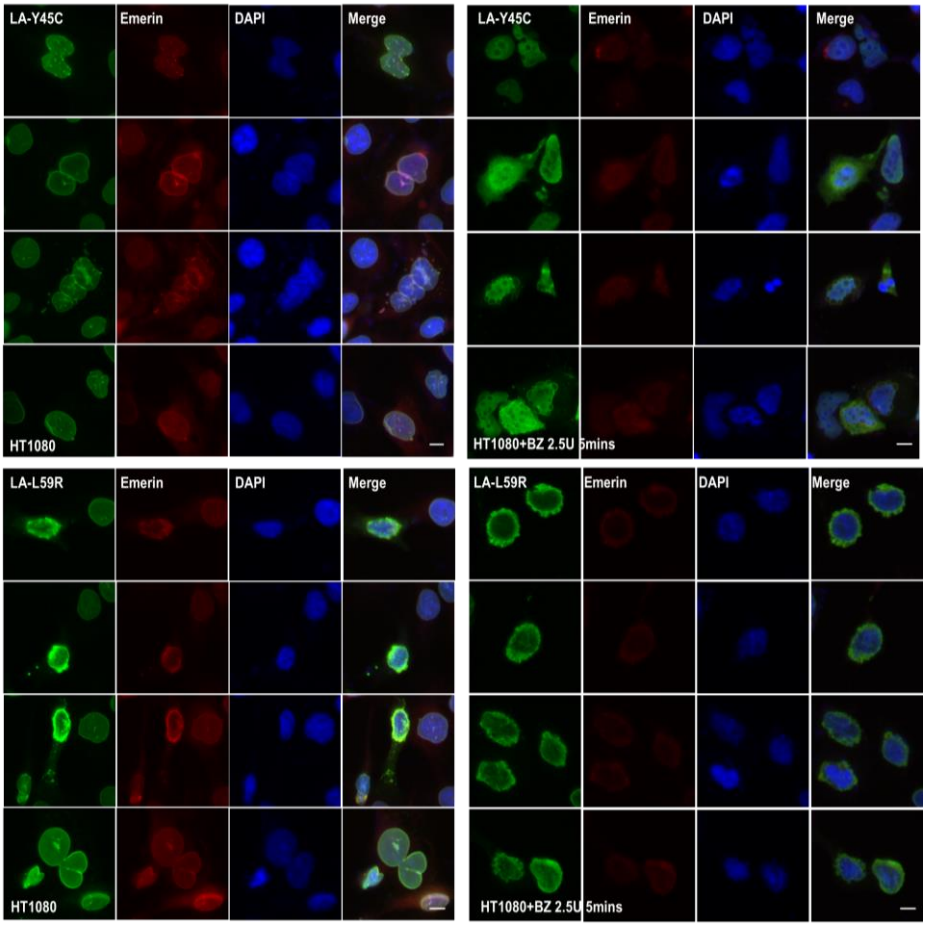

Figure 2.19. Immunofluorescence assay for visualization of nuclear shapes and distribution of the Y45C and L59R mutants of lamin A/C

Nuclear morphology was examined using fluorescence confocal microscopy after transfection of wild type or the Y45C or L59R mutant form of lamin A/C into HT1080 cells with or without benzonase. Cells were transfected with the indicated vectors for 24 h and treated 2.5 U/ml

benzonase for 5 min during permeabilization with 0.1% (v/v) Triton X-100. For visualization of the nuclear membrane, cells were stained with lamin A/C (green), emerin (red) and DAPI for DNA (blue). Scale bar: 10 μm. * The immunofluorescence assay was conducted by Bum-Joon Park's lab.

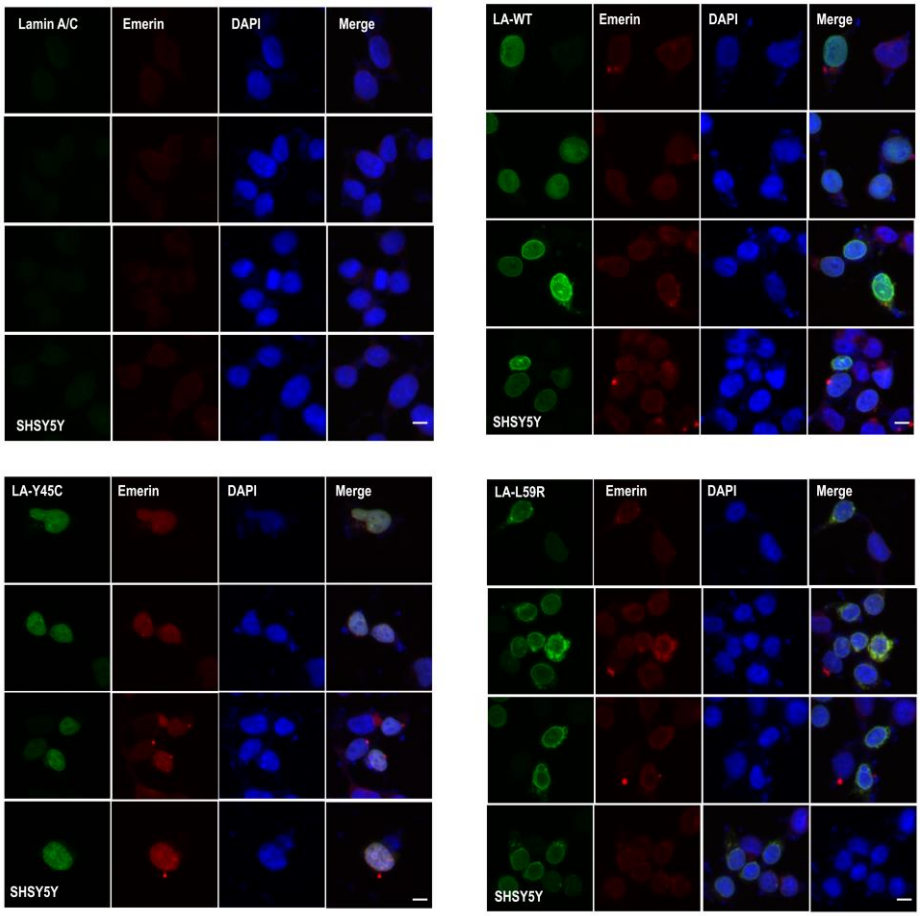

Figure 2.20. Nuclear shape and distribution of lamin A/C in the human neuroblastoma cell line (SHSY5Y) transfected with Y45C or L59R mutant lamin A/C

Nuclear morphology was examined using fluorescence confocal microscopy after the transfection of wild type or the Y45C or L59R mutant form of lamin A/C into SHSY5Y cells. For visualization of the

nuclear membrane, the cells were stained with lamin A/C (green), emerin (red) and DAPI for DNA (blue). Scale bar: 10 μm. * The immunofluorescence assay was conducted by Bum-Joon Park's lab.

2.4. Discussion

There are many different models for lamin and vimentin, some of which are based on the EM images of refolded proteins or their paracrystalline forms at a low resolution (Aziz et al., 2012; Ben-Harush et al., 2009; Chernyatina and Strelkov, 2012; Dhe-Paganon et al., 2002; Dittmer and Misteli, 2011). However, to understand the physiological structure of IF proteins, I now need to focus on the structures representing the native state and high-resolution structures. In this study, I determined the crystal structure of a fragment of lamin containing all the linker segments, directly displaying the A11 interaction between two coiled-coil dimers. This structure was long enough to extend and to connect the previous lamin structures determined by Strelkov and colleagues (Aziz et al., 2012; Kapinos et al., 2011; Strelkov et al., 2004), visualizing most structural features of the full-length lamin. A cross-linking study with MS/MS analysis further discovered an interaction, called an eA22 interaction, which acts presumably synergistically with the A11 interaction. By combining the two interactions, a complete assembly model was built at a molecular level, which agrees well with the *in situ* cryo-ET structure representing the native lamin filament recently provided by Turgay el al (Turgay et al., 2017).

Typical IF proteins, such as vimentin, form thicker filament structures than lamins (Henderson et al., 2012; Schietke et al., 2006). The α-helical rod domain of vimentin has a 42 residue-long gap sequence corresponding to the central compartment of coil 1b of lamin, with substantial length differences in the N- and C- terminal unstructured regions (Figures. 2.7a, 2.8, and 2.9). The central rod domain of vimentin is shorter by ~6-nm than that of lamin due to the gap 42 residues. However, the gap 42 residues seemed not to affect the A11 and eA22 interactions because the central compartment of coil 1b was not directly involved in the filament formation of lamin. Thus, it is likely that the overall structures of the α-helical rod domain of typical IF proteins would be shared with those of lamins (Wallace et al., 1998). Additional interactions, which are present only in typical IF proteins, but not in lamin, would be required to form the final 10-nm thick filament, which consists of four to six lamin-like filaments with a shortened interval.

In conclusion, two essential interactions were discovered for lamin assembly by the crystal structures and biochemical studies. These interactions could provide a key to understanding the nuclear function and the assembly mechanisms for IF proteins at the molecular level.

Chapter 3.

The separation of lamin coil 1a for the eA22 interaction and its implications to laminopathies

3.1. Introduction

Intermediate filament (IFs) proteins provide vital mechanical support in cells of higher eukaryotes. All IF proteins share the tripartite structural organization: a central rod domain is flanked by non-α helical N-terminal (head) and C-terminal (tail) domains, despite the difference of their biochemical properties (Gu et al., 2004; Herrmann et al., 2007; Herrmann et al., 1999; Parry and Steinert, 1999). The sequence-based prediction suggested that central rod domain consists of three a-helical coiled-coils (coil 1a, coil 1b, and coil 2), which interrupted by flexible linkers (L1 and L12) (Parry and Steinert, 1999; Parry et al., 2007; Smith et al., 2002). Since the central rod domains have a high propensity to form coiled-coil dimer followed heptad repeat pattern, a dimer of the IF proteins has been considered as the minimal oligomeric form (Heitlinger et al., 1991; Hess et al., 2002; Koster et al., 2015; Parry et al., 1985). Interestingly, the consensus motifs which have the highly conserved sequences of the various IF proteins were observed in the N-terminal of coil 1a and C-terminal of coil 2 (Burkhard et al., 2001; Herrmann and Strelkov, 2011; Herrmann et al., 2000; Kouklis et al., 1992; Schaffeld et al., 2001). It has been suggested that coil 1a of vimentin regulates the filament elongation as a molecular switch (Chernyatina et al., 2015;

Meier et al., 2009; Premchandar et al., 2016). The separation of coil 1a, divided into two α-helices, was considered a prerequisite for longitudinal elongation to form the filaments.

Recently, two major interactions, A11 and eA22 interactions, were presented concerning for the lamin assembly (Ahn et al., 2019). A11 interaction represents the coiled-coil dimers arranged in an anti-parallel manner centered on residues 146. It was supposed that coil 2 of the coiled-coil dimer was inserted to the tetramer by the eA22 interaction with ~14 nm-long overlapping during the lamin assembly process. However, the role of the coil 1a on the eA22 interaction is still lack understood at the molecular level. Interestingly, many genetic mutations causing laminopathies were mapped on the interfaces of the eA22 interaction. It allowed me to hypothesize that coil 1a plays as a molecular switch in regulating the eA22 interaction and the malfunction of a molecular switch might suppress the normal function of nuclear lamin.

Here, it was observed that the altered binding strength of eA22 interaction introducing mutations to residues at a, d position in the coil 1a. By using isothermal titration calorimetry, the altered binding strength of eA22 interaction was quantitatively estimated. When the lamin mutants were overexpressed in the cell lines, an abnormal nuclear shapes

and the distribution of the lamin A/C were observed. This study provides insight to understand the role of coil 1a as a molecular switch in the eA22 interaction, which contributes to the molecular basis for the development of a new treatment against laminopathies.

3.2. Materials and Methods

3.2.1. Plasmid construction

To overexpress the human lamin 300 and C-terminal coil 2 fragments, the genes encoding each proteins were amplified DNA fragments coding for residues 1-300 (wild-type, L35V, Y45C, L59R, and I63S mutants) and 250-400 of lamin A/C were inserted into the pProEx-HTa vector (Thermo Fisher Scientific, MA, USA). The resulting plasmids encode the hexahistidine tag and the tobacco etch virus (TEV) protease cleavage site at the N-terminus of the lamin proteins. The plasmids encoding the lamin proteins were transformed into the E. coli BL21 (DE3) strain. For immunofluorescence staining, amplified DNA fragments encoding wild type and the L35V and I63S mutants of full-length lamin A/C were inserted into the pcDNA3.1(+) vector (Thermo Fisher Scientific, MA, USA).

3.2.2. Purification of the recombinant proteins

The transformed cells were cultured in 3 L of Terrific Broth medium containing 100 μg/ml ampicillin and 34 μg/ml chloramphenicol at 37°C until an OD600 of 1.0 was measured, and then the expression of proteins was induced using 0.1 mM IPTG at 30°C for 6 hours. After the cell harvest by centrifugation, cells were resuspended in lysis buffer containing 20 mM Tris-HCl (pH 8.0), 150 mM NaCl, and 2 mM 2-mercaptoethanol. The cells were disrupted by using a continuous-type French press (Constant Systems Limited, United Kingdom) at 23 kpsi pressure. After centrifugation at 19,000 g for 30 min at 4°C, the cell debris was removed. The supernatant was loaded onto a Cobalt-talon affinity agarose resin (GE Healthcare). The target protein was eluted with lysis buffer supplemented with 250 mM imidazole and 0.5 mM EDTA. Lamin 250-400 protein was treated with TEV protease to cleave the hexahistidine tag. Then the target proteins were loaded onto a HiTrap Q column (GE Healthcare, USA). A linear gradient of increasing NaCl concentration was applied to the HiTrap Q column. The fractions containing the protein were pooled, applied onto a size-exclusion chromatography column (HiLoad 26/600 Superdex 200 pg, GE

Healthcare) pre-equilibrated with lysis buffer. The purified protein was concentrated and stored at -80°C until used for biochemical assays.

3.2.3. Pull-down assays

A pull-down assay was conducted by using His-tagged lamin 300 proteins immobilized on the Ni-NTA resin as bait. His-tag cleaved lamin 250-400 proteins as prey were incubated on the His-lamin immobilized resin pre-equilibrated in a 20 mM Tris-HCl (pH 8.0) buffer containing 150 mM NaCl (or 50 mM NaCl) at room temperature for 30 min. After washing with the lysis buffer supplemented with 20 mM imidazole, the resin and elute were analysed using SDS-PAGE.

3.2.4. Isothermal Titration Calorimetry

Isothermal titration calorimetry (ITC) experiments were carried out using an Auto-iTC200 Microcalorimeter (GE healthcare) at Korea Basic Science Institute (Ochang, Korea). His-tagged wild type, L35V, Y45C, L59R or I63S mutants of lamin 300 fragment (25 μM; 0.7 mg/ml) were prepared in the sample cell (370 μL) and TEV cleaved 250-400 fragment (180 μM; 3 mg/ml) was loaded into the injectable syringe. All samples were dialyzed with PBS for overnight. Titration measurements of 19

injections (2 μL) with 150 sec spacing were performed at 25°C while the syringe was stirred at 750 rpm. The data were analyzed using the MicroCal Origin™ software.

3.2.5. Immunofluorescence staining

A human fibrosarcoma cell line (HT1080) and human neuroblastoma cell line (SH-SY-5Y) obtained from ATCC were maintained in liquid medium (DMEM) containing 10% (v/v) FBS, 1% (v/v) antibiotics at 37°C. HT1080 or SH-SY-5Y cells were seeded on a cover glass and transfected with the plasmid coding wild type, Y45C or L59R mutant of full-length lamin A/C using jetPEI (Polyplus Transfection). After fixing with 1% (w/v) paraformaldehyde (PFA) for 1 h at 4°C, cells were permeabilized with 0.1% (v/v) Triton X-100 including 2.5 U/ml benzonase (Calbiochem; 71206-3) or mock for 5 min and incubated with a blocking buffer containing PBS and anti-human antibodies (1:400) for 1 h. After washing with PBS twice, the cells were incubated with anti-lamin A/C (sc-376248; Santa Cruz Biotechnology) and anti-emerin (sc-15378; Santa Cruz Biotechnology) primary antibodies (1:200) in the blocking buffer overnight, followed by secondary antibodies (anti-mouse Ab-FITC and anti-rabbit Ab-rhodamine; 1:400) in the blocking

buffer for 7 h and mounted. The nucleus was stained with DAPI. The immunofluorescence signal was detected using fluorescence microscopy (Logos).

3.3. Results

3.3.1. The highly conserved sequence of coil 1a

The α-helical rod domain followed the heptad repeats at conserved lengths except for lamin which contains additional 42 amino acids on the coil 1b (Figure. 3.1). The linkers L1 and L12 cause a phase shift in heptad periodicity between coils by one amino acid in lamins and two amino acids in vimentin. The highly conserved sequences was identified in the N-terminal of coil 1a and C-terminal of coil 2 based on the sequence alignment of human lamin A/C with putative IF proteins (vimentin, keratin 5, and keratin 14) (Figure. 3.1). It has been experimentally verified that the mutations in these motifs disturb the filament formation in keratins and vimentins (Hatzfeld and Weber, 1991; Hesse et al., 2007; Schietke et al., 2006).

Since the properties of coiled-coils are conserved in all IF proteins, the coiled-coil regions of IF proteins might be share a common important role to form filament structure. In the human vimentin, coil 1a suggested as an ‘oligomeric switch’ to regulate the elongation for the filament formation (Meier et al., 2009). The unwinding of vimentin coil 1a might be turning on the switch of the longitudinal elongation referred

to eA22 interaction in lamin. However, the detailed understanding of the structural change of coil 1a to generate the eA22 interaction is limited.

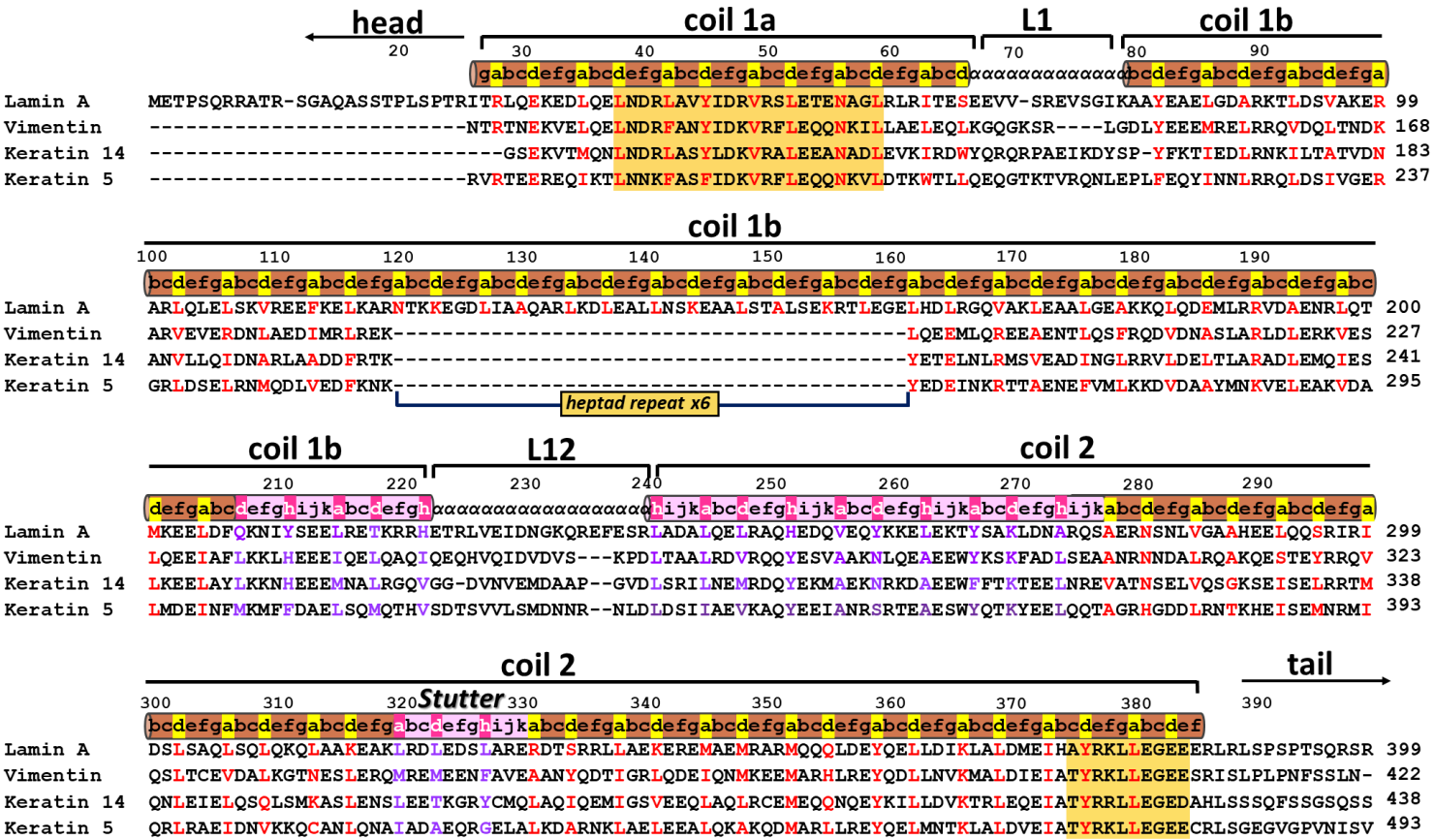
head
coil 1a
L1
coil 1b
Lamin A
Vimentin
Keratin 14
Keratin 5
heptad repeat x6
L12
coil 2
tail
Stutter

Figure 3.1. The sequence alignment of IF rod domain in the IF proteins

Multiple sequence alignment of lamin (human LaminA; P02545.1) and putative IF proteins (human Vimentin; NP_003371.2, human Keratin 5; P13647.3, and human Keratin 14; P02533.4). The sequence periodicity in the heptad (brown) or hendecad (pink) repeat, which was previously predicted (Chernyatina et al., 2015; Parry, 2006), is displayed above sequences. The yellow boxes indicated the highly conserved residues (consensus motif). The hydrophobic residues (a, d, and h) are highlighted in red for heptad or purple for hendecad repeats. An α-helix which does not follow the heptad nor the hendecad rules shown in 'α'.

3.3.2. The two possible conformational changes of coil 1a

Interestingly, previous data have shown the significant bending in the L1 region between coil 1a and coil 1b in the lamin 300 crystal structure (Ahn et al., 2019). In the coil 1a and N-terminal of coil 1b, the residues in a and d positions of heptad repeat were involved in an inter-helical hydrophobic interaction stabilizing the coiled-coil dimers as shown in the lamin 300 crystal structure (Figure. 3.2; *left*). Due to the kinks, the L1 region showed a short α-helical segment without an inter-helical hydrophobic interaction. The bending region of L1 would be straightened, when the coiled-coil dimers are joined by eA22 interaction. Simultaneously, the bending strain would be mounted on the L1 as it is straightened maintaining the coiled-coil dimer of coil 1a.

Two separated α-helices of coil 1a in a straightened conformation were observed in the crystal structure of short fragments in human vimentin (Figure. 3.2; *right*). The residues at a and d position of coil 1b are involved in the formation of a stable coiled-coil dimer, while those of coil 1a exposed to the other side despite their sequence predicted to follow heptad repeat pattern (Figure. 3.1). The exposed hydrophobic patches of coil 1a might be interpreted as a result of relieving the bending strain generated when the bending is straightened.

These observations indicate that the dissociation and association of the α-helices might be reversible or dynamic depending on the oligomerization states, which might be important in the assembly of the IF proteins. To gain more insight into the dynamic conformational changes of coil 1a at the molecular level, four mutations (L35V, Y45C, L59R and I63S) at a or d positions of coil 1a were selected which are related to muscular dystrophy (Figure. 3.2; *left*, coloured in red)(Dittmer and Misteli, 2011; Kang et al., 2018; Maraldi et al., 2005; Muchir et al., 2004; Strelkov et al., 2004)

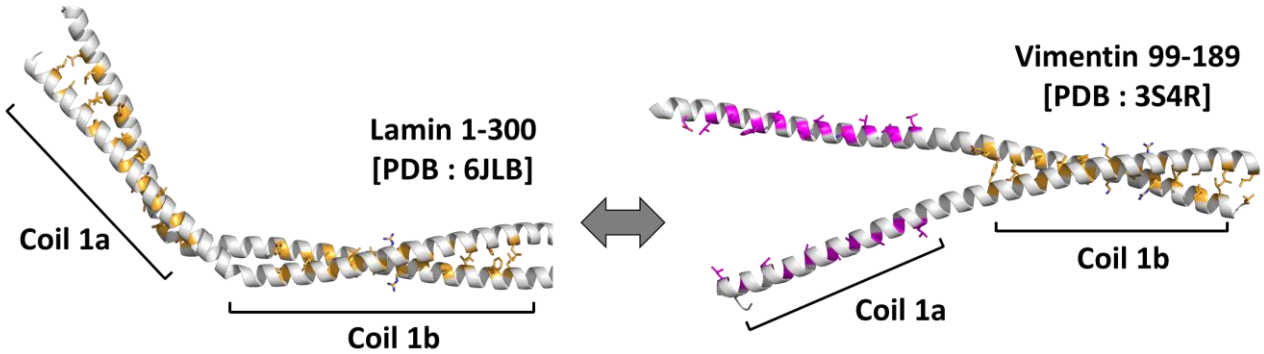
Lamin 1-300
[PDB : 6JLB]
Coil 1a
Coil 1b
Vimentin 99-189
[PDB : 3S4R]
Coil 1b
Coil 1a

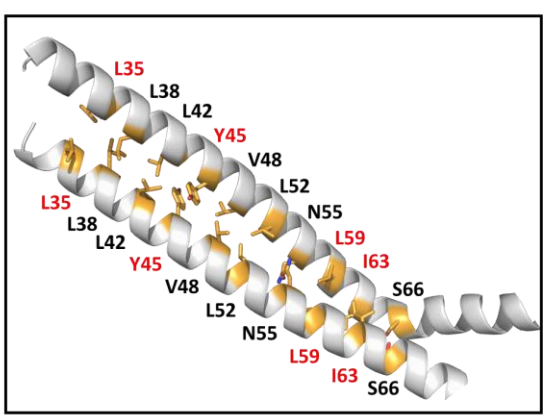
L35
L38
L42
Y45
V48
L52
N55
L59
I63
S66
L35
L38
L42
Y45
V48
L52
N55
L59
I63
S66

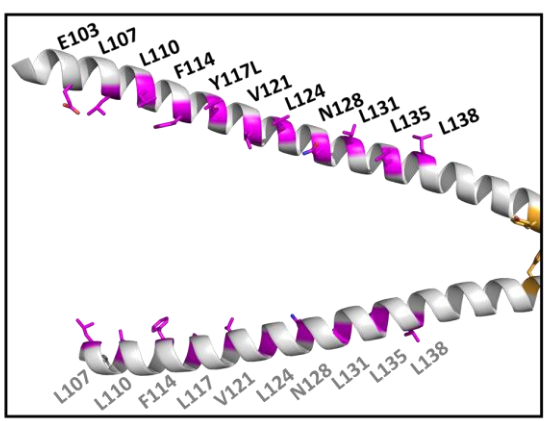
E103
L107
L110
F114
Y117L
V121
L124
N128
L131
L135
L138
L107
L110
F114
L117
V121
L124
N128
L131
L135
L138

Figure 3.2. Two different conformations of coil 1a in the crystal structure of lamin and vimentin

Structural comparison of the N-terminal region of rod domain between lamin (PDB code: 6JLB, (Ahn et al., 2019), residues 1-300) and vimentin (PDB code: 3S4R, (Chernyatina et al., 2012), residues 99-189). The inter-helical hydrophobic residues were shown in the stick representations and coloured in yellow. The residues positioned in *a* and *d* of heptad repeat without forming coiled-coil dimer were coloured in magenta. Coil 1a regions are enlarged in the bottom panel (*left* for lamin and *right* for vimentin). The selected mutations for further biochemical assay coloured in red.

3.3.3. The role of hydrophobic residues of coil 1a on the eA22 interaction

Introducing the L35V, Y45C, L59R, and I63S mutants into the lamin 300 fragment, the pull-down assay was performed to evaluate the altered binding affinity between the lamin 1-300 fragments to the C-terminal part of coil 2 (residues 250-400). It was compared that the binding affinity of the lamin 1- 300 fragments to the C-terminal part of coil 2 in a low-salt buffer containing 50 mM NaCl (Figure. 3.3; *left*), where the eA22 interaction was strengthened more than that in a high-salt buffer containing 150 mM NaCl (Figure. 3.3; *right*). In the L35V and Y45C mutation of lamin 300 fragment, it was observed that the binding strength of eA22 interaction was reduced in the low and high-salt buffer (Figure. 3.3). In contrast, it was observed that the L59R and I63S mutations of lamin 300 fragment increased the eA22 interaction more than wild type in both buffer conditions (Figure. 3.3).

Furthermore, the quantitative binding affinity between the lamin 300 fragments and the C-terminal part of coil 2 was calculated by using isothermal titration calorimetry (ITC). The previous data have shown a ~50-fold higher binding affinity of L59R mutation than the wild type against the C-terminal part of coil 2 in the phosphate-buffered saline,

based on K_D values (Figure. 2.18, represented in chapter 2). The binding affinity of Y45C mutant was measured to be reduced up to ~5-fold compared to the wild type (Figure. 3.4c). I63S mutant showed a slight increase while L35V mutant showed a slight decrease in binding affinity of them compared to wild-type (Figures. 3.4b and d). The results indicated that L35V or Y45C variants of lamin 300 fragment attenuates the eA22 interaction, simultaneously it is reinforced by introducing of L59R or I63S mutations to lamin 300 fragment.

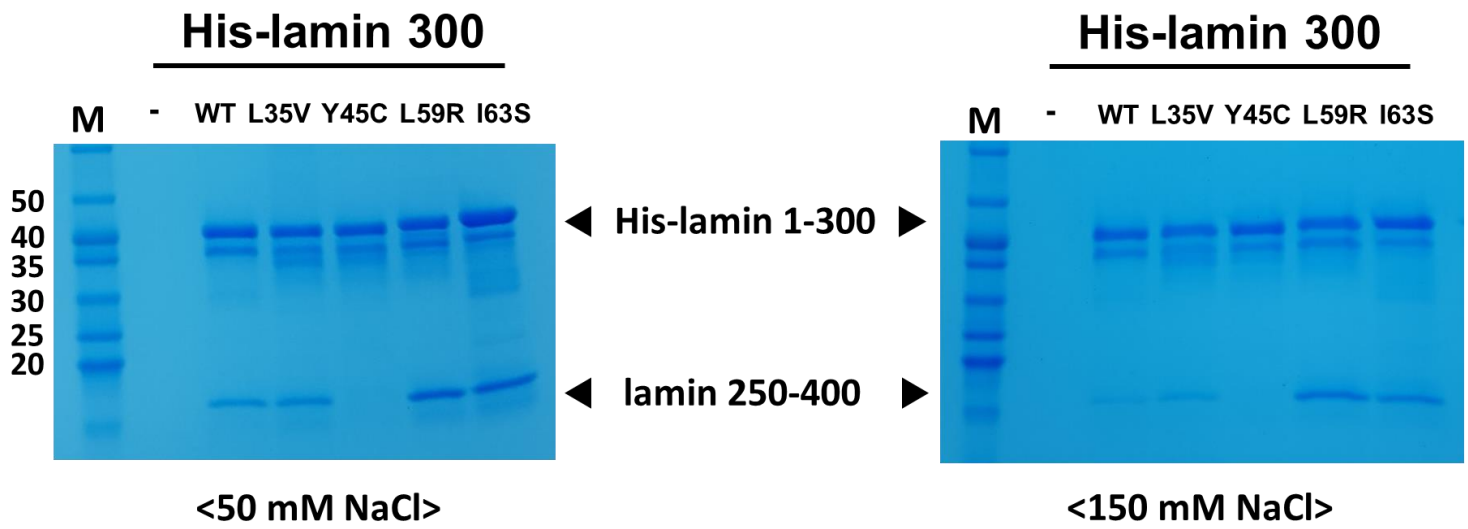

Figure 3.3. The laminopathy-related mutations correlate with the eA22 interaction

Altered eA22 interaction by mutations L35V, Y45C, L59R, and I63S revealed by *in vitro* binding assay. Wild type

and L35V, Y45C, L59R, and I63S mutant proteins of the His-tagged lamin 300 fragments were immobilized on Ni-NTA resin. Lamin 250-400 fragments were incubated on the empty (-) or His-lamin-bound (+) Ni-NTA resins. The resins were pre-equilibrated and washed with the 20 mM Tris-HCl (pH 8.0) buffer containing 50 mM (*left*) or 150 mM NaCl (*right*). After washing, the bound proteins were analysed using SDS-PAGE. Molecular weights (kDa) of the marker (M) are labeled on the left.

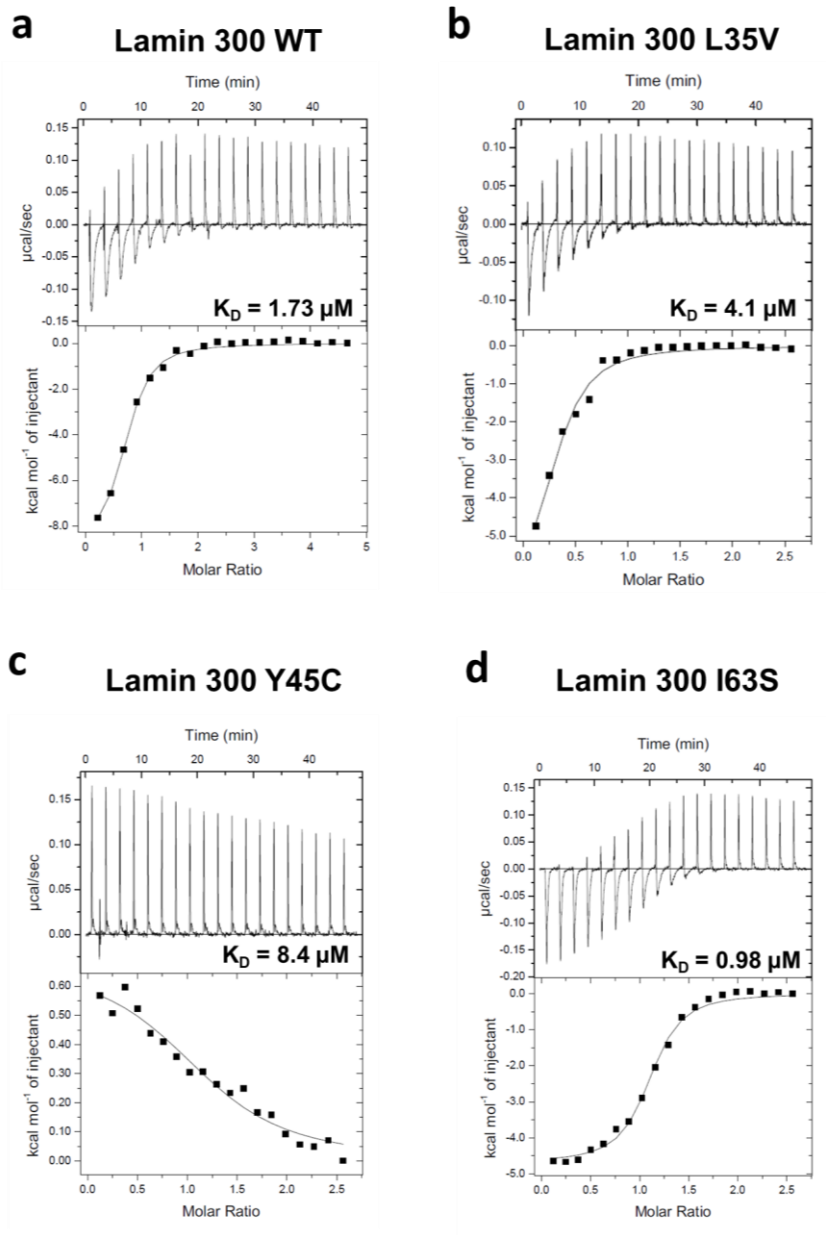

Figure 3.4. The quantitative analysis for the binding of lamin 300 fragments (WT; a, L35V; b, Y45C; c, and I63S; d) to the coil 2

fragment (residues 250-400) by Isothermal titration calorimetry (ITC)

The *top* panels represent the raw data plots as a series of peaks corresponding to the heat change (μcal/s) resulting from titration of lamin 300 fragment (20 μM; 370 μL) with 19 injections of the coil 2 fragment (160 μM; 2 μL per one injection). The *bottom* panels show the integrated heat pulses in the *top* panels.

3.3.4. Structure and biochemical analysis of the role of coil 1a on eA22 interaction

To explain the opposite effects of mutations to eA22 interaction, each mutant was superposed to coil 1a region in the lamin structure (Figure. 3.5). The distance between coiled-coils might be close by introducing L35V mutation since the valine contains a smaller side chain compared to the Leucine residue (Figure. 3.5a *right*). Y45C mutation rapidly forms a disulfide bond, which confirmed in the previous data and induces more stable coiled-coil dimers in coil 1a (Figure. 3.5b). Although L35V is assumed to be involved a slight change, L35V and Y45C might contribute to forming stable coiled-coil dimers. Conversely, mutations of L59R and I63S are likely to weaken the stability of coiled-coil due to the loss of their hydrophobicity. In particular, L59R has a high propensity to collide with R60 residues located in the same direction (Figure. 3.5c). These variations would destabilize the coiled-coil interaction through the non-homologous change.

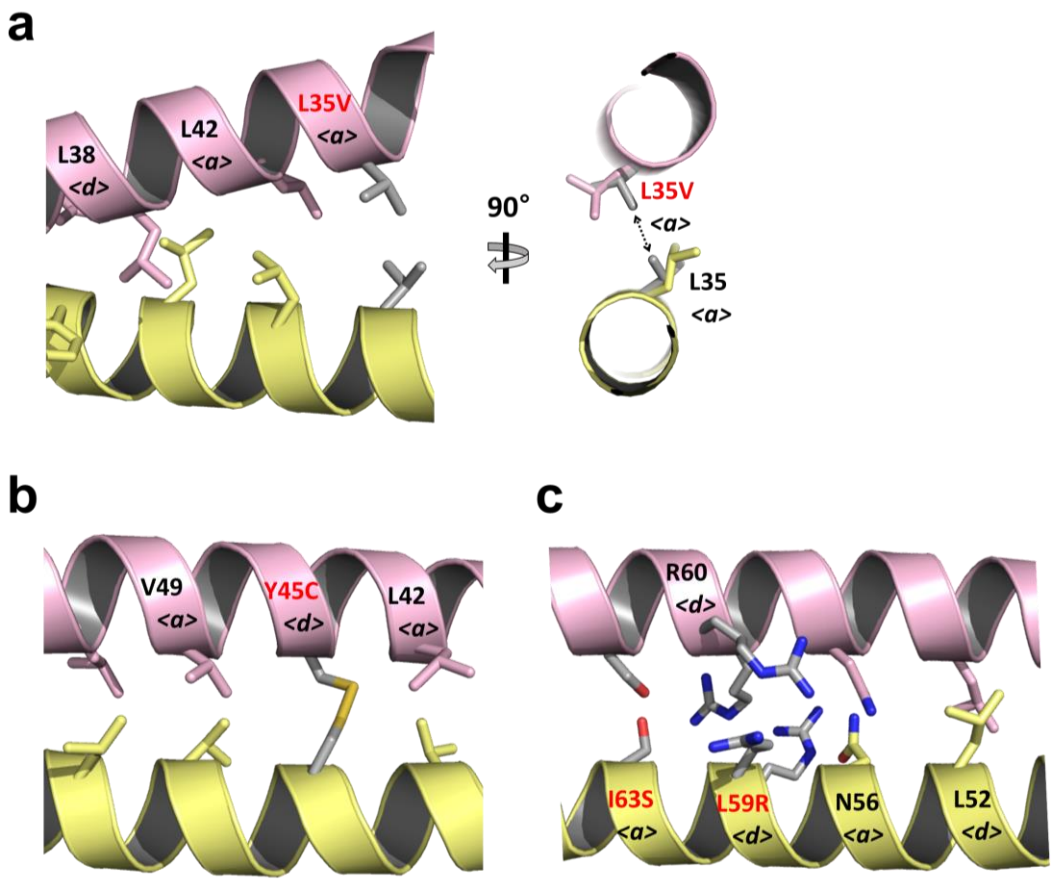
a
L38
<d>
L42
<a>
L35V
<a>
90°
L35V
<a>
L35
<a>
b
V49
<a>
Y45C
<d>
L42
<a>
c
R60
<d>
I63S
<a>
L59R
<d>
N56
<a>
L52
<d>

Figure 3.5. Modeling structure of L35V, L45C, L59R, and I63S mutant

The coiled-coil dimers (pink and yellow) around (a) L35V, (b) Y45C, and (c) L59R and I63S were presented as a ribbon diagram. The residues in *a* or *d* position of heptad repeat are shown as stick. The substituted residues (L35V, L45C, L59R, and I63S) are coloured in grey.

3.3.5. The correlation between laminopathies and eA22 interaction

Consistent results were obtained in the nuclear shapes and the distribution of the lamin A/C when the mutant lamin genes were overexpressed in the cell lines (HEK293). Lamin A-L35V and Y45C showed a lower level of lamin in the nucleus, and they diffused to the cytosol forming localized aggregations. When lamin A-L59R and I63S were overexpressed, stronger lamin aggregates were found at the peripheral region of the nuclear envelopes, probably by reinforced filament formation (Figure. 3.6).

Thus, these findings suggest that stronger or weaker interactions may be responsible for pathological states since both cases could cause adverse effects in the formation of robust nuclear structures. The malfunctions of coil 1a would deteriorate dynamic remodeling or correct mesh formation in cells for the robust nuclear envelope. These results imply that the dynamic conformational changes of coil 1a are necessary for maintaining the normal function of nuclear lamin.

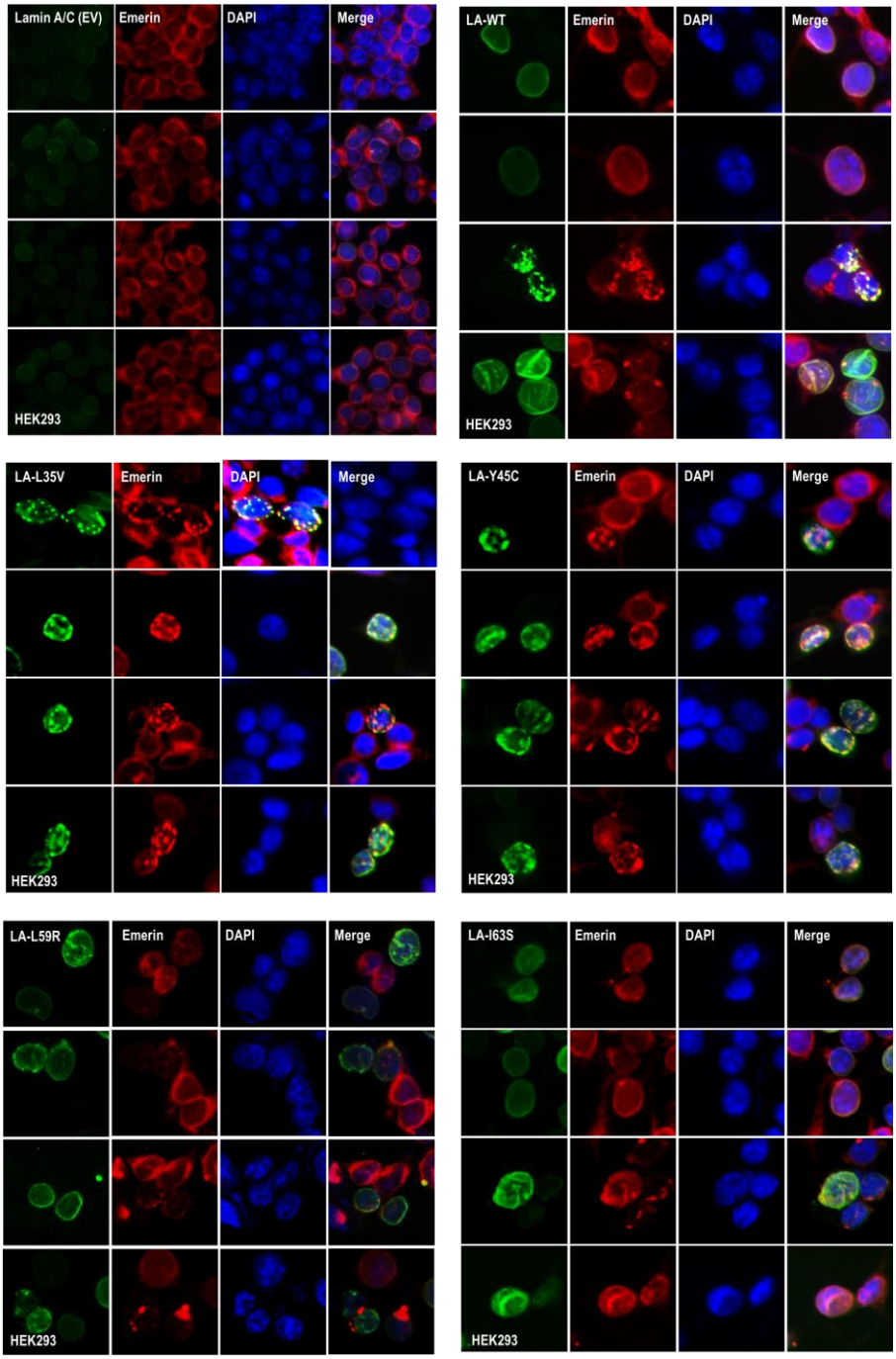
Lamin A/C (EV)
Emerin
DAPI
Merge
HEK293
LA-WT
Emerin
DAPI
Merge
HEK293
LA-L35V
Emerin
DAPI
Merge
HEK293
LA-Y45C
Emerin
DAPI
Merge
HEK293
LA-L59R
Emerin
DAPI
Merge
HEK293
LA-I63S
Emerin
DAPI
Merge
HEK293

Figure 3.6. The nuclear shapes and distribution of the mutants (L35V, Y45C, L59R, and I63S) of lamin A/C, visualized by immunofluorescence assay

Nuclear morphology was examined using fluorescence confocal microscopy after the transfection of wild type or the Y45C or L59R mutant form of lamin A/C into HEK293 cells. For visualization of the nuclear membrane, cells were stained with lamin A/C (green), emerin (red) and DAPI for DNA (blue). Merge indicates merged images of lamin A/C, emerin and DNA. * The immunofluorescence assay was conducted by Bum-Joon Park's lab.

3.4. Discussion

In this study, two possible conformations of coil 1a were observed in the crystal structure of human lamin and vimentin (Ahn et al., 2019; Chernyatina et al., 2012). To verify that the dissociation of coil 1a is essential for the elongation of the filament, pull-down assay was conducted to compare the altered binding affinity of the eA22 interaction by introducing four mutations to the lamin 300 fragments associated with the laminopathies. As a result, the eA22 interaction was weakened in the mutations which induce more stable coiled-coil dimers in coil 1a. In contrast, the mutations that cause instability of coiled-coil dimers due to the loss of hydrophobic properties of them enhanced the eA22 interaction more than the wild type.

Without the switch mode of coil 1a to control the filament elongation, the IF filaments might be extended endlessly. In fact, a cryo-electron tomography (cryo-ET) study revealed that the elongations and crossovers are properly regulated resulting in the rigid three-dimensional mesh of lamins by 3.5-nm-thick filaments (Turgay et al., 2017). These results suggested that the two possible conformations of coil 1a observed in the crystal structures reflected the actual motion of coil 1a in the cell.

When the coil 1a is separated for elongation, the exposed hydrophobic patches could be associated with another coil 2 regardless of the type of IF proteins since all IF proteins share the same pattern of heptad repeat. However, it is known that the filament formation of the IF proteins is only generated for protein-specific except for keratin proteins (Jacob et al., 2018). It could be explained if the length of the linkers determined the degree of the bending angle or the rotation of separated a-helices. The exposed position of the hydrophobic patches would be different depending on the IF proteins containing the different lengths of linkers.

In addition, it is well known that the polar residues of coil 1a and coil 2 in the consensus region involved in the eA22 interaction for filament elongation (Herrmann and Aebi, 2004; Herrmann et al., 2000; Kapinos et al., 2010; Kouklis et al., 1992). After mapping the genetic mutations containing many polar residues in the coil 1a, the mutations were positioned along with an α-helix forming stripe shape. These observations indicate that the stripe-shaped region concentrated on genetic mutations in the coil 1a participates in the combination of coil 2 for the filament elongation. It also gives an insight that some of the

laminopathies might be caused by the prevention of normal control of coil 1a in the process of forming filaments.

Although more biochemical and genetic studies are required to demonstrate the mechanisms of the switch-mode of coil 1a for elongation, this study provides a detailed molecular view of the structure of nuclear lamins and IF proteins in higher eukaryotes. The proposed mechanism will improve the understanding of the various biological processes and diseases related to IF proteins.

Chapter. 4

The flavonoid morin alleviates nuclear deformation of the aged cells by interrupting the progerin-lamin A/C binding

4.1. Introduction

Nuclear lamin proteins play an essential role in maintaining the structural integrity of the nuclear envelopes. Many mutations at lamin genes are related to human genetic disorders (Burke and Stewart, 2002b). Hutchinson-Gilford progeria syndrome (HGPS) is a rare autosomal dominant genetic disease that has a mutation at an intron of the *LMNA* gene encoding lamin A and C (lamin A/C) (Gordon et al., 2014). The mutation results in atypical splicing of mRNA expressing a shorter lamin A (called progerin) whose the C-terminal 50 amino acids are truncated. Progerin interferes the normal lamin A/C and finally results in the nuclear deformation, such as nuclear membrane blebs and reduction of nucleoplasmic lamin A. Since the atypical splicing of *LMNA* gene and the nuclear deformation are also detected in normal aged cells, studies of HGPS is important in understanding the normal physiological aging process.

A recent study revealed that the truncated C-terminal region of progerin makes an aberrant interaction with the Ig-like domain-containing region of the normal lamin A/C, leading to the nuclear deformation (Lee et al., 2016). A synthetic compound JH4 as an inhibitor

of the aberrant interaction was screened based on ELISA. JH4 ameliorated the diverse aging phenotypes in the HGPS cells and the normal aged cells and it expanded the lifespan of a mouse model of HGPS.

The human aging process can be explained by multiple factors. The ROS stress hypothesis proposed that the structural damage by ROS stress is the primary cause of the aging-associated functional losses (Sohal and Orr, 2012). Thus many antioxidants have been noted as anti-aging substances to reduce the level of ROS stress. In parallel, blocking the progerin-mediated interaction would also contribute to attenuate the aging-associated functional loss in the normal aged persons as well as HGPS patients. In this study, a natural compound was found that can be used as an anti-aging functional food ingredient to act as both antioxidant and progerin blocker.

4.2. Materials and Methods

4.2.1. Plasmids construction and purification

For the investigation of protein-protein interactions, recombinant proteins were generated. Recombinant lamin A middle region (residues 301-564) was used in a previous study (Lee et al., 2016). GST-fused recombinant progerin C-terminal region (566-606 and 657-664 in the lamin A numbering; GST-progerin) were produced by PCR cloning 100 aa upstream of the termination codon through PCR. Newly designed plasmid encoding human lamin A 406-553 with the hexahistidine tag was transformed into the E.coil BL21 (DE3) strain.

4.2.2. Purification of the recombinant proteins

The transformed cells were cultured in 2 L of Terrific Broth medium containing 100 μg/ml ampicillin and 34 μg/ml chloramphenicol at 37°C until an OD600 of 1.0 was measured, and then the expression of proteins was induced using 0.1 mM IPTG at 30°C for 6 hours. After the cell harvest by centrifugation, cells were resuspended in lysis buffer containing 20 mM Tris-HCl (pH 8.0), 150 mM NaCl, and 2 mM 2-mercaptoethanol. The cells were disrupted by using a continuous-type French press (Constant Systems Limited, United Kingdom) at 23 kpsi

pressure. After centrifugation at 19,000 g for 30 min at 4°C, the cell debris was removed. The supernatant was loaded onto a Cobalt-talon affinity agarose resin (GE Healthcare). The target proteins tagging with hexahistidine were eluted with lysis buffer supplemented with 250 mM imidazole and 0.5 mM EDTA. GST-fused recombinant progerin was purified by using GSH-agarose resin. Then the target proteins were loaded onto a HiTrap Q column (GE Healthcare, USA). A linear gradient of increasing NaCl concentration was applied to the HiTrap Q column. The purified protein was concentrated and stored at -80°C until used for biochemical assays.

4.2.3. Modified ELISA assay

To isolate progerin-lamin A binding inhibitors from the natural compounds library (L1400, lleckchem, Houston, TX, USA), an ELISA was established by modifying a previously described platform (Lee et al., 2016). His-LMNA-M was fixed on a 96-well plate using 2 mM Tris (bipyridine) ruthenium (II) chloride with 10 mM Sodium persulfate. After blocking and washing, 500 μM of natural compounds were applied on the plates. 96-well plates were washed with TBST and incubated with progerin. Then the anti-Gst-Ab (1: 1000, 2 hours) and anti-mouse-IgG-

HRP (1: 50000, 1 hour) were applied sequentially. After washing twice, plates were incubated with TMB solution (CL07; Calbiochem) and Stop solution (1N H_2SO_4) and the absorbance at 450 nm was determined.

GST-progerin was fixed on a 96-well plate using 0.5% paraformaldehyde. After drying and washing, His-LMNA-M with 10 μM of chemicals (final concentration) was incubated for 1 h. 96-well plates were washed with TBST and incubated with anti-His-Ab (1: 10000, 45 min), and anti-mouse-IgG-HRP (1: 50000, 30 min).

4.2.4. Isothermal Titration Calorimetry

Isothermal titration calorimetry (ITC) experiments were carried out using an Auto-iTC200 Microcalorimeter (GE healthcare) at the Ko rea Basic Science Institute (Ochang, Korea). His-tagged Ig-like do main (residues 406-553) was prepared in the sample cell (370 μL; 27 μM) and GST-fusion progerin (180 μL; 178 μM) was loaded i nto the injectable syringe. For the binding affinity of Ig-like dom ain with morin, 80 μM sample was prepared. The sample was di alyzed with PBS for overnight. Titration measurements of 19 inje ctions (2 μL) with 150-sec spacing were performed at 25°C while the syringe was stirred at 750 rpm. The data were analysed usin

g theMicroCal Origin™ software.

4.2.5. Immunoprecipitation and Western-blot analysis

For the binding assay, the resins accommodating GST-progerin was incubated with lysate from HEK293 cells that had been transfected with GFP–lamin A for 2 hours at room temperature. After washing twice with PBS and once with RIPA buffer (50 mM Tris, 150 mM NaCl, 1% NP-40, 0.5% deoxycholate, and 0.5% SDS), precipitated materials were collected and subjected to SDS-PAGE and Western blotting using anti-GFP antibodies.

4.3. Results

4.3.1. Screening of inhibitors of progerin-lamin A binding in the natural compound library

The synthetic compound JH4 was screened based on the ELISA with an immobilized lamin middle region fragment covering residues 301-565 (LMNA-M) and the truncated C-terminal 50 amino acid residues (progerin, residues 566-606, 657-664 in the lamin A numbering) (Lee et al., 2016). In this study, a similar ELISA was performed from a natural compound library consisting of 143 substances at 500 μM concentration. To firmly immobilize the lamin protein to the polystyrene ELISA plate, the photo-catalytic cross-linking reaction was applied by using Tris (bipyridine) ruthenium (II) chloride which is rapidly converted into Ruthenium (VIII)-oxide through 450 nm visible light in the presence of sodium persulfate (Fancy et al., 2000) (Figure. 4.1a). The screening identified 3-indolebutyric acid, gossypol, fisetin, and morin compounds as candidate inhibitors (Figures. 4.1b and c). Among the potential inhibitors, the flavonoid morin was decided to further investigate the activity by considering the toxicity and costs.

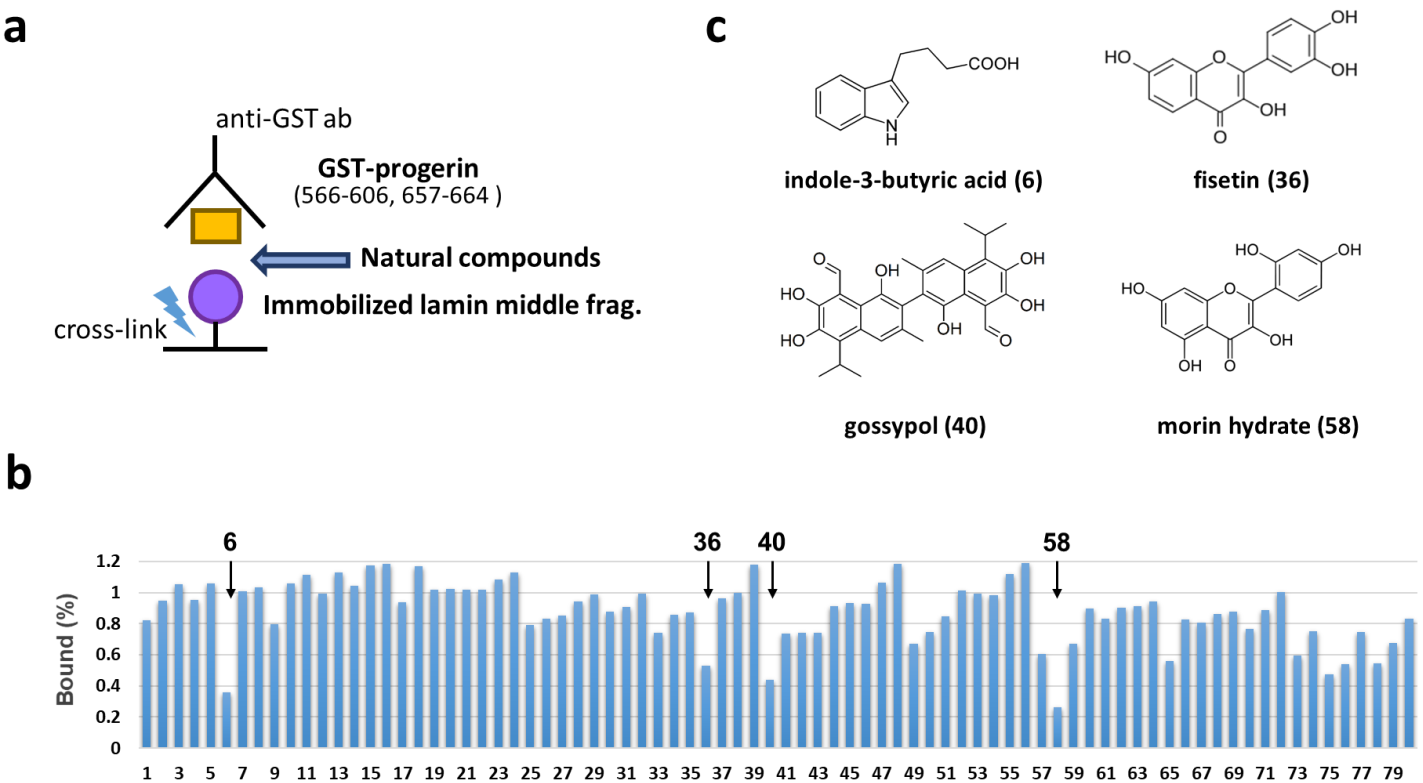

Figure 4.1. Screening of inhibitors of the progerin-lamin A interaction

(a) Experimental scheme for the screening of the natural compounds. The purified lamin A middle fragment (301-565) was immobilized by photo-initiated protein cross-linking reaction using Tris (bipyridine) ruthenium(II) chloride on the polypropylene plate. Each natural compound was incubated at 0.5 mM in each well. GST-progerin C-terminal region (1 uM; residues 566-606 and 658-664) was added to the well. The binding of GST-progerin was detected using ELISA with anti-GST antibody.

(b) Representative results of ELISA-based screening. The indicated bars were determined by the reaction without the natural compounds. The arrows indicate the hit compounds that inhibit the interaction of progerin and lamin A middle fragment (301-565).

(c) Molecular structures of selected natural compounds (6; indole-3-butyric acid, 36; fisetin, 40; gossypol, 58; morin hydrate).

4.3.2. The morin inhibits the interaction between Ig-like domain of lamin A and progerin

By ELISAs with immobilized LMNA-M and the GST-fused recombinant progerin, it was confirmed that morin inhibited the interaction of the two proteins as a dose-dependent manner (Figure. 4.3a). ITC assays were performed to estimate the quantitative binding affinity of LMNA-M with progerin or morin. Since the LMNA-M has separated into 3 specific fragments in the purification process, each band of them was analysed by protein N-terminal sequencing (Figure 4.2). It was identified that one of the separated short fragments is initiated with Ser406 residue. Considering the molecular weight of the fragment, lamin A 406-553 fragment was reconstructed and referred to Ig-like domain in this study. It was confirmed that Ig-like domain has a similar or higher specific affinity to progerin compared to LMNA-M fragment. The ITC results showed that the binding affinity between lamin A and morin is around 2-fold stronger than that of lamin A and progerin binding (Figure. 4.3b). These results indicate that the progerin combines with the Ig-like domain of lamin A fragment, and the morin restrains the interaction by coupling with Ig-like domain.

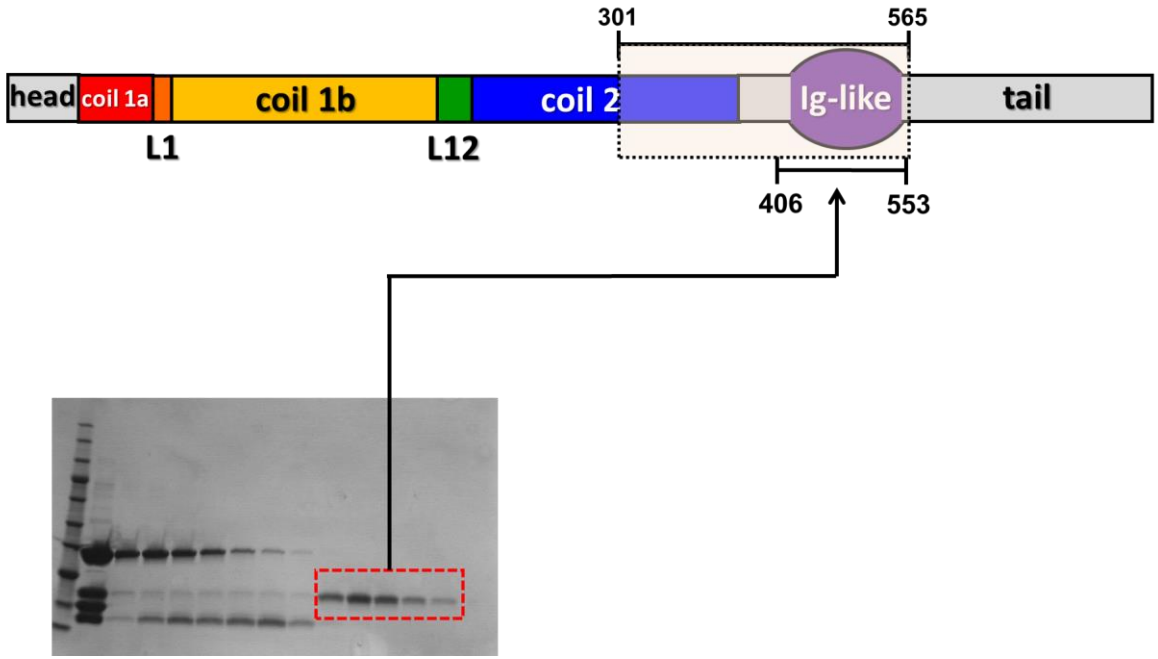

Figure 4.2. The minimum binding unit of lamin A to progerin

The constructs of the lamin middle region (301-565) and newly designed fragment (406-553) were represented in schematic bars on the full-length lamin A. The samples from size-exclusion chromatography were loaded on the SDS-

PAGE. The red box indicates the band applied for N-terminal sequencing corresponding to the 406-553 fragment. It was confirmed that Ig-like domain has a similar or higher specific affinity to progerin compared to LMNA-M fragment.

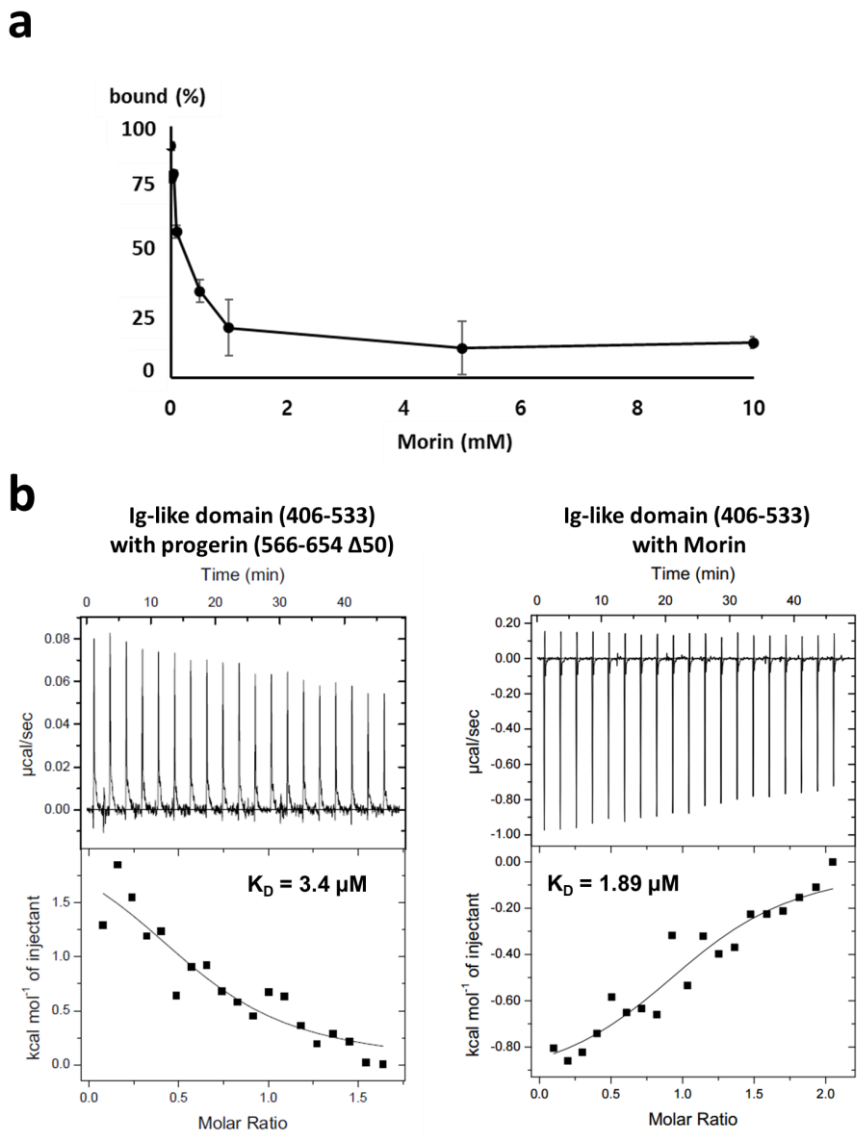

Figure 4.3. Morin inhibits the interaction between lamin A and progerin by coupling with Ig-like domain

(a) Dose-dependent relationship of the inhibition of the binding between

lamin A and progerin by morin. The concentration of morin was varied in the same ELISA.

(b) Isothermal titration calorimetry (ITC) analysis for the binding of la min A with progerin (*left*) or morin (*right*). The top panels represent th e raw data plots as a series of peaks corresponding to the heat chan ge (μcal/s) resulting from titration of lamin 406-553 (94 μM; 370 μ L) with 19 injections of the coil 2 fragment (500 μM; 2 μL per one injection). The bottom panels show the integrated heat pulses in th e *top* panels.

4.3.3. The flavonoid morin ameliorates the nuclear deformation of progerin-expressing cells

To examine the effect of morin in preventing the nuclear deformation of the cells causing by the interactions of lamin A and progerin, it was compared that the nuclear shapes of HEK293 cells expressing the normal full-length lamin A with the full-length progerin gene after treatment of morin. In this experiment, lamin A or progerin constructs were used which expressing GFP fusion proteins to visualize the cell envelop shapes. Progerin-expressing cells exhibited severe nuclear deformation unlike the normal lamin A-expressing cells (Figure. 4.4a). Morin drastically reduced the nuclear deformation of the progerin-expressing cells at 20 μM and showed a moderate effect at 10 μM (Figure. 4.4a). However, any effects of morin were not found in the cell expressing lamin A (Figure. 4.4b).

To confirm the inhibitory role of morin in the cell lysate, the GST-pull down assay was performed with the GST-fused progerin C-terminal region and the GFP-fused lamin A expressed in HEK293 cells. The cell lysate was incubated with the resin-bound to the GST-fused progerin in the absence or presence of morin. Morin reduced the binding between progerin and lamin A in a dose-dependent manner (Figure. 4.5). Since

normal aged cells express progerin albeit at a small amount (Jung et al., 2013), these findings suggest that morin could alleviate the normal aging phenotypes if the effective concentration of morin is maintained throughout the body.

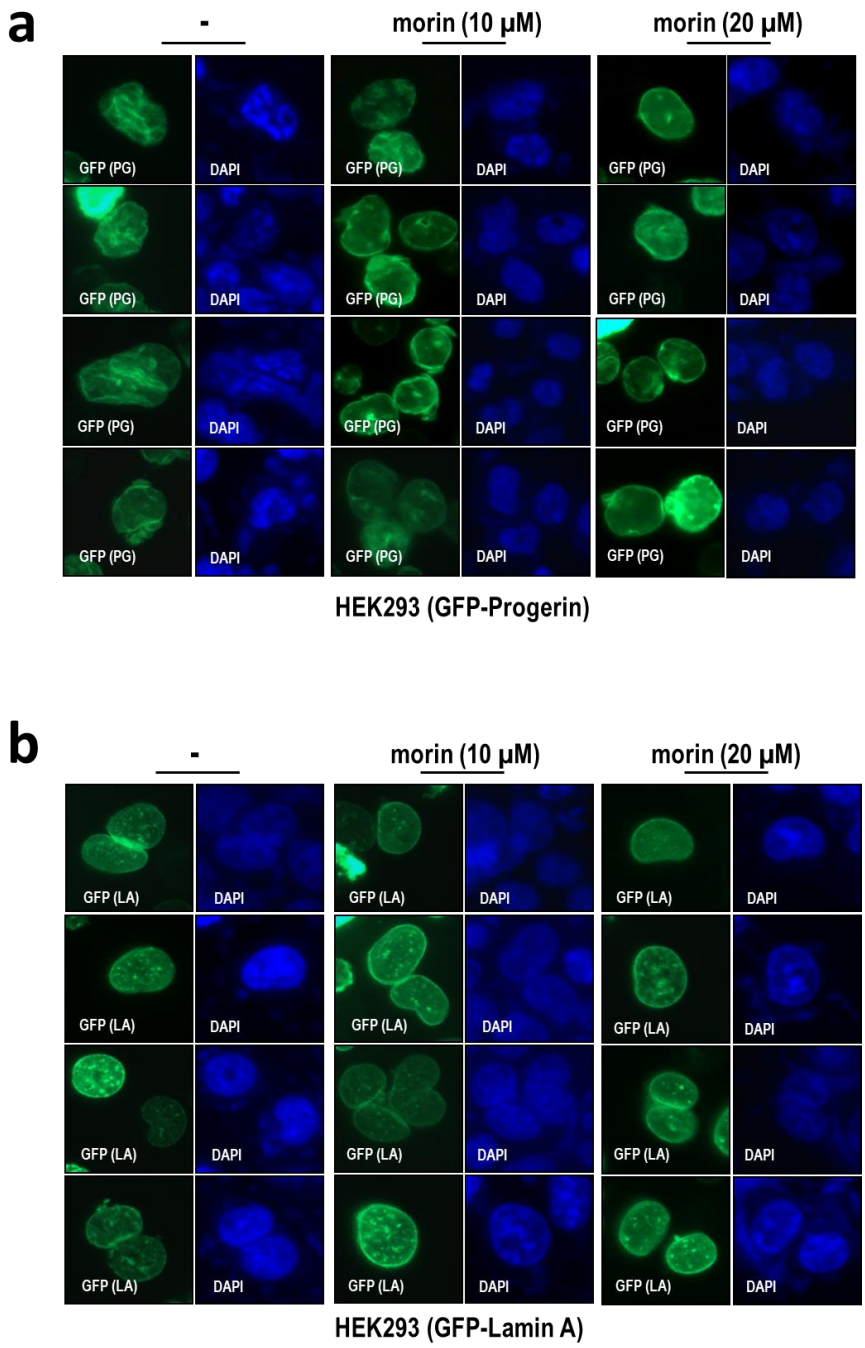

Figure 4.4. Effects of morin in HEK293 cells expressing progerin

HEK293 cells were transfected with GFP-fused progerin (A, full-length, PG) or GFP-fused lamin A (B, full-length, LA). The cell envelop was visualized by fluorescence from the GFP fusion proteins (green), and the chromosomes are stained by DAPI (blue). Morin was treated daily for three days at 0, 10, 20 μM. * The immunofluorescence assay was conducted by Bum-Joon Park's lab.

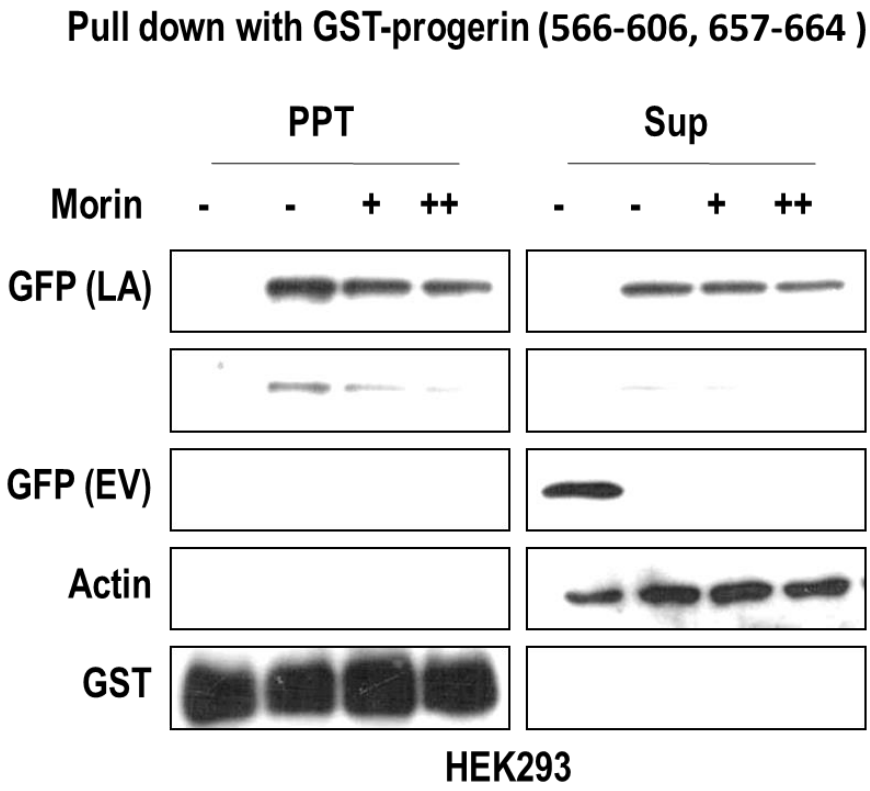

Figure 4.5. The effect of morin on the binding of lamin A and progerin

GST pull-down assay to examine the binding of progerin C-terminal fragment and lamin A expressed in HEK293 cells. HEK293 cells were transfected with GFP-lamin A (full-length, LA) or the parent GFP vector (EV). The resulting HEK293 cell lysates were incubated with the resin accommodating GST-progerin (residues 566-606 and 657-664). The

precipitated resin and the supernatant were analysed by western blotting with anti-GFP antibodies. * The immunofluorescence assay was conducted by Bum-Joon Park's lab.

4.3.4. Morin ameliorates the nuclear deformation of HGPS cells

Next, the effect of morin was examined on the nuclear deformation of the HGPS cells. The deformed nuclear envelopes of the HGPS cells were visualized by immunofluorescence with lamin A antibody (Figure 4.6). Treatment of 10 μM morin for 3 days to the HGPS cells reduced nuclear deformation by 50%. Furthermore, the numbers of the deformed nucleus were decreased to as low as 20% level by 20 μM morin treatment, which is similar to 5 μM treatment of the synthetic compound JH4 in control (Figure. 4.6a). The transcriptional level of lamin A or progerin was not affected despite the treatment of morin in the cells (Figure. 4.6b). These results suggest that morin is a promising candidate for the ingredients of the functional foods to alleviate the symptoms of HGPS.

The nuclear deformation was observed in the normal aged cells since the progerin has been generated during the normal aging (Jung et al., 2013). The effect of morin was checked on cell proliferation since an important feature of senescence is an irreversible cell proliferation arrest. When 20 μM morin was applied to HGPS cells for 5 days, the nuclear deformation was ameliorated but significant differences were not detected in the H3K9me3, the senescence marker (Figure. 4.7a). A slightly increased expression of H3K9me3 was found in the HGPS cells

treated with higher amounts (30 µM) of morin for 7 days (Figure. 4.7b).

a

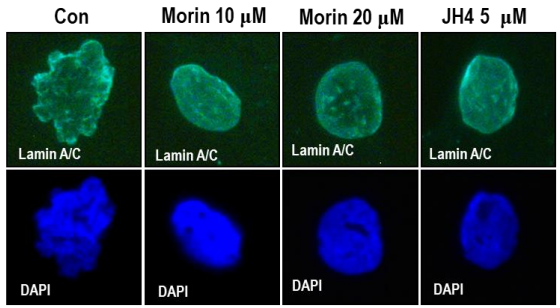

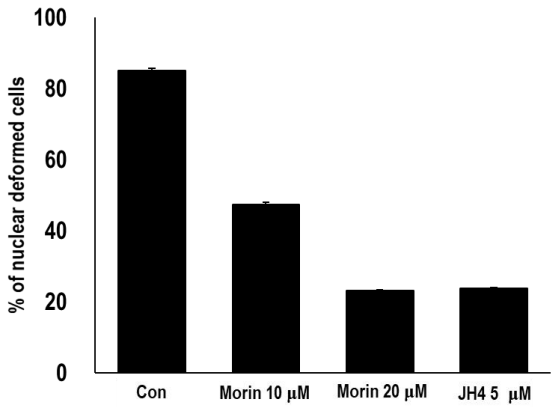

b

- Morin
  -> 3days treatment in daily

- PCR
- B.L : Blank (No template DNA)

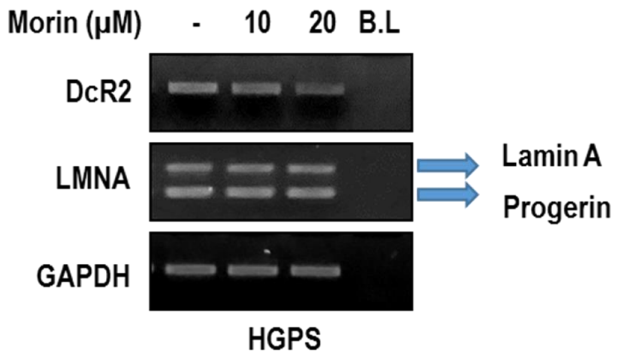

Figure 4.6. Effects of morin on the nuclear deformation in the HGPS cells

(a) Fibroblast cells from HGPS patients were treated with morin (10, or 20 μM) or JH4 (5 μM). The lamin A/C was stained by immunofluorescence with anti-lamin A antibody (green). The chromosomes were stained by DAPI (blue). The percent of cells with deformed nuclear morphology from the images indicated that morin ameliorated nuclear deformation of HGPS cells (*bottom*).

(b) The transcript levels of lamin A or progerin of the morin-treated HGPS cells. After the cells were washed, total RNA was extracted, and RT-PCR was performed. * The immunofluorescence assay was conducted by Bum-Joon Park's lab.

a

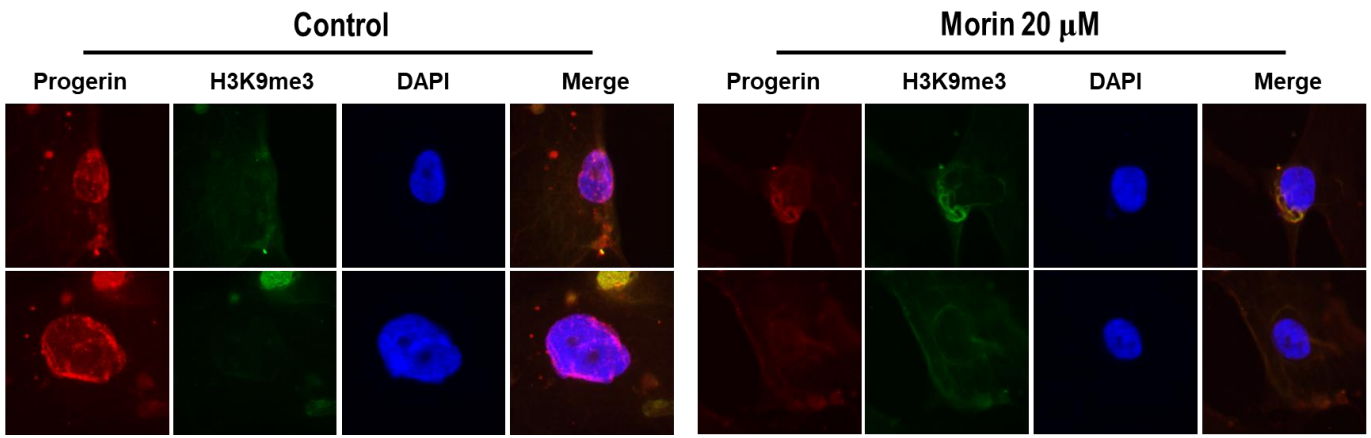
Control
Morin 20 μM
Progerin
H3K9me3
DAPI
Merge
Progerin
H3K9me3
DAPI
Merge

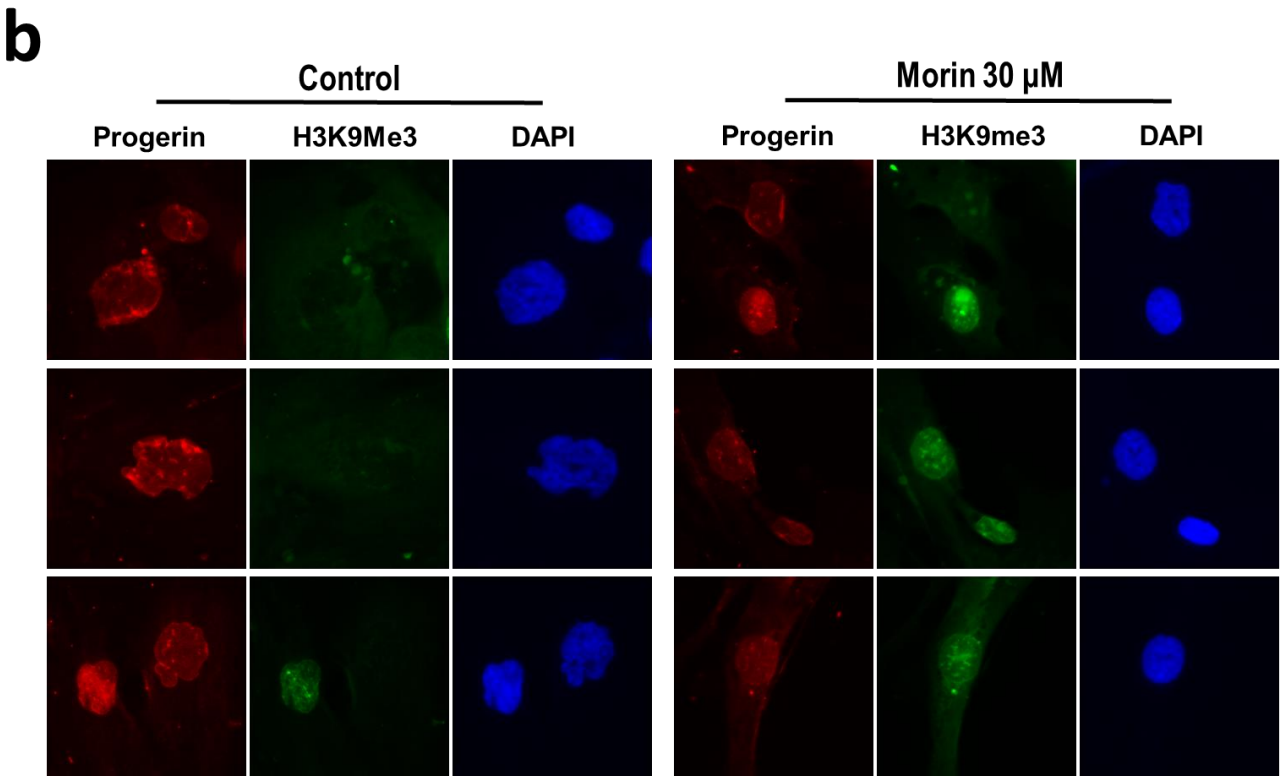
b
Control
Morin 30 μM
Progerin
H3K9Me3
DAPI
Progerin
H3K9me3
DAPI

Figure 4.7. Expression of H3K9Me3 treated with morin in the HGPS cells

HGPS cells were incubated with morin for 5 (***a***) or 7 (***b***) days and stained with H3K4Mes3 Ab. After being fixed with 100% MeOH, the cells were stained with lamin A/C Ab (red) and H3K9Me3 Ab (green). * The immunofluorescence assay was conducted by Bum-Joon Park's lab

4.4. Discussion

In this study, morin was screened and investigated as a direct inhibitor of the progerin-mediated protein interaction. Morin directly inhibited the aberrant interaction of progerin and lamin A. Although morin required 4 times higher concentration for preventing nuclear deformation of the HGPS cells than the synthetic compound JH4, morin has advantages as a daily food ingredient because of its potential low toxicity. Morin is known to have no toxicity in mice when used up to 100-1000 mM (Wu et al., 1994; Yugarani et al., 1992). Morin is 3, 5, 7, 2', 4'-pentahydroxylflavone, and is previously known to exhibit anti-oxidation activity that can protect cells against reactive oxygen species (ROS) damage. Morin is known to be produced by Mulberry figs, heartwood of old fustic (*Chlorophora tinctoria*), and many oriental medicinal herbs (Morris et al., 1951). Morin has diverse physiological effects, including anti-cancer effects (Chung et al., 2016; Zhang et al., 2018). Morin is also a direct inhibitor of GSK3beta, and thus morin attenuated Alzheimer's disease in the mice model by blocking GSK3beta-induced tau phosphorylation in vitro and a mouse model (Gong et al., 2011).

I believe that two important controllable factors to reduce the human aging rate. One factor is to reduce the cellular ROS level, and the

other factor is to reduce the aberrant function of progerin. Because morin is a strong antioxidant and an inhibitor of the progerin-mediated protein interaction, morin could show the beneficial effects in reducing the human aging rate in terms of both factors. Since morin also can alleviate Alzheimer's disease by a different mechanism (Gong et al., 2011), morin is a promising candidate to control age and age-related disease although further clinical and mechanistic studies are needed.

Bibliography

Aaronson, R.P., and Blobel, G. (1975). Isolation of nuclear pore complexes in association with a lamina. Proc Natl Acad Sci U S A ***72***, 1007-1011.

Aebi, U., Cohn, J., Buhle, L., and Gerace, L. (1986). The Nuclear Lamina Is a Meshwork of Intermediate-Type Filaments. Nature ***323***, 560-564.

Afonine, P.V., Grosse-Kunstleve, R.W., Echols, N., Headd, J.J., Moriarty, N.W., Mustyakimov, M., Terwilliger, T.C., Urzhumtsev, A., Zwart, P.H., and Adams, P.D. (2012). Towards automated crystallographic structure refinement with phenix.refine. Acta Crystallogr D ***68***, 352-367.

Afonine, P.V., Mustyakimov, M., Grosse-Kunstleve, R.W., Moriarty, N.W., Langan, P., and Adams, P.D. (2010). Joint X-ray and neutron refinement with phenix.refine. Acta Crystallogr D Biol Crystallogr ***66***, 1153-1163.

Ahn, J., Jo, I., Kang, S.M., Hong, S., Kim, S., Jeong, S., Kim, Y.H., Park, B.J., and Ha, N.C. (2019). Structural basis for lamin assembly at the molecular level. Nat Commun ***10***, 3757.

Andres, V., and Gonzalez, J.M. (2009). Role of A-type lamins in

signaling, transcription, and chromatin organization. J Cell Biol ***187***, 945-957.

Aziz, A., Hess, J.F., Budamagunta, M.S., FitzGerald, P.G., and Voss, J.C. (2009). Head and rod 1 interactions in vimentin: identification of contact sites, structure, and changes with phosphorylation using site-directed spin labeling and electron paramagnetic resonance. J Biol Chem ***284***, 7330-7338.

Aziz, A., Hess, J.F., Budamagunta, M.S., Voss, J.C., Kuzin, A.P., Huang, Y.J., Xiao, R., Montelione, G.T., FitzGerald, P.G., and Hunt, J.F. (2012). The structure of vimentin linker 1 and rod 1B domains characterized by site-directed spin-labeling electron paramagnetic resonance (SDSL-EPR) and X-ray crystallography. J Biol Chem ***287***, 28349-28361.

Bank, E.M., Ben-Harush, K., Feinstein, N., Medalia, O., and Gruenbaum, Y. (2012). Structural and physiological phenotypes of disease-linked lamin mutations in C. elegans. J Struct Biol ***177***, 106-112.

Baricheva, E.A., Berrios, M., Bogachev, S.S., Borisevich, I.V., Lapik, E.R., Sharakhov, I.V., Stuurman, N., and Fisher, P.A. (1996). DNA from Drosophila melanogaster beta-heterochromatin binds specifically to nuclear lamins in vitro and the nuclear envelope in situ. Gene ***171***, 171-176.

Ben-Harush, K., Wiesel, N., Frenkiel-Krispin, D., Moeller, D., Soreq,

E., Aebi, U., Herrmann, H., Gruenbaum, Y., and Medalia, O. (2009). The supramolecular organization of the C. elegans nuclear lamin filament. J Mol Biol ***386***, 1392-1402.

Bollati, M., Barbiroli, A., Favalli, V., Arbustini, E., Charron, P., and Bolognesi, M. (2012). Structures of the lamin A/C R335W and E347K mutants: Implications for dilated cardiolaminopathies. Biochem Bioph Res Co ***418***, 217-221.

Bonne, G., Di Barletta, M.R., Varnous, S., Becane, H.M., Hammouda, E.H., Merlini, L., Muntoni, F., Greenberg, C.R., Gary, F., Urtizberea, J.A., *et al.* (1999). Mutations in the gene encoding lamin A/C cause autosomal dominant Emery-Dreifuss muscular dystrophy. Nat Genet ***21***, 285-288.

Bonne, G., Mercuri, E., Muchir, A., Urtizberea, A., Becane, H.M., Recan, D., Merlini, L., Wehnert, M., Boor, R., Reuner, U., *et al.* (2000). Clinical and molecular genetic spectrum of autosomal dominant Emery-Dreifuss muscular dystrophy due to mutations of the lamin A/C gene. Ann Neurol ***48***, 170-180.

Bouzid, T., Kim, E., Riehl, B.D., Esfahani, A.M., Rosenbohm, J., Yang, R., Duan, B., and Lim, J.Y. (2019). The LINC complex, mechanotransduction, and mesenchymal stem cell function and fate. J Biol Eng ***13***, 68.

Broers, J.L., Peeters, E.A., Kuijpers, H.J., Endert, J., Bouten, C.V.,

Oomens, C.W., Baaijens, F.P., and Ramaekers, F.C. (2004). Decreased mechanical stiffness in LMNA-/- cells is caused by defective nucleo-cytoskeletal integrity: implications for the development of laminopathies. Hum Mol Genet ***13***, 2567-2580.

Brown, C.A., Lanning, R.W., McKinney, K.Q., Salvino, A.R., Cherniske, E., Crowe, C.A., Darras, B.T., Gominak, S., Greenberg, C.R., Grosmann, C., *et al.* (2001). Novel and recurrent mutations in lamin A/C in patients with Emery-Dreifuss muscular dystrophy. Am J Med Genet ***102***, 359-367.

Brunger, A.T. (1992). Free R value: a novel statistical quantity for assessing the accuracy of crystal structures. Nature ***355***, 472-475.

Burke, B., and Stewart, C.L. (2002a). Life at the edge: The nuclear envelope and human disease. Nat Rev Mol Cell Bio ***3***, 575-585.

Burke, B., and Stewart, C.L. (2002b). Life at the edge: the nuclear envelope and human disease. Nat Rev Mol Cell Biol ***3***, 575-585.

Burke, B., and Stewart, C.L. (2013). The nuclear lamins: flexibility in function. Nat Rev Mol Cell Biol ***14***, 13-24.

Burkhard, P., Stetefeld, J., and Strelkov, S.V. (2001). Coiled coils: a highly versatile protein folding motif. Trends Cell Biol ***11***, 82-88.

Cao, H., and Hegele, R.A. (2000). Nuclear lamin A/C R482Q mutation

in canadian kindreds with Dunnigan-type familial partial lipodystrophy. Hum Mol Genet ***9***, 109-112.

Capell, B.C., and Collins, F.S. (2006). Human laminopathies: nuclei gone genetically awry. Nat Rev Genet ***7***, 940-952.

Chernyatina, A.A., Guzenko, D., and Strelkov, S.V. (2015). Intermediate filament structure: the bottom-up approach. Curr Opin Cell Biol ***32***, 65-72.

Chernyatina, A.A., Nicolet, S., Aebi, U., Herrmann, H., and Strelkov, S.V. (2012). Atomic structure of the vimentin central alpha-helical domain and its implications for intermediate filament assembly. P Natl Acad Sci USA ***109***, 13620-13625.

Chernyatina, A.A., and Strelkov, S.V. (2012). Stabilization of vimentin coil2 fragment via an engineered disulfide. J Struct Biol ***177***, 46-53.

Chou, P.Y., and Fasman, G.D. (1978). Empirical predictions of protein conformation. Annu Rev Biochem ***47***, 251-276.

Chung, S.S., Oliva, B., Dwabe, S., and Vadgama, J.V. (2016). Combination treatment with flavonoid morin and telomerase inhibitor MST312 reduces cancer stem cell traits by targeting STAT3 and telomerase. Int J Oncol ***49***, 487-498.

Columbaro, M., Capanni, C., Mattioli, E., Novelli, G., Parnaik, V.K., Squarzoni, S., Maraldi, N.M., and Lattanzi, G. (2005). Rescue of heterochromatin organization in Hutchinson-Gilford progeria by drug treatment. Cell Mol Life Sci ***62***, 2669-2678.

Conway, J.F., and Parry, D.A.D. (1988). Intermediate Filament Structure .3. Analysis of Sequence Homologies. Int J Biol Macromol ***10***, 79-98.

Crisp, M., Liu, Q., Roux, K., Rattner, J.B., Shanahan, C., Burke, B., Stahl, P.D., and Hodzic, D. (2006). Coupling of the nucleus and cytoplasm: role of the LINC complex. J Cell Biol ***172***, 41-53.

Croft, J.A., Bridger, J.M., Boyle, S., Perry, P., Teague, P., and Bickmore, W.A. (1999). Differences in the localization and morphology of chromosomes in the human nucleus. J Cell Biol ***145***, 1119-1131.

Dahl, K.N., Kahn, S.M., Wilson, K.L., and Discher, D.E. (2004). The nuclear envelope lamina network has elasticity and a compressibility limit suggestive of a molecular shock absorber. J Cell Sci ***117***, 4779-4786.

De Sandre-Giovannoli, A., Bernard, R., Cau, P., Navarro, C., Amiel, J., Boccaccio, I., Lyonnet, S., Stewart, C.L., Munnich, A., Le Merrer, M., *et al.* (2003). Lamin a truncation in Hutchinson-Gilford progeria. Science ***300***, 2055.

Dechat, T., Adam, S.A., Taimen, P., Shimi, T., and Goldman, R.D. (2010). Nuclear lamins. Cold Spring Harb Perspect Biol ***2***, a000547.

Dechat, T., Pfleghaar, K., Sengupta, K., Shimi, T., Shumaker, D.K., Solimando, L., and Goldman, R.D. (2008). Nuclear lamins: major factors in the structural organization and function of the nucleus and chromatin. Genes Dev ***22***, 832-853.

Dessev, G.N., Iovcheva-Dessev, C., and Goldman, R.D. (1990). Lamin dimers. Presence in the nuclear lamina of surf clam oocytes and release during nuclear envelope breakdown. J Biol Chem ***265***, 12636-12641.

Dhe-Paganon, S., Werner, E.D., Chi, Y.I., and Shoelson, S.E. (2002). Structure of the globular tail of nuclear lamin. J Biol Chem ***277***, 17381-17384.

Dittmer, T.A., and Misteli, T. (2011). The lamin protein family. Genome biology ***12***, 222.

Emsley, P., and Cowtan, K. (2004). Coot: model-building tools for molecular graphics. Acta Crystallogr D Biol Crystallogr ***60***, 2126-2132.

Eriksson, M., Brown, W.T., Gordon, L.B., Glynn, M.W., Singer, J., Scott, L., Erdos, M.R., Robbins, C.M., Moses, T.Y., Berglund, P., *et al.* (2003). Recurrent de novo point mutations in lamin A cause Hutchinson-Gilford progeria syndrome. Nature ***423***, 293-298.

Fancy, D.A., Denison, C., Kim, K., Xie, Y., Holdeman, T., Amini, F., and Kodadek, T. (2000). Scope, limitations and mechanistic aspects of the photo-induced cross-linking of proteins by water-soluble metal complexes. Chem Biol ***7***, 697-708.

Foisner, R., and Gerace, L. (1993). Integral membrane proteins of the nuclear envelope interact with lamins and chromosomes, and binding is modulated by mitotic phosphorylation. Cell ***73***, 1267-1279.

Franke, W.W., Schmid, E., Winter, S., Osborn, M., and Weber, K. (1979). Widespread occurrence of intermediate-sized filaments of the vimentin-type in cultured cells from diverse vertebrates. Exp Cell Res ***123***, 25-46.

Fuchs, E., and Cleveland, D.W. (1998). A structural scaffolding of intermediate filaments in health and disease. Science ***279***, 514-519.

Furukawa, K. (1999). LAP2 binding protein 1 (L2BP1/BAF) is a candidate mediator of LAP2-chromatin interaction. J Cell Sci ***112*** *(Pt 15)*, 2485-2492.

Ghosh, S., and Zhou, Z. (2014). Genetics of aging, progeria and lamin disorders. Curr Opin Genet Dev ***26***, 41-46.

Goldberg, M.W., Huttenlauch, I., Hutchison, C.J., and Stick, R. (2008). Filaments made from A- and B-type lamins differ in structure and organization. J Cell Sci ***121***, 215-225.

Goldman, R.D. (1971). The role of three cytoplasmic fibers in BHK-21 cell motility. I. Microtubules and the effects of colchicine. J Cell Biol ***51***, 752-762.

Goldman, R.D., Gruenbaum, Y., Moir, R.D., Shumaker, D.K., and Spann, T.P. (2002). Nuclear lamins: building blocks of nuclear architecture. Genes Dev ***16***, 533-547.

Gong, E.J., Park, H.R., Kim, M.E., Piao, S., Lee, E., Jo, D.G., Chung, H.Y., Ha, N.C., Mattson, M.P., and Lee, J. (2011). Morin attenuates tau hyperphosphorylation by inhibiting GSK3beta. Neurobiol Dis ***44***, 223-230.

Gonzalez, J.M., Navarro-Puche, A., Casar, B., Crespo, P., and Andres, V. (2008). Fast regulation of AP-1 activity through interaction of lamin A/C, ERK1/2, and c-Fos at the nuclear envelope. Journal of Cell Biology ***183***, 653-666.

Goodchild, R.E., and Dauer, W.T. (2005). The AAA+ protein torsinA interacts with a conserved domain present in LAP1 and a novel ER protein. J Cell Biol ***168***, 855-862.

Gordon, L.B., Rothman, F.G., Lopez-Otin, C., and Misteli, T. (2014). Progeria: a paradigm for translational medicine. Cell ***156***, 400-407.

Gruber, M., and Lupas, A.N. (2003). Historical review: another 50th anniversary--new periodicities in coiled coils. Trends Biochem Sci ***28***,

679-685.

Gruenbaum, Y., and Foisner, R. (2015). Lamins: nuclear intermediate filament proteins with fundamental functions in nuclear mechanics and genome regulation. Annu Rev Biochem ***84***, 131-164.

Gruenbaum, Y., Margalit, A., Goldman, R.D., Shumaker, D.K., and Wilson, K.L. (2005). The nuclear lamina comes of age. Nat Rev Mol Cell Biol ***6***, 21-31.

Gu, L., Troncoso, J.C., Wade, J.B., and Monteiro, M.J. (2004). In vitro assembly properties of mutant and chimeric intermediate filament proteins: insight into the function of sequences in the rod and end domains of IF. Exp Cell Res ***298***, 249-261.

Guzenko, D., Chernyatina, A.A., and Strelkov, S.V. (2017). Crystallographic Studies of Intermediate Filament Proteins. Subcell Biochem ***82***, 151-170.

Hatzfeld, M., and Weber, K. (1991). Modulation of Keratin Intermediate Filament Assembly by Single Amino-Acid Exchanges in the Consensus Sequence at the C-Terminal End of the Rod Domain. J Cell Sci ***99***, 351-362.

Headd, J.J., Echols, N., Afonine, P.V., Grosse-Kunstleve, R.W., Chen, V.B., Moriarty, N.W., Richardson, D.C., Richardson, J.S., and Adams, P.D. (2012). Use of knowledge-based restraints in

phenix.refine to improve macromolecular refinement at low resolution. Acta Crystallogr D Biol Crystallogr ***68***, 381-390.

Heessen, S., and Fornerod, M. (2007). The inner nuclear envelope as a transcription factor resting place. Embo Rep ***8***, 914-919.

Heitlinger, E., Peter, M., Haner, M., Lustig, A., Aebi, U., and Nigg, E.A. (1991). Expression of chicken lamin B2 in Escherichia coli: characterization of its structure, assembly, and molecular interactions. J Cell Biol ***113***, 485-495.

Helbling-Leclerc, A., Bonne, G., and Schwartz, K. (2002). Emery-Dreifuss muscular dystrophy. Eur J Hum Genet ***10***, 157-161.

Henderson, P., Wilson, D.C., Satsangi, J., and Stevens, C. (2012). A role for vimentin in Crohn disease. Autophagy ***8***, 1695-1696.

Hennekes, H., Peter, M., Weber, K., and Nigg, E.A. (1993). Phosphorylation on protein kinase C sites inhibits nuclear import of lamin B2. J Cell Biol ***120***, 1293-1304.

Henrich, B., Bergamaschi, A., Broennimann, C., Dinapoli, R., Eikenberry, E.F., Johnson, I., Kobas, M., Kraft, P., Mozzanica, A., and Schmitt, B. (2009). PILATUS: A single photon counting pixel detector for X-ray applications. Nucl Instrum Meth A ***607***, 247-249.

Herrmann, H., and Aebi, U. (2004). Intermediate filaments: molecular

structure, assembly mechanism, and integration into functionally distinct intracellular Scaffolds. Annu Rev Biochem ***73***, 749-789.

Herrmann, H., and Aebi, U. (2016). Intermediate Filaments: Structure and Assembly. Cold Spring Harb Perspect Biol ***8***.

Herrmann, H., Bar, H., Kreplak, L., Strelkov, S.V., and Aebi, U. (2007). Intermediate filaments: from cell architecture to nanomechanics. Nat Rev Mol Cell Biol ***8***, 562-573.

Herrmann, H., Haner, M., Brettel, M., Ku, N.O., and Aebi, U. (1999). Characterization of distinct early assembly units of different intermediate filament proteins. J Mol Biol ***286***, 1403-1420.

Herrmann, H., and Strelkov, S.V. (2011). History and phylogeny of intermediate filaments: now in insects. BMC Biol ***9***, 16.

Herrmann, H., Strelkov, S.V., Feja, B., Rogers, K.R., Brettel, M., Lustig, A., Haner, M., Parry, D.A., Steinert, P.M., Burkhard, P., *et al.* (2000). The intermediate filament protein consensus motif of helix 2B: its atomic structure and contribution to assembly. J Mol Biol ***298***, 817-832.

Hess, J.F., Budamagunta, M.S., Voss, J.C., and FitzGerald, P.G. (2004). Structural characterization of human vimentin rod 1 and the sequencing of assembly steps in intermediate filament formation in vitro using site-directed spin labeling and electron paramagnetic resonance. J

Biol Chem ***279***, 44841-44846.

Hess, J.F., Voss, J.C., and FitzGerald, P.G. (2002). Real-time observation of coiled-coil domains and subunit assembly in intermediate filaments. J Biol Chem ***277***, 35516-35522.

Hesse, M., Grund, C., Herrmann, H., Brohl, D., Franz, T., Omary, M.B., and Magin, T.M. (2007). A mutation of keratin 18 within the coil 1A consensus motif causes widespread keratin aggregation but cell type-restricted lethality in mice. Experimental Cell Research ***313***, 3127-3140.

Hoffman, P.N., and Lasek, R.J. (1975). The slow component of axonal transport. Identification of major structural polypeptides of the axon and their generality among mammalian neurons. J Cell Biol ***66***, 351-366.

Hoger, T.H., Krohne, G., and Kleinschmidt, J.A. (1991). Interaction of Xenopus lamins A and LII with chromatin in vitro mediated by a sequence element in the carboxyterminal domain. Exp Cell Res ***197***, 280-289.

Holaska, J.M., Wilson, K.L., and Mansharamani, M. (2002). The nuclear envelope, lamins and nuclear assembly. Curr Opin Cell Biol ***14***, 357-364.

Holtz, D., Tanaka, R.A., Hartwig, J., and McKeon, F. (1989). The CaaX motif of lamin A functions in conjunction with the nuclear localization signal to target assembly to the nuclear envelope. Cell ***59***,

969-977.

Ishikawa, H., Bischoff, R., and Holtzer, H. (1968). Mitosis and intermediate-sized filaments in developing skeletal muscle. J Cell Biol ***38***, 538-555.

Ivorra, C., Kubicek, M., Gonzalez, J.M., Sanz-Gonzalez, S.M., Alvarez-Barrientos, A., O'Connor, J.E., Burke, B., and Andres, V. (2006). A mechanism of AP-1 suppression through interaction of c-Fos with lamin A/C (vol 20, pg 307, 2006). Gene Dev ***20***, 747-747.

Jacob, J.T., Coulombe, P.A., Kwan, R., and Omary, M.B. (2018). Types I and II Keratin Intermediate Filaments. Cold Spring Harb Perspect Biol ***10***.

Jung, Y.S., Lee, S.J., Lee, S.H., Chung, J.Y., Jung, Y.J., Hwang, S.H., Ha, N.C., and Park, B.J. (2013). Loss of VHL promotes progerin expression, leading to impaired p14/ARF function and suppression of p53 activity. Cell Cycle ***12***, 2277-2290.

Kang, S.M., Yoon, M.H., and Park, B.J. (2018). Laminopathies; Mutations on single gene and various human genetic diseases. BMB Rep ***51***, 327-337.

Kapinos, L.E., Burkhard, P., Herrmann, H., Aebi, U., and Strelkov, S.V. (2011). Simultaneous formation of right- and left-handed anti-parallel coiled-coil interfaces by a coil2 fragment of human lamin A. J

Mol Biol ***408***, 135-146.

Kapinos, L.E., Schumacher, J., Mucke, N., Machaidze, G., Burkhard, P., Aebi, U., Strelkov, S.V., and Herrmann, H. (2010). Characterization of the head-to-tail overlap complexes formed by human lamin A, B1 and B2 "half-minilamin" dimers. J Mol Biol ***396***, 719-731.

Koster, S., Weitz, D.A., Goldman, R.D., Aebi, U., and Herrmann, H. (2015). Intermediate filament mechanics in vitro and in the cell: from coiled coils to filaments, fibers and networks. Curr Opin Cell Biol ***32***, 82-91.

Kouklis, P.D., Traub, P., and Georgatos, S.D. (1992). Involvement of the Consensus Sequence Motif at Coil-2b in the Assembly and Stability of Vimentin Filaments. J Cell Sci ***102***, 31-41.

Krimm, I., Ostlund, C., Gilquin, B., Couprie, J., Hossenlopp, P., Mornon, J.P., Bonne, G., Courvalin, J.C., Worman, H.J., and Zinn-Justin, S. (2002). The Ig-like structure of the C-terminal domain of lamin A/C, mutated in muscular dystrophies, cardiomyopathy, and partial lipodystrophy. Structure ***10***, 811-823.

Kubben, N., Voncken, J.W., and Misteli, T. (2010). Mapping of protein-and chromatin-interactions at the nuclear lamina. Nucleus *1*, 460-471.

Laguri, C., Gilquin, B., Wolff, N., Romi-Lebrun, R., Courchay, K., Callebaut, I., Worman, H.J., and Zinn-Justin, S. (2001). Structural

characterization of the LEM motif common to three human inner nuclear membrane proteins. Structure ***9***, 503-511.

Lammerding, J., Fong, L.G., Ji, J.Y., Reue, K., Stewart, C.L., Young, S.G., and Lee, R.T. (2006). Lamins A and C but not lamin B1 regulate nuclear mechanics. J Biol Chem ***281***, 25768-25780.

Lazarides, E., and Hubbard, B.D. (1976). Immunological characterization of the subunit of the 100 A filaments from muscle cells. Proc Natl Acad Sci U S A ***73***, 4344-4348.

Lee, S.J., Jung, Y.S., Yoon, M.H., Kang, S.M., Oh, A.Y., Lee, J.H., Jun, S.Y., Woo, T.G., Chun, H.Y., Kim, S.K., *et al.* (2016). Interruption of progerin-lamin A/C binding ameliorates Hutchinson-Gilford progeria syndrome phenotype. J Clin Invest ***126***, 3879-3893.

Lendahl, U., Zimmerman, L.B., and McKay, R.D. (1990). CNS stem cells express a new class of intermediate filament protein. Cell ***60***, 585-595.

Leukel, M., and Jost, E. (1995). Two conserved serines in the nuclear localization signal flanking region are involved in the nuclear targeting of human lamin A. Eur J Cell Biol ***68***, 133-142.

Lin, F., and Worman, H.J. (1993). Structural organization of the human gene encoding nuclear lamin A and nuclear lamin C. J Biol Chem ***268***, 16321-16326.

Liu, B., Wang, J., Chan, K.M., Tjia, W.M., Deng, W., Guan, X., Huang, J.D., Li, K.M., Chau, P.Y., Chen, D.J., *et al.* (2005). Genomic instability in laminopathy-based premature aging. Nat Med ***11***, 780-785.

Liu, B., and Zhou, Z. (2008). Lamin A/C, laminopathies and premature ageing. Histol Histopathol ***23***, 747-763.

Lupas, A.N., and Bassler, J. (2017). Coiled Coils - A Model System for the 21st Century. Trends Biochem Sci ***42***, 130-140.

Machowska, M., Piekarowicz, K., and Rzepecki, R. (2015). Regulation of lamin properties and functions: does phosphorylation do it all? Open Biol ***5***.

Malhas, A.N., Lee, C.F., and Vaux, D.J. (2009). Lamin B1 controls oxidative stress responses via Oct-1. J Cell Biol ***184***, 45-55.

Mall, M., Walter, T., Gorjanacz, M., Davidson, I.F., Thi, B.N.L.H., Ellenberg, J., and Mattaj, I.W. (2012). Mitotic lamin disassembly is triggered by lipid-mediated signaling. Journal of Cell Biology ***198***, 981-990.

Manilal, S., Recan, D., Sewry, C.A., Hoeltzenbein, M., Llense, S., Leturcq, F., Deburgrave, N., Barbot, J., Man, N., Muntoni, F., *et al.* (1998). Mutations in Emery-Dreifuss muscular dystrophy and their effects on emerin protein expression. Hum Mol Genet ***7***, 855-864.

Maraldi, N.M., Squarzoni, S., Sabatelli, P., Capanni, C., Mattioli, E., Ognibene, A., and Lattanzi, G. (2005). Laminopathies: involvement of structural nuclear proteins in the pathogenesis of an increasing number of human diseases. J Cell Physiol ***203***, 319-327.

Markiewicz, E., Dechat, T., Foisner, R., Quinlan, R.A., and Hutchison, C.J. (2002). Lamin A/C binding protein LAP2alpha is required for nuclear anchorage of retinoblastoma protein. Mol Biol Cell ***13***, 4401-4413.

Martin, C., and Zhang, Y. (2005). The diverse functions of histone lysine methylation. Nat Rev Mol Cell Biol ***6***, 838-849.

Martin, L., Crimaudo, C., and Gerace, L. (1995). cDNA cloning and characterization of lamina-associated polypeptide 1C (LAP1C), an integral protein of the inner nuclear membrane. J Biol Chem ***270***, 8822-8828.

Mattout, A., Dechat, T., Adam, S.A., Goldman, R.D., and Gruenbaum, Y. (2006). Nuclear lamins, diseases and aging. Curr Opin Cell Biol ***18***, 335-341.

McCoy, A.J., Grosse-Kunstleve, R.W., Adams, P.D., Winn, M.D., Storoni, L.C., and Read, R.J. (2007). Phaser crystallographic software. J Appl Crystallogr ***40***, 658-674.

McPherson, E., Turner, L., Zador, I., Reynolds, K., Macgregor, D.,

and Giampietro, P.F. (2009). Ovarian failure and dilated cardiomyopathy due to a novel lamin mutation. Am J Med Genet A ***149A***, 567-572.

Meier, M., Padilla, G.P., Herrmann, H., Wedig, T., Hergt, M., Patel, T.R., Stetefeld, J., Aebi, U., and Burkhard, P. (2009). Vimentin coil 1A-A molecular switch involved in the initiation of filament elongation. J Mol Biol ***390***, 245-261.

Morris, Q., Gage, T., and SH, W. (1951). The isolation and purification of morin on an ion-exchange resin. Journal of the American Pharmaceutical Association ***73***, 3340-3341.

Muchir, A., Bonne, G., van der Kooi, A.J., van Meegen, M., Baas, F., Bolhuis, P.A., de Visser, M., and Schwartz, K. (2000). Identification of mutations in the gene encoding lamins A/C in autosomal dominant limb girdle muscular dystrophy with atrioventricular conduction disturbances (LGMD1B). Hum Mol Genet ***9***, 1453-1459.

Muchir, A., Medioni, J., Laluc, M., Massart, C., Arimura, T., van der Kooi, A.J., Desguerre, I., Mayer, M., Ferrer, X., Briault, S., *et al.* (2004). Nuclear envelope alterations in fibroblasts from patients with muscular dystrophy, cardiomyopathy, and partial lipodystrophy carrying lamin A/C gene mutations. Muscle Nerve ***30***, 444-450.

Naetar, N., and Foisner, R. (2009). Lamin complexes in the nuclear interior control progenitor cell proliferation and tissue homeostasis. Cell

Cycle ***8***, 1488-1493.

Nguyen, D., Leistritz, D.F., Turner, L., MacGregor, D., Ohson, K., Dancey, P., Martin, G.M., and Oshima, J. (2007). Collagen expression in fibroblasts with a novel LMNA mutation. Biochem Biophys Res Commun ***352***, 603-608.

Nicolet, S., Herrmann, H., Aebi, U., and Strelkov, S.V. (2010). Atomic structure of vimentin coil 2. J Struct Biol ***170***, 369-376.

Nikolova, V., Leimena, C., McMahon, A.C., Tan, J.C., Chandar, S., Jogia, D., Kesteven, S.H., Michalicek, J., Otway, R., Verheyen, F., *et al.* (2004). Defects in nuclear structure and function promote dilated cardiomyopathy in lamin A/C-deficient mice. J Clin Invest ***113***, 357-369.

Nitta, R.T., Jameson, S.A., Kudlow, B.A., Conlan, L.A., and Kennedy, B.K. (2006). Stabilization of the retinoblastoma protein by A-type nuclear lamins is required for INK4A-mediated cell cycle arrest. Mol Cell Biol ***26***, 5360-5372.

Otwinowski, Z., and Minor, W. (1997). Processing of X-ray diffraction data collected in oscillation mode. Methods Enzymol ***276***, 307-326.

Ozaki, T., Saijo, M., Murakami, K., Enomoto, H., Taya, Y., and Sakiyama, S. (1994). Complex-Formation between Lamin-a and the Retinoblastoma Gene-Product - Identification of the Domain on Lamin-a Required for Its Interaction. Oncogene ***9***, 2649-2653.

Parry, D.A. (2006). Hendecad repeat in segment 2A and linker L2 of intermediate filament chains implies the possibility of a right-handed coiled-coil structure. J Struct Biol ***155***, 370-374.

Parry, D.A., and Steinert, P.M. (1999). Intermediate filaments: molecular architecture, assembly, dynamics and polymorphism. Q Rev Biophys ***32***, 99-187.

Parry, D.A., Steven, A.C., and Steinert, P.M. (1985). The coiled-coil molecules of intermediate filaments consist of two parallel chains in exact axial register. Biochem Biophys Res Commun ***127***, 1012-1018.

Parry, D.A., Strelkov, S.V., Burkhard, P., Aebi, U., and Herrmann, H. (2007). Towards a molecular description of intermediate filament structure and assembly. Exp Cell Res ***313***, 2204-2216.

Peter, M., Nakagawa, J., Doree, M., Labbe, J.C., and Nigg, E.A. (1990). In vitro disassembly of the nuclear lamina and M phase-specific phosphorylation of lamins by cdc2 kinase. Cell ***61***, 591-602.

Premchandar, A., Mucke, N., Poznanski, J., Wedig, T., Kaus-Drobek, M., Herrmann, H., and Dadlez, M. (2016). Structural Dynamics of the Vimentin Coiled-coil Contact Regions Involved in Filament Assembly as Revealed by Hydrogen-Deuterium Exchange. J Biol Chem ***291***, 24931-24950.

Qin, Z., Kalinowski, A., Dahl, K.N., and Buehler, M.J. (2011). Structure and stability of the lamin A tail domain and HGPS mutant. J Struct Biol ***175***, 425-433.

Quinlan, R.A., Hatzfeld, M., Franke, W.W., Lustig, A., Schulthess, T., and Engel, J. (1986). Characterization of dimer subunits of intermediate filament proteins. J Mol Biol ***192***, 337-349.

Raffaele Di Barletta, M., Ricci, E., Galluzzi, G., Tonali, P., Mora, M., Morandi, L., Romorini, A., Voit, T., Orstavik, K.H., Merlini, L., *et al.* (2000). Different mutations in the LMNA gene cause autosomal dominant and autosomal recessive Emery-Dreifuss muscular dystrophy. Am J Hum Genet ***66***, 1407-1412.

Rice, L.M., Earnest, T.N., and Brunger, A.T. (2000). Single-wavelength anomalous diffraction phasing revisited. Acta Crystallogr D Biol Crystallogr ***56***, 1413-1420.

Rodriguez, J., Calvo, F., Gonzalez, J.M., Casar, B., Andres, V., and Crespo, P. (2010). ERK1/2 MAP kinases promote cell cycle entry by rapid, kinase-independent disruption of retinoblastoma-lamin A complexes. J Cell Biol ***191***, 967-979.

Scaffidi, P., and Misteli, T. (2006). Lamin A-dependent nuclear defects in human aging. Science ***312***, 1059-1063.

Schaffeld, M., Herrmann, H., Schultess, J., and Markl, J. (2001).

Vimentin and desmin of a cartilaginous fish, the shark Scyliorhinus stellaris: sequence, expression patterns and in vitro assembly. Eur J Cell Biol ***80***, 692-702.

Scharner, J., Brown, C.A., Bower, M., Iannaccone, S.T., Khatri, I.A., Escolar, D., Gordon, E., Felice, K., Crowe, C.A., Grosmann, C., *et al.* (2011). Novel LMNA mutations in patients with Emery-Dreifuss muscular dystrophy and functional characterization of four LMNA mutations. Human mutation ***32***, 152-167.

Schietke, R., Brohl, D., Wedig, T., Mucke, N., Herrmann, H., and Magin, T.M. (2006). Mutations in vimentin disrupt the cytoskeleton in fibroblasts and delay execution of apoptosis. Eur J Cell Biol ***85***, 1-10.

Schmidt, M., and Krohne, G. (1995). In vivo assembly kinetics of fluorescently labeled Xenopus lamin A mutants. Eur J Cell Biol ***68***, 345-354.

Schreiber, K.H., and Kennedy, B.K. (2013). When Lamins Go Bad: Nuclear Structure and Disease. Cell ***152***, 1365-1375.

Schweizer, J., Bowden, P.E., Coulombe, P.A., Langbein, L., Lane, E.B., Magin, T.M., Maltais, L., Omary, M.B., Parry, D.A., Rogers, M.A., *et al.* (2006). New consensus nomenclature for mammalian keratins. J Cell Biol ***174***, 169-174.

Shackleton, S., Lloyd, D.J., Jackson, S.N.J., Evans, R., Niermeijer,

M.F., Singh, B.M., Schmidt, H., Brabant, G., Kumar, S., Durrington, P.N., *et al.* (2000). LMNA, encoding lamin A/C, is mutated in partial lipodystrophy. Nature Genetics ***24***, 153-156.

Sheldrick, G.M. (2010). Experimental phasing with SHELXC/D/E: combining chain tracing with density modification. Acta Crystallogr D Biol Crystallogr ***66***, 479-485.

Shumaker, D.K., Dechat, T., Kohlmaier, A., Adam, S.A., Bozovsky, M.R., Erdos, M.R., Eriksson, M., Goldman, A.E., Khuon, S., Collins, F.S., *et al.* (2006). Mutant nuclear lamin A leads to progressive alterations of epigenetic control in premature aging. Proc Natl Acad Sci U S A ***103***, 8703-8708.

Shumaker, D.K., Lee, K.K., Tanhehco, Y.C., Craigie, R., and Wilson, K.L. (2001). LAP2 binds to BAF.DNA complexes: requirement for the LEM domain and modulation by variable regions. EMBO J ***20***, 1754-1764.

Smith, T.A., Strelkov, S.V., Burkhard, P., Aebi, U., and Parry, D.A. (2002). Sequence comparisons of intermediate filament chains: evidence of a unique functional/structural role for coiled-coil segment 1A and linker L1. J Struct Biol ***137***, 128-145.

Sohal, R.S., and Orr, W.C. (2012). The redox stress hypothesis of aging. Free Radic Biol Med ***52***, 539-555.

Sosa, B.A., Rothballer, A., Kutay, U., and Schwartz, T.U. (2012). LINC complexes form by binding of three KASH peptides to domain interfaces of trimeric SUN proteins. Cell ***149***, 1035-1047.

Starr, D.A., and Han, M. (2003). ANChors away: an actin based mechanism of nuclear positioning. J Cell Sci ***116***, 211-216.

Steinert, P.M., Marekov, L.N., and Parry, D.A. (1993). Diversity of intermediate filament structure. Evidence that the alignment of coiled-coil molecules in vimentin is different from that in keratin intermediate filaments. J Biol Chem ***268***, 24916-24925.

Strelkov, S.V., and Burkhard, P. (2002). Analysis of alpha-helical coiled coils with the program TWISTER reveals a structural mechanism for stutter compensation. J Struct Biol ***137***, 54-64.

Strelkov, S.V., Herrmann, H., Geisler, N., Lustig, A., Ivaninskii, S., Zimbelmann, R., Burkhard, P., and Aebi, U. (2001). Divide-and-conquer crystallographic approach towards an atomic structure of intermediate filaments. J Mol Biol ***306***, 773-781.

Strelkov, S.V., Schumacher, J., Burkhard, P., Aebi, U., and Herrmann, H. (2004). Crystal structure of the human lamin A coil 2B dimer: implications for the head-to-tail association of nuclear lamins. J Mol Biol ***343***, 1067-1080.

Stuurman, N., Sasse, B., and Fisher, P.A. (1996). Intermediate

filament protein polymerization: molecular analysis of Drosophila nuclear lamin head-to-tail binding. J Struct Biol ***117***, 1-15.

Sullivan, T., Escalante-Alcalde, D., Bhatt, H., Anver, M., Bhat, N., Nagashima, K., Stewart, C.L., and Burke, B. (1999). Loss of A-type lamin expression compromises nuclear envelope integrity leading to muscular dystrophy. J Cell Biol ***147***, 913-920.

Sylvius, N., Bilinska, Z.T., Veinot, J.P., Fidzianska, A., Bolongo, P.M., Poon, S., McKeown, P., Davies, R.A., Chan, K.L., Tang, A.S., *et al.* (2005). In vivo and in vitro examination of the functional significances of novel lamin gene mutations in heart failure patients. J Med Genet ***42***, 639-647.

Szeverenyi, I., Cassidy, A.J., Chung, C.W., Lee, B.T., Common, J.E., Ogg, S.C., Chen, H., Sim, S.Y., Goh, W.L., Ng, K.W., *et al.* (2008). The Human Intermediate Filament Database: comprehensive information on a gene family involved in many human diseases. Human mutation ***29***, 351-360.

Tapley, E.C., and Starr, D.A. (2013). Connecting the nucleus to the cytoskeleton by SUN-KASH bridges across the nuclear envelope. Curr Opin Cell Biol ***25***, 57-62.

Thompson, L.J., Bollen, M., and Fields, A.P. (1997). Identification of protein phosphatase 1 as a mitotic lamin phosphatase. J Biol Chem ***272***, 29693-29697.

Todorova, A., Halliger-Keller, B., Walter, M.C., Dabauvalle, M.C., Lochmuller, H., and Muller, C.R. (2003). A synonymous codon change in the LMNA gene alters mRNA splicing and causes limb girdle muscular dystrophy type 1B. J Med Genet ***40***, e115.

Tu, Y., Sanchez-Iglesias, S., Araujo-Vilar, D., Fong, L.G., and Young, S.G. (2016). LMNA missense mutations causing familial partial lipodystrophy do not lead to an accumulation of prelamin A. Nucleus ***7***, 512-521.

Turgay, Y., Eibauer, M., Goldman, A.E., Shimi, T., Khayat, M., Ben-Harush, K., Dubrovsky-Gaupp, A., Sapra, K.T., Goldman, R.D., and Medalia, O. (2017). The molecular architecture of lamins in somatic cells. Nature ***543***, 261-264.

Van Berlo, J.H., Voncken, J.W., Kubben, N., Broers, J.L., Duisters, R., van Leeuwen, R.E., Crijns, H.J., Ramaekers, F.C., Hutchison, C.J., and Pinto, Y.M. (2005). A-type lamins are essential for TGF-beta1 induced PP2A to dephosphorylate transcription factors. Hum Mol Genet ***14***, 2839-2849.

Vigouroux, C., and Capeau, J. (2005). A-type lamin-linked lipodystrophies. Novartis Found Symp ***264***, 166-177; discussion 177-182, 227-130.

Wallace, P., Signer, E., Paton, I.R., Burt, D., and Quinlan, R. (1998).

The chicken CP49 gene contains an extra exon compared to the human CP49 gene which identifies an important step in the evolution of the eye lens intermediate filament proteins. Gene ***211***, 19-27.

Waterham, H.R., Koster, J., Mooyer, P., Noort Gv, G., Kelley, R.I., Wilcox, W.R., Wanders, R.J., Hennekam, R.C., and Oosterwijk, J.C. (2003). Autosomal recessive HEM/Greenberg skeletal dysplasia is caused by 3 beta-hydroxysterol delta 14-reductase deficiency due to mutations in the lamin B receptor gene. Am J Hum Genet ***72***, 1013-1017.

Wickert, U., Mucke, N., Wedig, T., Muller, S.A., Aebi, U., and Herrmann, H. (2005). Characterization of the in vitro co-assembly process of the intermediate filament proteins vimentin and desmin: mixed polymers at all stages of assembly. Eur J Cell Biol ***84***, 379-391.

Wilson, K.L., and Foisner, R. (2010). Lamin-binding Proteins. Cold Spring Harb Perspect Biol ***2***, a000554.

Worman, H.J., and Bonne, G. (2007). "Laminopathies": A wide spectrum of human diseases. Experimental Cell Research ***313***, 2121-2133.

Wu, T.W., Zeng, L.H., Wu, J., and Fung, K.P. (1994). Morin: a wood pigment that protects three types of human cells in the cardiovascular system against oxyradical damage. Biochem Pharmacol ***47***, 1099-1103.

Yates, J.R., and Wehnert, M. (1999). The Emery-Dreifuss Muscular

Dystrophy Mutation Database. Neuromuscul Disord ***9***, 199.

Yuan, J., Simos, G., Blobel, G., and Georgatos, S.D. (1991). Binding of Lamin-a to Polynucleosomes. Journal of Biological Chemistry ***266***, 9211-9215.

Yugarani, T., Tan, B.K., Teh, M., and Das, N.P. (1992). Effects of polyphenolic natural products on the lipid profiles of rats fed high fat diets. Lipids ***27***, 181-186.

Zhang, Q., Zhang, F., Thakur, K., Wang, J., Wang, H., Hu, F., Zhang, J.G., and Wei, Z.J. (2018). Molecular mechanism of anti-cancerous potential of Morin extracted from mulberry in Hela cells. Food Chem Toxicol ***112***, 466-475.

[국문초록]

중간 필라멘트(Intermediate Filament) 단백질은 고등진핵생물 세포에 필수적이며, 외부에서 가해지는 힘에 대해 물리적인 지지를 제공하는 유연한 섬유 구조를 형성한다. 핵의 구조와 기능은 중간 필라멘트에 속하는 라민에 의해 조절된다. 따라서 핵의 구조와 기능에 대해 이해하기 위해서는 라민의 조립 메커니즘 규명이 필수적이다. 하지만 짧은 조각의 라민 구조만 규명되어 왔으며, 전자현미경을 이용한 낮은 해상도를 가지는 구조의 한계에 의해 라민의 조립 메커니즘에 대한 분자적 수준의 이해가 부족한 상황이었다. 본 연구에서는 라민의 전체 길이를 보여줄 만큼 긴 결정 구조를 3.2 Å 해상도로 규명하였다. 결정 구조에서는 두개의 코일형 이중체 (coiled-coil dimers)가 나란한 방향으로 배열되어 사중체를 형성하고 있는 것을 확인할 수 있었는데, 이는 기존 중간 필라멘트 비멘틴에서 관찰된 A11 결합과 유사하였다. 더 나아가 케미컬 크로스링커와 질량분석법을 적용하여 라민 필라멘트의 연장에 관여하는 새로운

결합 (eA22 interaction)을 발견하였다. 이러한 두가지 결합 (A11, eA22 결합)을 통해 라민 조립 메커니즘을 분자적으로 제시하였으며, 이는 최근 제시된 초저온 전자토모그래피 (Electron cryotomography; Cryo-ET) 이미지와도 일치하였다.

또한 필라멘트가 세로방향으로 확장될 때 코일 1a의 역할을 밝히기 위해 코일 1a의 a와 d 위치에 존재하는 아미노산 잔기의 변형을 도입하여 eA22 결합의 결합강도가 변화되는 것을 관찰하였다. 실험 결과 코일 1a의 안정도에 따라서 eA22 결합이 변화된다는 것을 확인할 수 있었다. 여러 세포에 돌연변이 라민 유전자를 과발현시켜 핵의 모양과 라민 단백질의 분포를 관찰하였을 때에도 일관된 결과를 얻었다. 이러한 연구는 코일 1a가 eA22 결합을 위한 분자적 스위치로 역할을 한다는 것을 시사하며 라민과 관련된 질병을 위한 치료제 개발에 분자적 기반을 마련할 것으로 기대한다.

라민 A/C 유전자의 무성 돌연변이 (silent mutation) 가 발생하면 C-말단이 잘려진 상태의 단백질인 프로제린 (progerin)

이 생성되며 이는 허친슨-길포드 프로게리아 증후군 (Hutchinson-Gilford progeria syndrome; HGPS)을 일으킨다. 기형적인 핵 모양은 HGPS 세포의 특징으로, 정상적인 노화 세포에서도 이와 같은 특징이 나타난다. 최근 연구에서는 프로제린이 라민 A/C의 중간 파편과 직접 상호작용하여 핵변형을 일으킨다는 사실이 밝혀졌다. 해당 상호작용을 차단하는 합성 화합물 (JH4)은 세포와 마우스 모델 모두에서 노화 표현형을 개선하는 효과를 보였다. 본 연구에서는 프로제린과 정상적인 라민의 결합을 억제하는 천연물을 스크리닝하였다. 여러가지 후보물질 중 플라보노이드 계열의 모린을 최종 후보물질로 선택하였다. 모린은 프로제린과 라민의 결합을 억제하는 효과를 나타내었다. 프로제린을 과발현시킨 세포와 HGPS 세포에 모린을 처리하였더니 핵이 변형되는 현상이 완화되었고, 이는 기존에 합성된 JH4 물질과 비슷한 수준으로 효과를 보였다. 모린은 항산화 효과를 가지고 있는 자연물질이기 때문에 모린을 기능성 식품으로 개발한다면 HGPS 환자들뿐만 아니라 정상적인 노화 작용에 대하여 수명과 건강을 향상시키는 효과를 기대할 수 있을 것이다.